



Synthesis and Characterization of Titanium Dioxide

Wissanu Choychangtong

Master of Science Thesis in Inorganic Chemistry

Prince of Songkla University

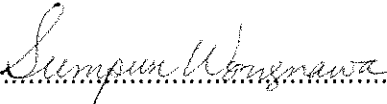
2004

T

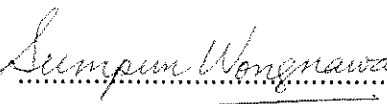
เลขที่	00181.T6 W57 2004 C.2
Bib Key	241642
	23 S.A. 2547

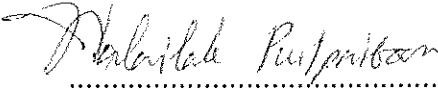
Thesis Title Synthesis and Characterization of Titanium Dioxide
Author Mr. Wissanu Choychangtong
Major Program Inorganic Chemistry

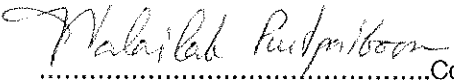
Advisory Committee



.....Chairman
(Associate Professor Dr. Sumpun Wongnawa)

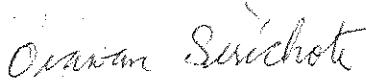
Examining Committee


.....Chairman
(Associate Professor Dr. Sumpun Wongnawa)


.....Committee
(Dr. Walailak Puetpaiboon)


.....Committee
(Dr. Walailak Puetpaiboon)


.....Committee
(Dr. Weena Aemage)


.....Committee
(Assistant Professor Dr. Orawan Sirichote)

The Graduate School, Prince of Songkla University, has approved this thesis as partial fulfillment of the requirement for the Master of Science degree in Inorganic Chemistry.


.....

(Surapon Arrykul, Ph.D.)
Associate Professor and Dean
Graduated School

ชื่อวิทยานิพนธ์	การสังเคราะห์และศึกษาคุณลักษณะของไทเทเนียมไดออกไซด์
ผู้เขียน	นายวิษณุ ช้อยช่างทอง
สาขาวิชา	เคมีอนินทรีย์
ปีการศึกษา	2546

บทคัดย่อ

ไทเทเนียมไดออกไซด์ที่มีโครงสร้างเป็นแบบรูทิล (แทนด้วยสัญลักษณ์ RU) และโครงสร้างแบบอนาเทสและรูทิลผสมกัน (แทนด้วยสัญลักษณ์ AR) สามารถเตรียมที่อุณหภูมิต่ำประมาณ 95°C โดยวิธี sol-gel จากปฏิกิริยาการย่อยสลายด้วยน้ำและปฏิกิริยาการควบแน่นของสารละลายไทเทเนียมเตตระคลอไรด์ จากนั้นทำสารละลายให้เป็นกลางด้วยสารละลายแอมโมเนีย ผลจากการศึกษาสารตัวอย่างด้วยเทคนิค XRD, FT-IR, N_2 absorption study, TGA, DTA, SEM, TEM และ UV-Vis พบว่าสารตัวอย่าง RU มีโครงสร้างแบบรูทิลมีขนาดอนุภาคเฉลี่ย 9.0 นาโนเมตรและพื้นที่ผิว 101.36 ตารางเมตรต่อกรัม นอกจากนี้ยังพบว่าสารตัวอย่างข้างต้นมีการจับตัวของอนุภาคที่เป็นระเบียบซึ่งประกอบไปด้วยอนุภาครูปรางคล้ายเส้นใยเล็กๆ กรณีของสารตัวอย่าง AR พบว่าลักษณะการจับตัวของอนุภาคมีความเป็นระเบียบน้อยกว่าสารตัวแรก มีขนาดพื้นที่ผิวประมาณ 218.38 ตารางเมตรต่อกรัม สารตัวอย่างนี้มีโครงสร้างทั้งแบบอนาเทสและรูทิลผสมกัน โดยที่โครงสร้างแบบแรกมีขนาดอนุภาคเฉลี่ย 5.2 นาโนเมตร ส่วนโครงสร้างแบบที่สองมีขนาดอนุภาคเฉลี่ย 7.8 นาโนเมตร การเกิดโครงสร้างแบบอนาเทสและรูทิลในสารตัวอย่างคาดว่าเกิดจากผลของปริมาณของน้ำในปฏิกิริยาเคมีซึ่งจะมีผลต่อลักษณะการจัดเรียงตัวของโครงสร้างพื้นฐานที่จะเกิดการจัดเรียงตัวเป็นโครงสร้างแบบอนาเทสและรูทิลในปฏิกิริยา

Thesis Title	Synthesis and Characterization of Titanium Dioxide
Author	Mr. Wissanu Choychangtong
Major Program	Inorganic Chemistry
Academic Year	2003

Abstract

Titanium dioxide in rutile phase (RU) and mixture of anatase and rutile phase (AR) were prepared by the sol-gel method at relatively low temperature (95°C) from the hydrolysis and condensation reaction of titanium tetrachloride and neutralized by ammonia solution. The oxides obtained were characterized by XRD, FT-IR, N₂ absorption study, TGA, DTA, SEM, TEM and UV-Vis techniques. The RU sample showed only the present of rutile phase with average particle size 9.0 nm, 101.36 m²/g, and surface area. While The AR sample showed the present of both anatase and rutile phase with surface area of 218.38 m²/g and average particle size of 5.2 and 7.8 nm for anatase and rutile, respectively. The morphology results indicated that Ru sample consisted of tenuous fibers of rutile with high aggregation of particles. For AR sample, it consisted of point-like of anatase and tenuous fibers of rutile with few aggregation of particles. The difference in crystalline phase formation of synthesized TiO₂ proposed from the stereochemistry of original nuclei which may resulted from the water content in the preparation condition.

Acknowledgements

I would like to express my sincere thanks to my advisor, Associate Professor Dr. Sumpun Wongnawa, who suggested this research problem, for his numerous suggestions, encouragement and criticism without which I would have been unable to complete this work.

I am very grateful to thanks Assistant Professor Phadoong Boonsin for the valuable comments on my thesis. I would like to thank the Department of Chemistry, Faculty of Science, Prince of Songkla University, for all necessary laboratory facilities used throughout this research.

I am grateful to the Development and Promotion of Science and Technology Talents Project (DPST) for the scholarship supports of the education program.

I am grateful to the Postgraduate Education and Research Program in Chemistry (PERCH) and the Graduate School, Prince of Songkla University, for the financial supports of this research.

I also would like to thank all of my collaborators who helped creating an enjoyable atmosphere to be working in and for their helpful in many countless ways throughout the years.

Wissanu Choychangtong

Contents

	Page
บทคัดย่อ	(3)
Abstract	(4)
Acknowledgements	(5)
Contents	(6)
List of Tables	(8)
List of Figures	(9)
1. Introduction	1
Introduction	1
Review of Literatures	4
Objectives	32
2. Methods of study	33
Materials	33
Instruments	33
Methods	34
Synthesis of titanium dioxide	35
Characterization of titanium dioxide	36
3. Results	40
Synthesis and characterization of titanium dioxide	40

Contents. (continued)

	Page
4. Discussions	63
5. Summary	91
references	94
Vitae	107

List of Tables

Table	Page
1 Properties of titanium	3
2 X-ray data on TiO ₂ modifications (Clark, 1968 : 268)	4
3 Properties of the three modifications of titanium dioxide (Clark, 1968 : 270)	5
4 Percent weight and peak area of rutile at $2\theta = 27.5$ of RU and AR TiO ₂	44
5 Percent weight and peak area of anatase at $2\theta = 25.5$ of AR TiO ₂	42
6 Particle size of TiO ₂	44
7 Surface area of TiO ₂	46
8 Porosity of TiO ₂	48
9 Assignment of the FT-IR bands of RU TiO ₂ (from Figure 16 and 17)	49
10 Assignment of the FT-IR bands of AR TiO ₂ (from Figure 16 and 17)	54
11 The onset of absorption and band gap energy of TiO ₂	60
12 Band gap energy from direct and indirect method	62
13 IUPAC classification of the pore	68
14 Energies of Direct and Indirect Transitions in a TiO ₂ semiconductor	83

List of Figures

Figure	Page
1 Crystal structure of TiO ₂ , (a) Anatase, (b) Rutile, (c) Brookite	6
2 TiO ₂ pigment manufactured by the sulfate process (Büchner, et al., 1989 : 526)	7
3 TiO ₂ pigment manufactured by the chloride process (Büchner, et al., 1989 : 528)	8
4 An overview of products prepared by Sol-Gel methods. (Chemat Technology, Inc., 1998)	11
5 Flow chart of the preparation of TiO ₂ powders by Sol-Gel method	38
6 Synthesized TiO ₂	40
7 XRD patterns of the TiO ₂ (a) RU TiO ₂ (b) AR TiO ₂ (c) P25 : Degussa (d) anatase : Carlo Erba (e) rutile : TOA Co, Thailand.	43
8 Standard addition calibration curve of synthetic rutile	45
9 Standard addition calibration curve of synthetic anatase	45
10 Nitrogen adsorption isotherm of RU TiO ₂	49
11 Nitrogen adsorption isotherm of AR TiO ₂	50
12 t-plot of Nitrogen adsorption isotherm of RU TiO ₂	50
13 t-plot of Nitrogen adsorption isotherm of AR TiO ₂	51
14 Pore size distribution curve of RU TiO ₂	51
15 Pore size distribution curve of AR TiO ₂	52
16 FT-IR spectrum (reflectance mode) of TiO ₂ (syn) in the range 4000-400 cm ⁻¹	53
17 FT-IR spectrum (reflectance mode) of TiO ₂ (syn) in the range 900-400 cm ⁻¹	53

List of Figures (continued)

Figure		Page
18	TGA curve of synthesized TiO ₂	55
19	DTA curve of synthesized TiO ₂	56
20	SEM image of synthesized TiO ₂ (RU : 18a and 18b, AR : 18c and 18d)	57
21	TEM images of synthesized TiO ₂ (RU : 21a and 21b, AR : 21c and 21d)	58
22	Diffuse UV-Vis absorption spectra of TiO ₂	59
23	Plot of $(\alpha h\nu)^{1/2}$ versus E_{phot} for indirect transition of TiO ₂ . The band gap (E_g) are obtained by extrapolation to $\alpha = 0$	61
24	Plot of $(\alpha h\nu)^2$ versus E_{phot} for direct transition of TiO ₂ . The band gap (E_g) are obtained by extrapolation to $\alpha = 0$	62
25	IUPAC classification of adsorption isotherms (Ryu et al., 1999)	68
26	SEM images of commercial TiO ₂ ; (26a) anatase : Carlo Erba (26b) rutile : TOA Co, Thailand, and (26c) P25 : Degussa	75
27	SEM images of TiO ₂ from the study of Yu et al., (2003)	76
28	TEM images of TiO ₂ ; (28a) anatase : Zhang et al., (2000) (28b) rutile : Yang et al., (2002) and (28c) P25 : Degussa : Liquang et al., (2003)	77
29	TEM images of rutile TiO ₂ ; Wang et al., (2001) (29a) tenuous fiber of rutile phase (29b) : higher magnification of the dark area in (29a)	79
30	Short energy level diagram illustrating the relative energy level in TiO ₂ (Serpone et al., 1995)	82

List of Figures (continued)

Figure		Page
31	Proposed pathway for the TiO ₂ nuclei of rutile (a) and anatase (b) starting from octahedral cations $[\text{Ti}(\text{OH})_2(\text{OH}_2)_4]^{2+}$ (Yanqing et al., 2001).	85
32	The <i>cis</i> - and <i>trans</i> -isomers of $[\text{Ti}(\text{OH})_2(\text{OH}_2)_4]^{2+}$ monomers.	86
33	Possible pathway for the formation of anatase and rutile type nuclei starting from octahedral cations (a) <i>trans</i> - $[\text{Ti}(\text{OH})_2(\text{OH}_2)_4]^{2+}$, (b) <i>cis</i> - $[\text{Ti}(\text{OH})_2(\text{OH}_2)_4]^{2+}$ in equatorial positions, in apical positions, and (d) <i>trans</i> - and <i>cis</i> - $[\text{Ti}(\text{OH})_2(\text{OH}_2)_4]^{2+}$.	87
34	Details of Figure 33 (c) showing the formation of each nuclei.	88
35	Possible pathway for the TiO ₂ of RU sample starting from octahedral cations <i>trans</i> - $[\text{Ti}(\text{OH})_2(\text{OH}_2)_4]^{2+}$	88
36	Possible pathway for the TiO ₂ of AR sample starting from octahedral cations (a) <i>trans</i> - $[\text{Ti}(\text{OH})_2(\text{OH}_2)_4]^{2+}$, (b) <i>cis</i> - $[\text{Ti}(\text{OH})_2(\text{OH}_2)_4]^{2+}$ in equatorial positions and (c) <i>cis</i> - $[\text{Ti}(\text{OH})_2(\text{OH}_2)_4]^{2+}$ in apical positions and (d) both <i>cis</i> - and <i>trans</i> - $[\text{Ti}(\text{OH})_2(\text{OH}_2)_4]^{2+}$.	90

1. Introduction

1.1 Introduction

Titanium is a chemical element with symbol Ti, atomic number 22 and atomic weight 47.90. It belongs to the fourth group of the periodic table, and its chemistry shows similarities to that of silicon and zirconium. Titanium occurs in nature as ilmenite (FeTiO_3), rutile (tetragonal TiO_2), anatase (tetragonal TiO_2), brookite (rhombohedral TiO_2), perovskite (CaTiO_3), sphene (CaTiSiO_6), and geikielite (MgTiO_3) (Kirk and Othmer, 1985 : 1182).

Titanium is a silvery, ductile metal with important industrial possibilities because it is less dense than iron, much stronger than aluminium, and almost as corrosion-resistant as platinum. Although it is unlikely ever to be as steel, its rare combination of properties makes it ideal for a variety of uses, particularly in engines, aircraft frames, some marine equipment, in industrial plant and in laboratory equipment. Certain properties may be improved by alloying it with aluminium (Clark, 1968 : 4-5). Some properties of titanium are given in Table 1.

The most important industrial use of titanium is in the form of titanium dioxide (TiO_2) which is widely used as a pigment for paint, coating ink, paper, plastic, cosmetic products, catalyst supports, photoconductors, dielectric materials, and so on because of its very whiteness, outstanding hiding property and non-toxicity. Titanium dioxide exists in three types according to its crystal structure: anatase, rutile, and brookite.

The brookite type cannot be used in industries because of its instability at room temperature. The anatase type has the problems of poor light and heat resistance and of gradually decreasing whiteness due to the weather. The anatase type also has drawbacks for applications involving adsorption technology owing to its low surface energy. The rutile type has outdoor applicability because of its good light resistance and can be applied to surfaces by the use of adsorption technology without advanced skills or sophisticated equipment (Kim and Chung, 2001).

In recent years, titanium dioxide photocatalysis has been studied extensively as a potential technique for the treatment of pollutants (both organic and inorganic) and microorganisms. In addition, there are many studies that used titanium dioxide for solid-phase extraction (SPE) because of its high chemical stability and high ion-exchange capacity (Poznyak, et al., 1999). Generally, titanium dioxide is obtained either from minerals or from a solution of titanium salts or alkoxides. However, the conversion of the production preparation of titanium dioxide usually requires calcination at high temperature. So, in this research it is desirable to find a lower temperature method for synthesis of anatase or rutile phase without calcination at high temperature and compare some properties to commercial titanium dioxide. The method simplification leads to lower production costs, energy saving and no pollution.

Table 1 Properties of titanium

Property	value
^a Electronic structure	3d ² 4s ²
^b Melting point, °C	1668 ± 5
^b Boiling point, °C	3260
^b Density, g/cm ³	
α phase at 20 °C	4.507
β phase at 885 °C	4.35
^b Thermal conductivity at 25 °C, W/(m·K)	21.9
^b Electrical resistivity at 20 °C, nΩ·m	420
^b Magnetic susceptibility, mks	180 x 10 ⁻⁶
^b Modulus of elasticity, Gpa	
tension	ca. 101
compression	103
shear	44
^a Metallic radius (Å)	1.47
^a Entropy S ^o ₂₉₈ (cal/deg/mol)	7.33
^a E ^o (M ²⁺ /M) volts, 25 °C	-1.63
^a E ^o (M ³⁺ /M ²⁺) volts, 25 °C	-0.37
^a Heat of atomisation (kcal/g·atom)	112.6

a (Clark, 1968 : 6), b (Kirk and Othmer, 1985 : 1183)

1.2 Review of Literatures

Titanium dioxide has three crystal structures: anatase, brookite, and rutile as shown in Figure 1. The crystallographic data on the three oxide modifications are summarised in Table 2. Both anatase and rutile are tetragonal, whereas brookite is orthorhombic. In all three forms, each titanium atom is coordinated to six almost equidistant oxygen atoms, and each oxygen atom to three titanium atoms (Clark, 1968 : 269). All three oxide modifications are birefringent ; anatase is uniaxial negative, brookite is biaxial positive and rutile is uniaxial positive. Further data are given in Table 3.

Table 2 X-ray data on TiO₂ modifications (Clark, 1968 : 268).

	Space group	Z	Cell parameters (Å)			Ti-O (Å) ^b
			A	B	C	
Anatase	$C_{4h}^{19} = C4/amc$	8	5.36		9.53	1.91(2) 1.95(4)
Brookite	$D_{2h}^{15} = Pbca$	8	9.15	5.44	5.14	1.84-2.03
Rutile	$D_{4h}^{14} = P4_2/mnm$	2	4.954		2.959	1.944(4) 1.988(2)
α - PbO ₂ form	$D_{2h}^{14} = Pbcn$	4	4.515	5.497	4.939	1.91(4) 2.05(2)

^b The numbers in parentheses refer to the number of equivalent oxygen atoms at the stated distance from a titanium atom.

Table 3 Properties of the three modifications of titanium dioxide
(Clark, 1968 : 270).

	<i>Anatase</i>	<i>Brookite</i>	<i>Rutile</i>
Density (g/cc)	3.90	4.13	4.27
Hardness (Mohs's scale)	5.5-6.0	5.5-6.0	6.0-6.5
Melting Point ($^{\circ}\text{C}$)	change to rutile	change to rutile	1840 ± 10
Entropy $S_{298.16}^{\circ}$ (cal/deg/m)	11.93	-	12.01
Refractive Index (25°C) ($\lambda = 5893 \text{ \AA}$)	n_{ω} 2.5612 n_{ϵ} 2.4880	n_{α} 2.5831 n_{β} 2.5843 n_{γ} 2.7004	n_{ω} 2.6124 n_{ϵ} 2.8993
Dielectric Constant (powder)	$\epsilon = 48$	$\epsilon = 78$	$\epsilon_{av} \approx 110$ $\epsilon_{\parallel} = 180$ at 3×10^5 c/s 25°C $\epsilon_{\perp} = 89$, at 3×10^5 c/s 25°C

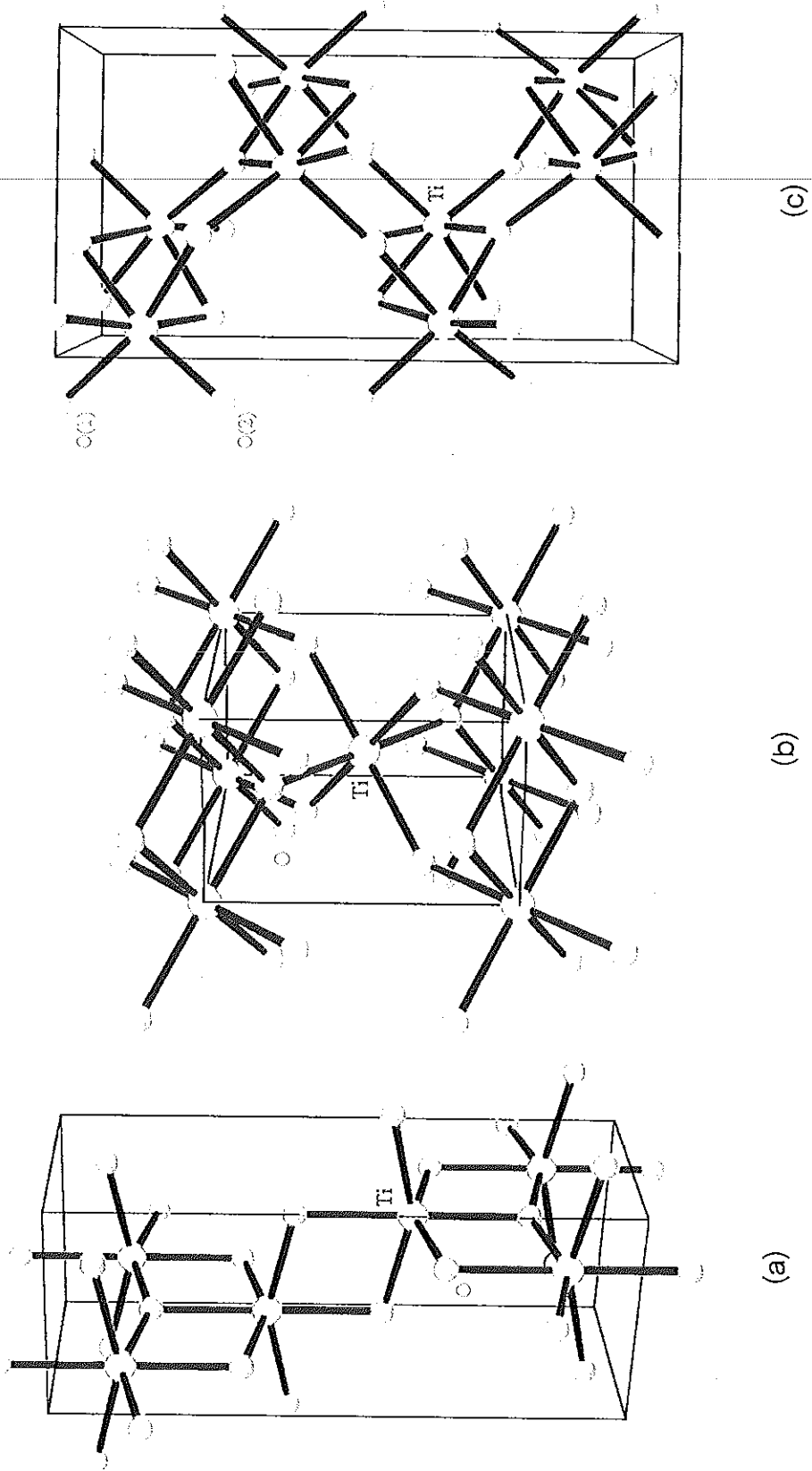


Figure 1 Crystal structures of TiO_2 , (a) Anatase, (b) Rutile, (c) Brookite.

Generally, TiO_2 pigments are industrially produced by the older sulfate or newer chloride processes. The economics of the two processes are very much dependent upon the raw material available. The starting materials for TiO_2 production are ilmenite and titaniferous slag in the case of the sulfate process (Figure 2) and leucoxene, rutile, synthetic rutile, and in the future possibly also anatase for the chloride process (Figure 3) (Büchner, et al., 1989 : 523-525).

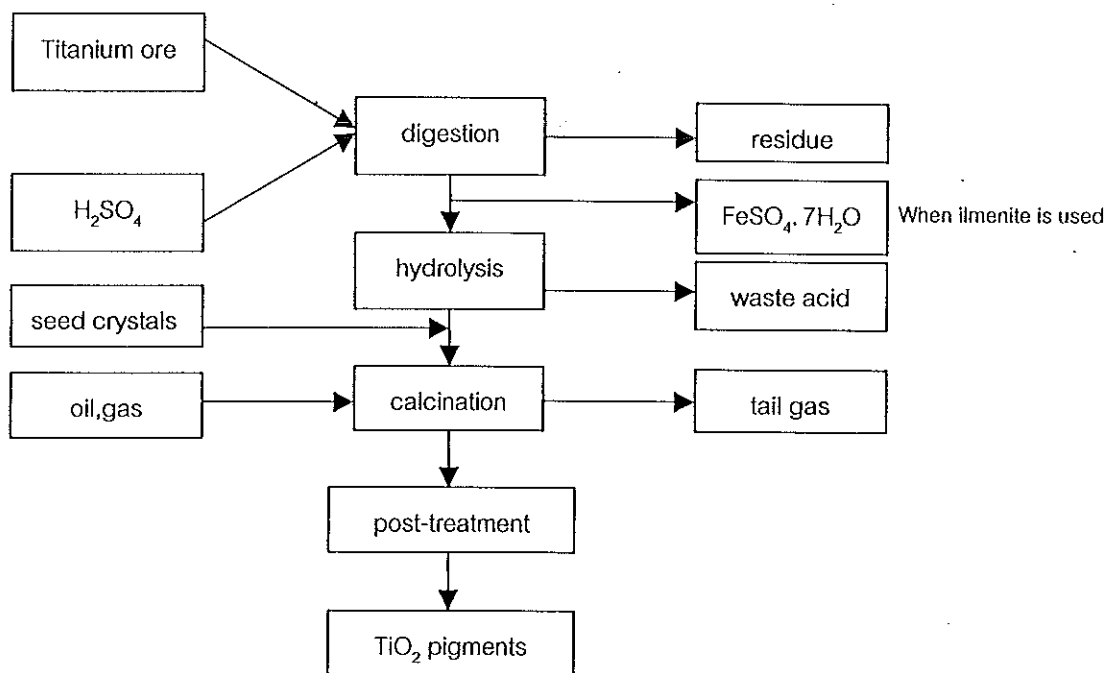


Figure 2 TiO_2 pigment manufactured by the sulfate process
(Büchner, et al., 1989 : 526).

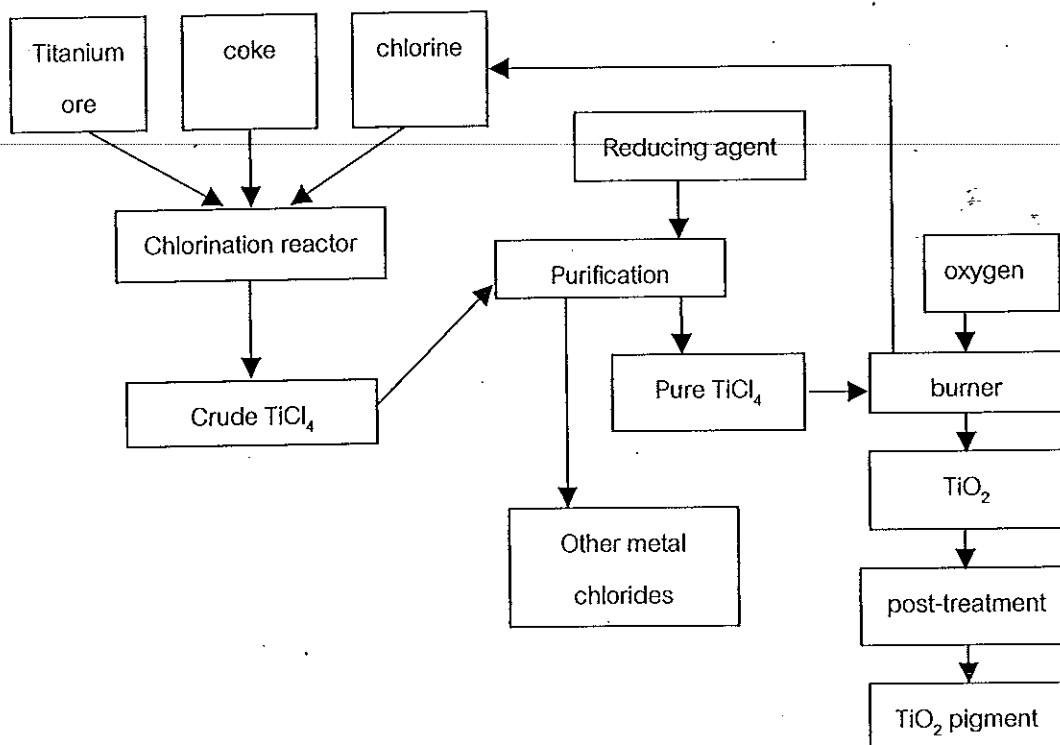


Figure 3 TiO₂ pigment manufactured by the chloride process
(Büchner, et al., 1989 : 528).

The sulfate process was the first commercial scale technology used to convert ilmenite to TiO₂. The process started from digestion the finely ground raw materials in an exothermic reaction with concentrated sulfuric acid, the digested cake dissolved in cold water and the residue separated off. To prevent their precipitation during the subsequent hydrolysis the Fe(III) ions are reduced to Fe(II) by adding a Ti(III) solution or scrap-ions. Upon evaporation of the solution, the large quantities of iron(II) sulfate heptahydrate is produced when ilmenite is used, and crystallize out. The titanium oxysulfate is then hydrolyzed to titanium oxyhydrate by heating the clarified solution with steam

at 95-110°C. TiO₂ seed crystals are added or formed before hydrolysis to ensure yields of 93-96 % TiO₂ and to obtain a hydrolysis product which yields the optimum particle size of ca. 0.2 μm upon firing. Diluted sulfuric acid remains as "waste acid". The hydrolysis product is washed, treated with a Ti (III) solution to remove adsorbed heavy metal ions (Fe, Cr, Mn, V) and calcined at temperature between 800-1,000°C. Anatase or rutile pigments can be produced in the calcination process depending upon the choice of additives, which determine the characteristics of the product. TiO₂ obtained in this way usually has the structure of anatase since the sulfate ions stabilize this modification (Hadjiivanov, *et al.*, 1996) which could not be removed during the process of washing, and it would benefit to the formation of anatase and the transformation temperature must take place at high temperature (about 1,000°C) to obtain rutile TiO₂(Yang, *et al.*, 2002).

The newer chloride process offers tighter product control, less labor intensive, avoids the iron sulfate waste problem and, at larger scales, is cheaper to operate. Currently about 60 % of 4 million tones of pigment produced world-wide is produced by this process. This process required the ilmenite to be processed to the rutile form (i.e. removal of the iron component to yield crude titanium dioxide(synthetic rutile)). The chloride process started from the reaction of chlorine with synthetic rutile to form raw titanium tetrachloride which is then mixed with reducing agent to convert impurities such as vanadium oxychloride, iron chloride to lower oxidation state compounds. It is then distilled yielding titanium tetrachloride in almost any required purity. Finally, it is combusted with pure oxygen to TiO₂ and chlorine, which is reused in the chlorination. Usually, TiO₂ prepared from this process

has the mixture structure of anatase and rutile with the average diameter about 20 nm. For instance, the typical commercial fumed TiO_2 (anatase) made by Degussa contain about 25 % rutile.

On a laboratory scale, titanium dioxide has been prepared by various methods, such as sol-gel method, hydrothermal method, combustion synthesis, inert-gas conversion and so on. The different preparation route and the experiment conditions of titanium dioxide result in products with different structures, morphology, particle size and contaminants (Hadjiivanov, et al., 1996). The metal alkoxide is usually used as a precursor on a laboratory scale to prepare titanium dioxide powders. However, strick control of the reaction conditions is required because of the intense hydrolysis of alkoxide in the air and the prices of the alkoxide limit the commercialization. So, the commercial inorganic compounds such as titanium tetrachloride (TiCl_4) and titanium disulfate ($\text{Ti}(\text{SO}_4)_2$) are more extensively used in the preparation of titanium dioxide than the metal alkoxide.

It is known that titanium dioxide prepared by sol-gel methods has been used in many applications in science and technology such as membranes, porous substrate, photocatalytic oxides, ceramics, glass materials and also in electronic devices (Kumar, et al., 1998). In general, the sol-gel method involves the transition of system from a liquid "sol" into solid "gel" phase. An overview of the sol-gel product is presented in Figure 4. The starting materials in the preparation of the "sol" are usually inorganic metal salts or metal organic compounds. In a typical sol-gel method, the precursor is subjected to a series of hydrolysis and polymerization (condensation) reactions to form a colloidal

suspension or a "sol". Further processing of the "sol" enables one to make ceramic materials in different forms. Thin films can be prepared on a piece of substrate by spin coating or dip-coating. When the "sol" is cast into a mold, a wet "gel" will form. With further drying and heat-treatment, the "gel" is converted into dense ceramic or glass articles. If the liquid in a wet "gel" is removed under a supercritical condition, a highly porous and extremely low density material called "aerogel" is obtained. As the viscosity of a "sol" is adjusted into a proper viscosity range, ceramic fibers can be drawn from the "sol". Ultra-fine and uniform ceramic powders are formed by precipitation, spray pyrolysis, or emulsion techniques (Chemat Technology, Inc., 1998).

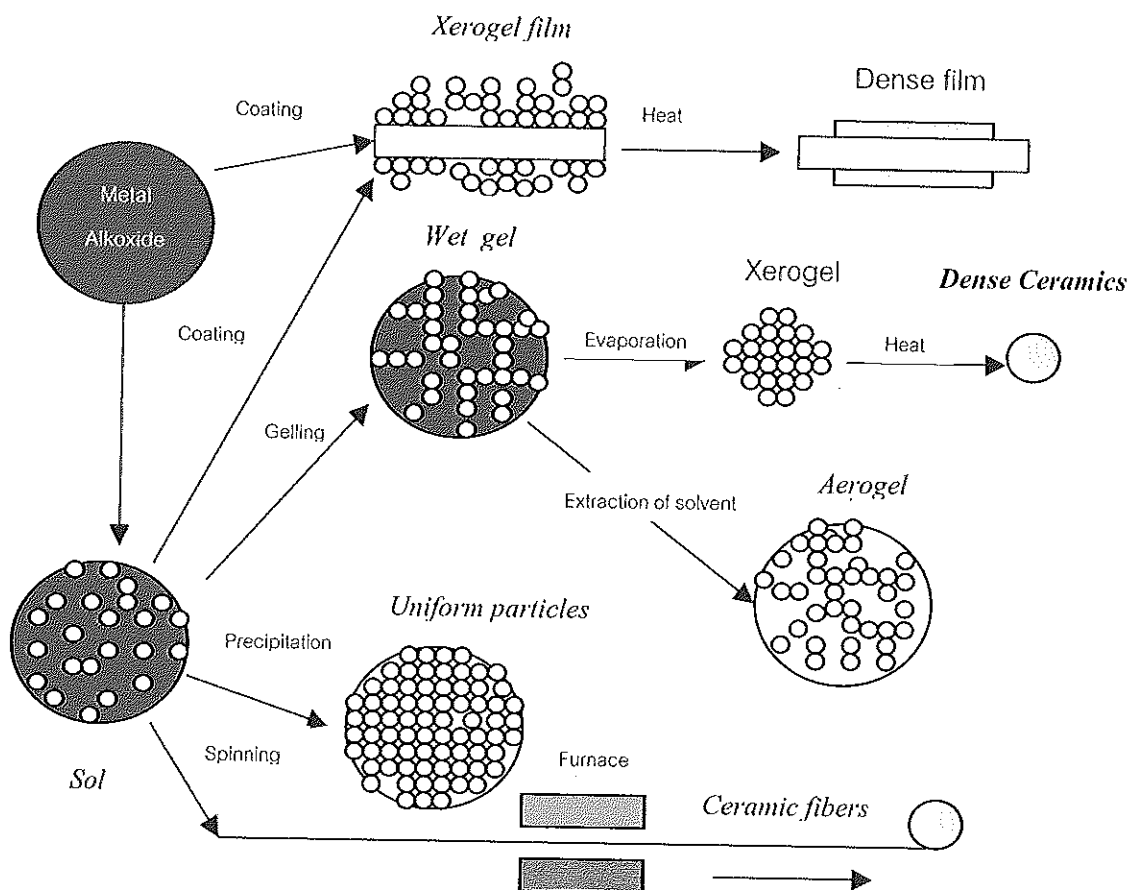


Figure 4 An overview of products prepared by sol-gel methods
(Chemat Technology, Inc., 1998)

In comparison to the other methods, the sol-gel method offers many advantages in easily control and strongly influenced by the synthesis conditions. Strick control on synthesis parameters is necessary to obtain reproducibility in sample with the desired characteristics and high level of chemical purity (Suresh, et al., 1998). Moreover, in these method precursor materials are metallic halide or alkoxide that favor the building of a solid network in a gel which eventually become a stable solid (Sanchez, et al., 1996). When this method is used for developing catalytic materials, it provides very interesting results. For instance, in metal supported catalysis, the active metal and the support can be prepared in one step. This allows an economy in the catalyst preparation, and also allows one to develop catalyst with new properties (Bokhimi, et al., 1995). Furthermore, the sol-gel method can be used for preparing the support alone, this supports determine the dispersion and stabilization of the active metal and has a specific surface area that can be regulated by controlling its particle size and porosity (Tauter, et al., 1978). Although, titanium dioxide powder prepared by hydrothermal method has high quality and shown high activity in photocatalytic reaction, the method required an autoclave to produce high temperature and high pressure conditions. In addition to these methods, it has been still difficult for continuous process up to now (Yang, et al., 2002). Many studies have shown that titanium dioxide powder obtained from sol-gel method has a good properties for application as follows.

Anderson, et al., (1995) synthesized mixed oxide of $\text{SiO}_2/\text{TiO}_2$ powders by sol-gel method. They also investigated the photodecomposition of rhodamine-6G (R-6G). The powders prepared from the reaction of

tetraisopropyl orthotitanate (TIOT) and tetraethoxysilane (TEOS). A mixture TIOT/TEOS with the desired Ti/Si ratio was prepared in a dry box, sealed, and then removed from the drybox. This solution was added dropwise to a solution of 250 mL anhydrous 2-propanol and 1 mL of concentrated HCl at 0°C with vigorous stirring. The mixture was allowed to age at room temperature in a covered beaker for 1 week after gelling. Solvent was then removed under vacuum, and while still under vacuum, the catalysts were heated to 200°C for 12 h. The resulting glassy materials were ground in a mixture mill for 1 h. The products were determined by XRD, BET surface area and UV-VIS techniques. Their studies indicated that SiO₂/TiO₂ powders with weight ratio of 30/70 show more efficient photocatalyst about 3 times for the destruction of R-6G than Degussa P25 TiO₂. The presence of an adsorbent (SiO₂) promoted efficiency by increasing the quantity of R-6G near the TiO₂ sites relative to the solution concentration of R-6G. Photogenerated oxidants from TiO₂ had been shown to be mobile either in solution or on the surface of SiO₂.

Anderson, et al., (1997) synthesized mixed oxides of TiO₂/SiO₂ and TiO₂/Al₂O₃ by sol-gel method and studied the photocatalytic decomposition of phenol and salicylic acid in an air-saturated aqueous solution. The first oxide was prepared by the same method as given above. The latter oxide was prepared from the reaction of tetraisopropyl orthotitanate (TIOT) and triisopropyl orthoaluminate (TIOA). A solution of 20 g TIOA in 500 mL of 2-propanol was prepared and stirred for 8 h. The solution was cooled to 0°C and TIOT was added dropwise with stirring for 1 h. The resulting solution was slowly warmed to room temperature and stirred for 8 h. The mixture was allowed to age in the liquor for 7 days. After aging the solvent was removed

under vacuum at room temperature. The dry powder was then heated and used as a photocatalyst. It was found that $\text{TiO}_2/\text{Al}_2\text{O}_3$ material showed more activity for the photocatalytic decomposition of salicylic acid than $\text{TiO}_2/\text{SiO}_2$ and TiO_2 -only materials. $\text{TiO}_2/\text{SiO}_2$ materials showed more activity for the photocatalytic decomposition of phenol when compare to the other materials. The increasing in efficiency was attributed to the presence of matrix-isolated TiO_2 quantum particles in the $\text{TiO}_2/\text{SiO}_2$ which promote the adsorption of phenol and a higher decomposition rate than $\text{TiO}_2/\text{Al}_2\text{O}_3$ and pure TiO_2 . While the $\text{TiO}_2/\text{Al}_2\text{O}_3$ materials behave more as a composite of the two bulk phases which adsorbed acidic species and showed more efficiency in photocatalytic decomposition of salicylic acid.

Ding, et al., (1997) synthesized nanocrystalline titanium dioxide by sol-gel method, and studied the influence of several factors during processing, such as hydrolysis catalyst used, hydrolysis degree, room temperature aging process, and some oxide dopants, on the microstructural evolution of these powders. The samples were investigated by TGA, XRD techniques. The product prepared by using tetrabutyl titanate ($\text{Ti}(\text{O-Bu})_4$) as precursor and anhydrous ethanol was used as the solvent. Either hydrochloric acid or acetylacetone ($\text{C}_5\text{H}_8\text{O}_2$) was added to monitor the hydrolysis reaction of $\text{Ti}(\text{O-Bu})_4$ in water. The molar ratio of these reactants was: $\text{Ti}(\text{O-Bu})_4$: H_2O : EtOH : catalyst (HCl or $\text{C}_5\text{H}_8\text{O}_2$) = 1 : r : 15 : 0.3 (r= 1 or 4 represents the hydrolysis water amount). In order to avoid strong hydrolysis reactions, $\text{Ti}(\text{O-Bu})_4$ was diluted with half the prescribed amount of ethanol at first, then water and catalyst dissolved in the remaining ethanol were added dropwise to the ethanolic solution of alkoxide with continuous stirring. Through a sequence of

hydrolysis and condensation reactions, the sol-gel transition took place gradually. The drying process of the wet-gel was performed in a vacuum tube (10^{-1} Pa) furnace at 333 K for 5 h. After mechanically grinding for 10 min, the dry-gel powders were heat-treated at various temperature for 2 h under oxygen atmosphere to obtain the nanostructure titanium dioxide powders. During sample processing, most of the dry-gel powders were heat-treated soon after the preparation. In order to examine the effect of the room temperature aging process on the structural evolution of the as-prepared dry-gel powder. The dry-gel powder was sealed in a small glass bottle and heat-treated after 1 year. In preparation the doped titanium dioxide powders, aluminum isopropoxide, tin tetrachloride and ferric nitride were used as the precursors of alumina, tin oxide, and ferric oxide, respectively. At first, one of these doping precursors was added into the mixed solution of $\text{Ti}(\text{O-Bu})_4$ -EtOH and this mixture was stirred by a magnetic mixer and ultrasonic wave successively. The next steps were the same as those in the preparation of pure titanium dioxide powders. The amount of dopants in the prepared powders was calculated to be 4 mole % according to the molar ratio between the precursors of titanium dioxide and doping oxides. The characterization of the product was determined by XRD, TGA analysis. The results showed that the structural evolution of the powders could be significantly influenced by preparation conditions. In comparison with $\text{C}_5\text{H}_8\text{O}_2$ -catalyzed titanium dioxide gel, the HCl-catalyzed one crystallized into anatase at a much lower temperature, and the crystalline size is smaller after the same heat treatments. On the other hand, pure rutile phase could be more easily obtained in the $\text{C}_5\text{H}_8\text{O}_2$ -catalyzed gel. In the lower hydrolysis water content samples, the grain size was smaller, and the starting temperature of the anatase to rutile

transformation was a little lower, in comparison with those higher water content samples. A long period of aging at room temperature evidently enhances the anatase to rutile transformation in the dry-gel powders. Some oxides additives, such as alumina, tin oxide and ferric oxide could effectively prevent the grain growth and quite different in anatase to rutile transformation in these nanocrystalline. Both tin oxide and ferric oxide dopants can enhance the anatase to rutile transformation, while alumina doping can significantly prevent this transformation.

Suresh, et al., (1998) prepared titanium dioxide powders by sol-gel method with acetic acid as a modifier at different pH conditions. The phase transformation during heat treatment was investigated by impedance spectroscopic measurements and the data were compared with those obtained from thermal analysis and XRD techniques. The samples were prepared by hydrolysis of 25 mL titanium isopropoxide dissolved in 48 mL acetic acid and was stirred for 0.5 h. To this solution 150 mL double distilled water was added dropwise under continuous stirring for 1 h. The pH was adjusted to 3 by adding 10 % ammonium hydroxide. The mixture was heat to 70°C in an air oven to get a gel. Similar procedures were followed to prepare titanium dioxide samples at pH values 4, 5 and 6. The studies showed that the anatase to rutile phase transformation was delayed in the case of acetic acid modified gel precursor at pH 3 and 4, showing the presence of anatase phase even at 1,000°C. On the other hand, in the sample precursor prepared at pH 6, anatase to rutile transformation was complete at 800°C, under identical conditions of heat-treatment.

Escobar, et al., (2000) prepared $\text{Al}_2\text{O}_3\text{-TiO}_2$ materials by the sol-gel method using aluminium tri-sec-butoxide and titanium (IV) isopropoxide as precursors with different synthesis additives: HNO_3 , NH_4OH , and CH_3COOH . The materials at two compositions: Al/Ti atomic ratio = 2 and 25 were synthesized at 278 K and calcined at temperature from 573 to 1173 K. These solids were characterized by TGA, DTA, XRD, BET and SEM. The complexing (CH_3COOH) and the basic (NH_4OH) additives led to solids with high pore volumes and broad pore size distributions. On the one hand, very high surface area: $525 \text{ m}^2/\text{g}$ for solids calcined at 773 K was found for samples prepared with CH_3COOH . On the other hand, high temperature stability was obtained with NH_4OH addition ($200 \text{ m}^2/\text{g}$, for Al_2O_3 -rich samples at 1173 K). HNO_3 catalyzed samples showed lower surface areas and pore volumes. Surface areas and sintering behavior were a function of titanium dioxide content. TiO_2 -rich samples showed higher surface area (773 K) than Al_2O_3 -rich samples, but at more severe conditions they suffered a severe specific area loss. The Al_2O_3 -rich formulations showed good stability in the whole range of temperature studied.

Harizonov, et al., (2001) studied the mixed oxide system TiO_2/MnO prepared by the sol-gel method using titanium ethoxide and manganese nitrate as precursors. The xerogels of the solutions dried at 80°C and treated at 560°C in air for 1 h and then characterized by XRD, FT-IR, DTA and UV-VIS techniques. The results showed that the sol-gel method could be used to prepare good quality nanocrystalline TiO_2 coatings. In addition, the presence of MnO in TiO_2 xerogels was effective in decreasing the anatase-rutile

transformation temperature. These coatings offered prospective applications in passive solar control glazing due to the relatively high refractive index.

Yamazaki, et al., (2001) reported novel titanium dioxide pellets which were obtained from the preparation process of sol-gel method in sulfuric acid and also investigated the efficiency of these products for the photocatalytic degradation of ethylene. The samples were prepared by the hydrolysis of 45 mL $\text{Ti}(\text{OC}_3\text{H}_7)_4$ in 540 mL water containing 3.9 mL HNO_3 , and the precipitation occurred immediately. Precipitates were stirred continuously at room temperature for 3 days. This peptization process formed a highly dispersed gel. This sol then dialyzed in a cleaned molecularly porous dialysis tube until a value of approximately pH 4 was obtained. The sol was concentrated in an oven at 40-50°C for 2 days. The resulting gel was fired at 100-500°C. On the other hand, when 2.6 mL H_2SO_4 was used instead of 3.9 mL HNO_3 to adjust pH in the precipitation methods, precipitates on hydrolysis were not dispersed to a colloidal solution during the precipitation for 10 days. The obtained fine precipitates were washed by repeating decantation to obtain a final pH of 3.7 and were filtered by aspirator. Finally, the solid was fired at 100-700°C. As-prepared products were characterized by XRD, XPS, BET surface area, ion chromatography, hardness testers and UV-VIS techniques. The results indicated that the use of sulfuric acid in the peptization process of sol-gel method produced sulphate ion incorporated titanium dioxide which was mechanically strong by firing at 200°C. Such oxide had larger surface area and retarded the phase transition from anatase to rutile compared with that prepared from the peptization with nitric acid. The XPS measurements indicated that sulfur exists mainly as sulphate ions. The titanium dioxide fired

at 400°C showed the highest photocatalytic activity for ethylene degradation. Especially, emphasized was put on the titanium dioxide sintered at 200°C because it was extremely hard in spite of such a low sintering temperature. This photocatalyst may provide a great potential for extensive applications as self-membranes.

Zhang, et al., (2001) prepared nanocrystalline iron doped titanium dioxide as a single-phase product by sol-gel method. The product synthesized from the reaction of titanium isopropoxide and $\text{Fe}(\text{NO}_3)_3 \cdot 9\text{H}_2\text{O}$ by varying the iron dopant amounts: 0, 1, 2, 3, 4, 5 and 6 atom %. The mixture was aged at ambient temperature for a few days. During this time liquid became progressively more viscous and eventually a dry gel formed. Crystallization was achieved by subsequent calcination of the dry gel in air at different temperatures. By transmission, scanning, and analytical electron microscopy as well as by complementary techniques it has been found that the as-prepared solids exhibit a narrow size distribution and that the iron is homogeneously distributed in the titanium dioxide matrix. The influence of the iron concentration on the phase transformations of the doped titanium dioxide was investigated by X-ray diffractometer. The formation of the iron titanium dioxide pseudobrookite, $\text{Fe}_2\text{Ti}_2\text{O}_5$, was observed above 670°C, but only for an iron content of more than 3 atom %. UV-spectroscopic measurement revealed that the absorption spectrum of the iron doped titanium dioxide is sensitively related to both the iron concentration and the calcination temperature. Whereas pure nanocrystalline titanium dioxide undergoes grain growth (sintering) when the calcination temperature is increased, iron doped titanium dioxide proves to be inert to grain growth, N_2 adsorption-desorption analysis

indicated that the products calcined between 390 and 600°C for 1 h in air have mesoporous structure and the distribution of mesopores is very narrowly, centered at 3.7 nm.

Zhang, et al., (2002) reported the preparation of mesoporous nanocrystalline titanium dioxide by sol-gel method and the effected of aging time for synthesis on its phase transition. The samples were analyzed by XRD, BET surface area, SEM, and TEM. The product synthesized at room temperature by using butanediol mixed with tetrapropylorthotitanate as precursors. The mixture was aged at ambient temperature for 1-8 weeks. During these days, the fluid became progressively viscous and eventually resulted in a dry-gel. After aging the dry-gel, it was heated at 300-800°C in air. The mesoporous nanophase titanium dioxide solid was obtained by annealing this dry-gel between 380 and 480°C for 2 h. The studies indicated that the aging time for the synthesis has evidently influenced on the phase transition of titanium dioxide and nucleation process. A very fine network texture made from uniform nanoparticles were revealed by SEM and TEM analysis. The mesoporous structure as-prepared titanium dioxide was maintained after heat treatment at 350 and 400°C for 1 h, exhibiting a significant thermal stability. Four titanium dioxide phase (amorphous, anatase, anatase-rutile, rutile) were observed at different calcination temperatures.

Liqiang, et al., (2003) prepared nanoparticle TiO₂/Ti films by the sol-gel method using Ti(OBu)₄ as raw material. The samples synthesized by mixing 10 mL Ti(OBu)₄ with 40 mL anhydrous ethanol in a dry atmosphere. The mixed Ti(OBu)₄/ethanol solution was then added dropwise into anatase mixture

consisting of 10 mL water and 10 mL anhydrous ethanol and 2 mL HNO_3 at room temperature under roughly stirring to carry out hydrolysis. After continuously stirring 3 h, the yellowish transparent sol was obtained. The as-prepared samples were also characterized by TGA, DTA, XRD, TEM, SEM, XPS, DRS, PL, SPS and EFIPS testing techniques. The results indicated that 600°C might be the most appropriate calcination temperature during the preparation process of nanoparticle TiO_2/Ti film photocatalyst by considering the main factor such as the properties of titanium dioxide nanoparticles, the adhesion of nanoparticles titanium dioxide film to Ti substrate and the surface characteristics and morphology of nanoparticle TiO_2/Ti film. The O element mainly existed on the $n\text{-TiO}_2/\text{Ti}$ film as three kinds of chemical states, i.e. the crystal lattice oxygen, hydroxyl oxygen, and adsorbed oxygen. The effects of quantum size on optical property were greater than that of the Coulomb and surface polarization. Its different PL spectra could be observed using the excited wavelength of 260, 310, and 450 nm, respectively, which possibly resulting from the recombination of photoinduced electrons and holes, free or trapped excitons emission and the surface states. These provided some important information about the electronic structure and the surface states of the titanium dioxide films, which are of significance to many uses. In addition, during the experimental process of the photocatalytic degradation of phenol, the TiO_2/film calcined at 600°C exhibited higher photocatalytic activity.

Recently, there has been increasing interest in application of nanocrystalline materials for catalyst, supports, ceramics, inorganic membranes, gas sensing, water purification, and solar energy conversion (Yang, et al., 2001). A unique property of nanocrystalline particles are their

extremely high surface area; they have many more sites for achieving property enhancements, making them ideal for a wide variety of applications. In the present, the synthesis of nanocrystalline particles with controlled size and composition are of technological increasing interest. Nanocrystalline titanium dioxide has attracted much attention for application because of its large effective surface area which enhances the surface reactions. It also has novel electronic optical and catalytic properties originating from the quantum confinement (Koshizaki, et al., 2002). Furthermore, photocatalysis of nanocrystalline titanium dioxide has a great many advantage on waste water treatment such as high catalysis efficiency, energy saving, no pollution, etc. and can degrade all kinds of organic pollutants from water effectively. All of those merits make photocatalysis of water treatment and it is supposed to be used widely in the future (Baolong, et al., 2003). Because of each application that is based on nanocrystalline titanium dioxide required a specific crystal structure, particle size and also surface area, thus, it is important to develop synthetic methods in which the properties of the particles could be controlled. There are many reports involved the preparation of nanocrystalline titanium dioxide as follows.

Aruna, et al., (2000) synthesized nanosized rutile titanium dioxide particles by hydrothermal method. The synthesis involved was by adding an aliquot 5 mL of titanium isopropoxide and 5 mL of dry isopropanol dropwise to a well-stirred 40 mL solution of 0.5 HNO₃. The solution was stirred for 8 h whereupon the isopropanol was evaporated by heating the solution to 82°C. The resulting solution was transferred into a Teflon container and placed in a titanium autoclave. The solution was stirred throughout the autoclaving period

using a homemade magnet-based system. The autoclaving process was carried out at 250°C for 26 h with a heating rate of 15°C.min⁻¹. Each synthesis was carried out twice, with and without stirring. The long aging experiments during the titanium dioxide synthesis involved the steps similar to above preparation but the pH of the solution was 0.5 in one case and 2.0 in the other and then the solutions were aged at room temperature for 6 months. As-prepared powders determined by XRD, TEM and BET surface area. The results indicated that nanosize rutile titanium dioxide particles had a diameter of 20 nm and large surface area about 45 m²/g with almost spherical shape and also relatively stable at high temperature. The significant effect of the stirring and long aging control experiments suggested that, at this composition, most of the condensation to titanium dioxide occurred during the autoclaving step. The large colloid size distribution and the formation of anatase structure in the absence of stirring were attributed to the inhomogeneity developed in the solution under the extreme conditions of the hydrothermal process.

Wu, et al., (2000) synthesized titanium dioxide nanoparticles capped with stearate anions by sol-gel methods. Their work dealt with the formation mechanism and the structure of organo-capped nanoparticles. The product prepared by the reaction of titanium tetrachloride diluted with acetone to control the reaction easily and stearic acid solution under vigorous stirring. With continuous vigorous stirring for 6 h, the solvent was removed by a rotary evaporator. The gel was then thoroughly rinsed with warm ethanol. Finally, a pale yellow powder was obtained, which can be dispersed stability in an organic solvent such as acetone, tetrahydrofuran or hydrocarbon. The

products were characterized by infrared spectroscopy, X-ray photoelectron spectroscopy, XRD, and TEM. The results showed that the stearate-capped titanium dioxide nanoparticles were obtained by controlling the hydrolysis of titanium tetrachloride. Both IR and XPS results confirmed the presence of an organic layer on the particle surfaces. It also could be inferred that the organic layer links the inorganic nuclei by chemical bonds. The XRD patterns indicated that as-prepared products were poorly crystallized. The mechanism of the formation of organo-capped titanium dioxide nanoparticles were polymerization process and inhibition process.

Zhang et al., (2000) prepared nanosized titanium dioxide powders by controlling the hydrolysis of titanium tetrachloride aqueous solution and characterized by TEM, HREM, XRD, ED and BET surface area techniques. They studied the effects of the temperature of hydrolysis and sulphate ions on crystallization and morphology of the products. The samples synthesized by dissolving TiCl_4 in distilled water in an ice-water bath. The concentration of titanium was adjusted to 3 M. This aqueous solution was then mixed with pure distilled water or $(\text{NH}_4)_2\text{SO}_4$ solution in a glass bottle and placed in a temperature-controlled bath. Temperatures were varied in the range 20 - 95°C. The mixture was stirred at high speed while the amount of TiCl_4 solution necessary for the desired $[\text{H}_2\text{O}]:[\text{Ti}]$ molar ratio was added dropwise. Maintaining at the same temperature for 1 h, the mixed solution was treated with 2.5 M diluted NH_4OH until the pH value was 7. Subsequently, the precipitated titanium hydroxide/hydrous titanium oxide ($\text{TiO}_2 \cdot n\text{H}_2\text{O}$) was separated from the solution by filtration and repeatedly washed with distilled water and dilute NH_4OH solution to make $\text{TiO}_2 \cdot n\text{H}_2\text{O}$ that was free of chloride

ions. The hydrous oxide was dried at room temperature ($\sim 30^{\circ}\text{C}$) under vacuum and ground to fine powder. The studies indicated that in the presence of sulphate ions, when titanium tetrachloride solution hydrolyzed at 70°C , the obtained powder was pure anatase and its particle size was 3.5 nm, which was finer than that of alkoxide-derived powders. Moreover, its anatase-rutile transformation was retarded. However, at the same temperature, in the absence of sulphate ions the synthetic powder was a mixture of the anatase and rutile, and the particle size in the rutile phase was 4.3 nm. The results of UV-VIS showed that the presence of sulphate ions accelerated the growth of titanium dioxide clusters to anatase.

Zhang, et al., (2000) synthesized nanosized titanium dioxide powders by titanium tetrachloride hydrolysis and studied the photoactivity of these products in the photocatalytic degradation of phenol. The resulting samples were characterized by HREM, XRD, BET and UV-VIS absorption spectrophotometer. The samples were prepared by the hydrolysis of titanium tetrachloride in distilled water and then mixed with $(\text{NH}_4)_2\text{SO}_4$ solution or distilled water to yield anatase or mixture of anatase and rutile, respectively. The mixture was stirred at the hydrolysis about 70°C for 1h and the mixed solution was then treated with 2.5 M diluted NH_4OH until the pH value was 7. For preparation of rutile phase, the titanium tetrachloride solution was diluted with 0.5 M HCl and was not treated with NH_4OH solution. Then, the mixed solution was placed into a constant temperature bath about 70°C for 15 h. Subsequently, the precipitated titanium dioxide ($\text{TiO}_2 \cdot n\text{H}_2\text{O}$) was separated from the solution by using centrifugation and repeatedly washed with distilled water to make $\text{TiO}_2 \cdot n\text{H}_2\text{O}$ that was free of chloride ions. The hydrous oxides

were dried at 110°C under vacuum and ground to fine powder. In some cases, the titanium dioxide powders were calcined at 400, 600 or 700°C for 2 h. Their studies showed that the quantum-sized catalyst particles (4 nm) in the anatase phase showed the highest selectivity for the photocatalytic degradation of phenol. HREM micrographs showed the quantum-sized catalyst was crystallized partially or many defects occurred on their crystal planes. Calcination was an effective treatment to increase the photoactivity of nanosized titanium dioxide photocatalysts resulting from the improvement of crystallinity. In all cases, the photoactivity of catalysts calcined at 400°C was higher than those catalysts calcined at 110°C. After calcination at 600°C, the photoactivities of these catalysts decrease significantly, since the larger size results in the recombination of photogenerated hole and electron at higher rate. Additionally, the mixed form of anatase and rutile phase exhibited higher photoactivity as well as effective degradation in comparison with pure anatase or rutile catalysts. The quantum-sized crystalline crystallites in the rutile phase (7.2 nm) exhibited higher photoactivity and lower selectivity for the same reaction than anatase.

It was well known that the preparation of TiO₂ crystalline in anatase and rutile structures usually affected by calcination at high temperature. Anatase structure was obtained when the temperature rose to 400°C and changed into rutile structure after 800°C. These transition temperatures could be lowered or raised depending on the preparation method, the type and amount of additives and atmosphere. These parameters significantly changed the transformation rate and activation energy and thus produced a transition temperature either higher or lower than that of pure TiO₂ (Yang et al., 1998).

Although, TiO_2 was conventionally fabricated by a sulfate or chloride process, but these two methods had their drawbacks either in purity or in controlling of the particle size and particle shape (Wang et al., 2000). For the sulfate process, the processing was very complicated and the transformation must take place at high temperature about $1,000^\circ\text{C}$ to obtain rutile structure. In the chloride process, TiO_2 powders with high purity rutile structure were obtained by reacting TiCl_4 with oxygen at high temperature than $1,400^\circ\text{C}$. So, the requirement for equipment were very harsh because of the high reaction temperature and strong corrosiveness of HCl or Cl_2 (Tang et al., 2002). It is therefore desirable to find a low temperature and less complicated route for the synthesis of anatase and rutile phases, to avoid calcination at high temperature. There were some studies showed that TiO_2 crystalline powders with various crystalline phases at low temperature could be prepared without calcination.

Seo, et al., (2001) synthesized anatase or mixture of anatase and rutile titanium dioxide crystalline by aging the NaOH -treated powder in boiling water or HCl solution. The powder could be prepared by the reaction between 0.5 M TiOCl_2 and $5\text{ M NH}_4\text{OH}$ solutions and the precipitates were vacuum-filtered and washed repeatedly using distilled water until chloride ions in the precipitates were completely removed. The filtered precipitates were treated in 5 M NaOH solution at various temperature for 24 h , resulting in titanate containing Na . The titanate was aged for 24 h in boiling water or in 0.5 M HCl solution at 60°C . Then, titanium dioxide nanocrystalline powder was synthesized after filtering and drying. To investigate the microstructures, the crystallinity of each aged powder was analyzed by means of XRD, TEM and

BET method. The results showed that the anatase and Na_2TiO_3 phase coexisted when the titanium hydroxide precipitates were reacted with 5 M NaOH solution. In the case of the boiling water treatment of the NaOH-treated powder, the broad peak of the anatase structure was found in the as-dried powder; however, heat treatment at 300°C contributed to the consumption of amorphous phase, followed by the formation of the anatase powder with good crystallinity. The surface area of the as-dried powder was $360\text{ m}^2/\text{g}$ but, after the heat treatment, it decreased to $170\text{ m}^2/\text{g}$. Titanium dioxide crystalline powder with a mixture of the anatase and rutile phase was obtained resulting from the exudation of Na in the Na_2TiO_3 by treating with HCl. The powder with a large surface area of $240\text{ m}^2/\text{g}$ consisted of spherical particles of less than 10 nm and triangular particles of 100-120 nm, and the EDS result revealed that the powder was the crystalline titanium dioxide and did not contain Na atoms.

Seo, et al., (2001) prepared titanium dioxide powder crystalline by ageing at low temperature and studied by XRD, BET surface area and TEM analysis techniques. Titanium dioxide powders were obtained from the reaction between 0.5 M TiOCl_2 and 5 M NH_4OH solutions and the precipitates were vacuum-filtered and washed repeatedly using distilled water until chloride ions in the precipitates were completely removed. The filtered precipitates were aged for 24 h. in boiling water or HCl solution of various concentration at 60°C . Then, titanium dioxide nanocrystalline powder was produced after filtering and drying. It had been found that varying aging conditions could control crystalline type and particle shape of the obtained titanium dioxide powders. The powder aged in the boiling water showed the anatase phase and was consisted of spherical particles with 20 nm in size. In

the case of the aging the powder in HCl solution, the anatase powder was obtained in 0.1 and 0.5 M HCl solution. The powder aged in 0.1 M solution was consisted of spherical particles of less than 10 nm, and spherical particles with 5-7 nm in size and small amount of triangular particles were formed in the powder aged in 0.5 M solution. However, the powder aged in 2 M solution consisted of rod-like particles of 50-70 nm and spherical ones were not found. The powder aged in those HCl solutions showed a large specific surface area of 240-250 m²/g.

Arroyo, et al., (2002) studied the effect of the distribution and content of Mn²⁺ ions on the structural properties of titanium dioxide materials. The products were characterized by XRD, BET surface area, and ESR techniques. The synthesis of doped titanium dioxide with different amounts of Mn²⁺ ions were achieved by adding, with stirring a solution of Ti[OCH(CH₃)₂]₄(TIPT) diluted with 2-propanol (TIPT : HOCH(CH₃)₂ = 1 : 2 molar ratio) to a solution of Mn(CH₃COO)₂·4H₂O in water and 2-propanol [(HOCH(CH₃)₂ : H₂O = 2 : 1 molar ratio)]. Precipitation occurred in seconds. This mixture was stirred at room temperature for 20 min. After which, 3 mole of deionized water were added, and a major precipitation occurred. The stirring was continued for another 60 min. The resultant mixture was aged for 72 h, and xerogels were obtained by heating at 80°C in a drying oven for 72 h. Later, the xerogels were divided in aliquots, which were treated at a heating rate of 2.5°C/min in a furnace at 100°C for 1 h and then, at a heating rate of 5°C/min at a selected temperature for 2 h in static air. Sample of titanium dioxide containing X mole % of Mn²⁺ ions were prepared (X values were 0, 0.1, 0.5, 1.0, 1.5, 2.0, and 2.5) and hereafter will be referred to as MTX. An impregnated sample, referred to

as IMT 1.0, means that it was prepared by adding 1 mole % of Mn^{2+} ions before the aging period. The sample was prepared by adding the manganese salt dissolved in the smallest amount of water and diluted with 10 mole of 2-propanol, and the reaction mixture stirred for 5 min more, and later, treated in the same manner as the other samples. It was found that when Mn^{2+} ions were added in low concentration up to 1.5 mole %, the Mn^{2+} ions were initially incorporated in interstitial positions in titanium dioxide, and as a consequence the anatase phase was stabilized. As the treatment temperature increase, the Mn^{2+} is oxidized to Mn^{4+} . The Mn^{4+} ions then entered substitutional position. When the Mn^{2+} concentration was 2 mole % and larger, the samples behave in a similar way as favor the nucleation of rutile in the surface and spread out their growth into titanium dioxide particles, lowering the anatase-rutile transformation temperature.

Tany, et al., (2002) studied the preparation of rutile titanium dioxide at low temperature from the reaction of $Ti(OC_4H_9)_4$ and 2.5 mole/L NH_4OH or HNO_3 solution with stirring to get transparent solution which was hydrolyzed at 40-50°C in water bath. For the basic and neutral solution, the hydrolysis product was a precipitate which was then washed, filtered, dried at 40-50°C in dry oven and finally calcined. For the acidic solution, the hydrolysis products were two layers of solution, the upper layer was organic from the hydrolysis, and the lower layer was a transparent solution. The sol was separated from the organic and was heated at 40-50°C in dry oven to get dry powder and the powder was finally calcined at different temperatures. The products were investigated by XRD, TGA, DTA and TEM. Their work suggested that the products of the hydrolysis of $Ti(OC_4H_9)_4$ solution were

different when the acidity of the solution was different. When the solution was basic or neutral, the dried gel was amorphous and rutile could not be obtained by calcining the dried gel at low temperature. By controlling the acidity and the ratio of water to $\text{Ti}(\text{OC}_4\text{H}_9)_4$ in the $\text{Ti}(\text{OC}_4\text{H}_9)_4$ solution, rutile could be obtained at about 40-50°C. The ratio of water to HNO_3 and the ratio of water to $\text{Ti}(\text{OC}_4\text{H}_9)_4$ were very important. When the ratio of water to $\text{Ti}(\text{OC}_4\text{H}_9)_4$ was increased, the ratio of HNO_3 to $\text{Ti}(\text{OC}_4\text{H}_9)_4$ should also be increased in order to get rutile titanium dioxide at low temperature.

Yang, et al., (2002) prepared titanium dioxide in rutile phase by liquid method at room temperature and characterized by XRD and TEM techniques. The powders were synthesized by adding 2 M NH_4OH or NaOH solution into $\text{Ti}(\text{SO}_4)_2$ solution while stirring at room temperature. Gelatinous white precipitates were formed instantly. The pH value of the liquor mixture was controlled to be 7-8 at the end of the precipitation reaction. The resulting precipitates were separated from the mother liquor by centrifugation and washed with distilled water to remove sulphate ions. Then, the precipitates were re-dispersed in an aqueous solution of HNO_3 at a constant temperature for peptization and after a certain time the mixture became clear and transparent indicating the formation of a sol. This sol was aged at room temperature to give crystalline precipitates and then washed using distilled water and dried in a vacuum oven at 60°C for 12 h to obtain the final white powders. Their results indicated that the preparation process of rutile titanium dioxide at room temperature by liquid method could be divided into two stages: precipitation reaction and peptization process. The main factor that influenced the structure of the resulted crystals was the peptizing temperature.

Rutile was formed at lower temperatures, with an increasing temperature to form anatase when progressively increased the temperature. The mechanism of the formation of rutile by crystallization in liquid phase could be confirmed by "growth unit" theory. In addition, temperature and molar ratio of the reactions of precipitation reaction and the content of sulphate in the system also had effect on the phase and crystal size of the product.

1.3 Objectives

- 1.3.1 To prepare titanium dioxide in anatase or rutile crystalline structure by sol-gel method from the hydrolysis and condensation reaction of titanium tetrachloride at low temperature and without calcination.
- 1.3.2 To study the difference in some properties of synthesized titanium dioxide and commercial titanium dioxide and also titanium dioxide prepared by other methods.

2. Methods of study

2.1 Materials

- 2.1.1 Ammonium hydroxide (Ammonia solution) 28.0 - 30.0%, NH_4OH , A.R., code no. 9721-03, J.T. Baker.
- 2.1.2 Silver nitrate, AgNO_3 , A.R., code no. 102333J, BDH, England.
- 2.1.3 Sodium hydroxide, NaOH , A.R., code no. 102525P, BDH, England.
- 2.1.4 Titanium tetrachloride, TiCl_4 , A.R., code no. VN1838, Merck.
- 2.1.5 Titanium dioxide (Anatase), TiO_2 , A.R., code no. 488257, Carlo Erba.
- 2.1.6 Titanium dioxide P25, code no. D-60287, Degussa AG, Frankfurt, Germany.
- 2.1.7 Hydrochloric acid, HCl , A.R., code no. 9535-03, J.T Baker.
- 2.1.8 Universal indicator , full range pH 1 – 14, Whatman, England.

2.2 Instruments

2.2.1 Chemistry Department, PSU

- 1. Fourier-transformed infrared spectrophotometer, FT-IR, EQUINOX55, Bruker, Germany.
- 2. Magnetic stirrer, Jenway 1000, JENWAY, UK.
- 3. Oven, National, Heinicke Company, U.S.A.
- 3. pHep-pH electronic paper, Hanna Instruments,
- 4. Ultraviolet-visible spectrophotometer, UV-VIS, UV-2401, Shimadzu, Japan.

2.2.2 Scientific Equipment Center, PSU

1. Differential thermal analyzer, DTA, DTA7, Perkin Elmer.
2. Scanning electron microscope, SEM, JEOL JSM-5800LV.
3. Thermogravimetric analyzer, TGA, TGA7, Perkin Elmer.
4. Transmission electron microscope, TEM, JEOL JEM-2010

2.2.3 Central Equipment Unit, Faculty of Science, PSU

1. X-ray diffractometer, XRD, PW 3710 mpd control,
Ni-filtered Cu K α radiation, Philips.

2.2.4 Chemical Engineering Department, PSU

1. Surface area / pore size study, SA 3100, Coulter, U.S.A.

2.3 Methods

In this work, rutile and the mixture of anatase and rutile titanium dioxide crystalline powders were prepared by sol-gel method at low temperature without calcination at high temperature. The products were then characterized by various techniques such as XRD, BET, FT-IR, TGA, DTA, SEM, TEM and UV-VIS.

2.3.1 Synthesis of titanium dioxide

2.3.1.1 Synthesis of rutile phase.

Titanium tetrachloride (TiCl_4) was used without any further purification. Titanium tetrachloride solution was prepared by dissolving 20 mL of TiCl_4 in 100 mL cold-distilled water. This solution was then mixed with 2 mL conc.HCl which used as hydrolysis catalyst in a 3-necked round bottom flask and placed at 95°C in a temperature-controlled bath under vigorous stirring to carry out hydrolysis and condensation reaction. Maintaining at the same temperature for 13 h, the mixed solution was slowly treated with conc. NH_3 solution until the pH value was 7. The reaction was maintained for a period of 13 h with continuous stirring. The experimental procedure was schematically shown in Figure 5. Through the hydrolysis and condensation reactions, the sol-gel transition took place gradually. Subsequently, the powders were separated from the solution by using vacuum-filtered and washed repeatedly using distilled water until free of chloride ions and ammonium ions (by AgNO_3 and NaOH solution tests, respectively). The powders were then dried at 105°C for 24 h and ground to fine powder and denoted as RU.

2.3.1.2 Synthesis of mixed anatase and rutile phase.

TiO_2 in the mixed phase of anatase and rutile could be prepared by the same method as given by section 2.3.1.1 but 200 mL of cold-distilled water was used for preparing TiCl_4 solution. This solution was then maintained at room temperature

for overnight until it transformed to homogeneous solution. The experimental procedure was also schematically shown in Figure 5.

2.3.2 Characterization of titanium dioxide

2.3.2.1 X-ray powder diffraction patterns (XRD)

The XRD was used for crystal phase identification and also estimated the crystallite size of each phase present. The XRD intensities of the anatase (101) peak at $2\theta = 25.5^\circ$ and the rutile (110) peak at 27.5° were analyzed. The spectra were obtained through the Equipment Division of the Faculty of Science, Prince of Songkla University, Hat Yai, Songkla using an X-ray diffractometer, PW 3710 mpd control, Ni-filtered Cu $K\alpha$ radiation, Philips.

2.3.2.2. Surface area / pore size

The specific surface area and pore size were measured by the BET method (Coulter, model SA3100, U.S.A). All data were acquired by the Department of Chemical Engineering, Faculty of Engineering, Prince of Songkla University, Hat Yai, Songkla.

2.3.2.3 Fourier-transformed infrared spectrophotometer

(FT-IR)

The functional groups were checked by FT-IR in diffused reflectance mode at $4000-400\text{ cm}^{-1}$ with KBr as blank (EQUINOX 55, BRUKER, Germany).

2.3.2.4 Thermogravimetric analysis (TGA)

Mass change with temperature was studied in the range 50-1,300°C under nitrogen atmosphere with heating rate of 10 °C per minute (TGA7, Perkin Elmer, U.S.A). All data were acquired by the Scientific Equipment Center, Prince of Songkla University, Hat Yai, Songkla.

2.3.2.5 Differential thermal analysis (DTA)

The change of phase with temperature was studied in the temperature range of 50-1,300°C under nitrogen atmosphere with heating rate of 10 °C per minute (DT7, Perkin Elmer, Singapore). All data were acquired by the Scientific Equipment Center, Prince of Songkla University, Hat Yai ; Songkla.

2.3.2.6 Scanning electron microscope (SEM)

The texture, topography, and surface features of powders were studied by SEM (SEM: JEOL JSM-5800LV) using high vacuum mode with secondary electron image conditions and electron micrograph technique. All data were acquired by the Scientific Equipment Center, Prince of Songkla University, Hat Yai , Songkla

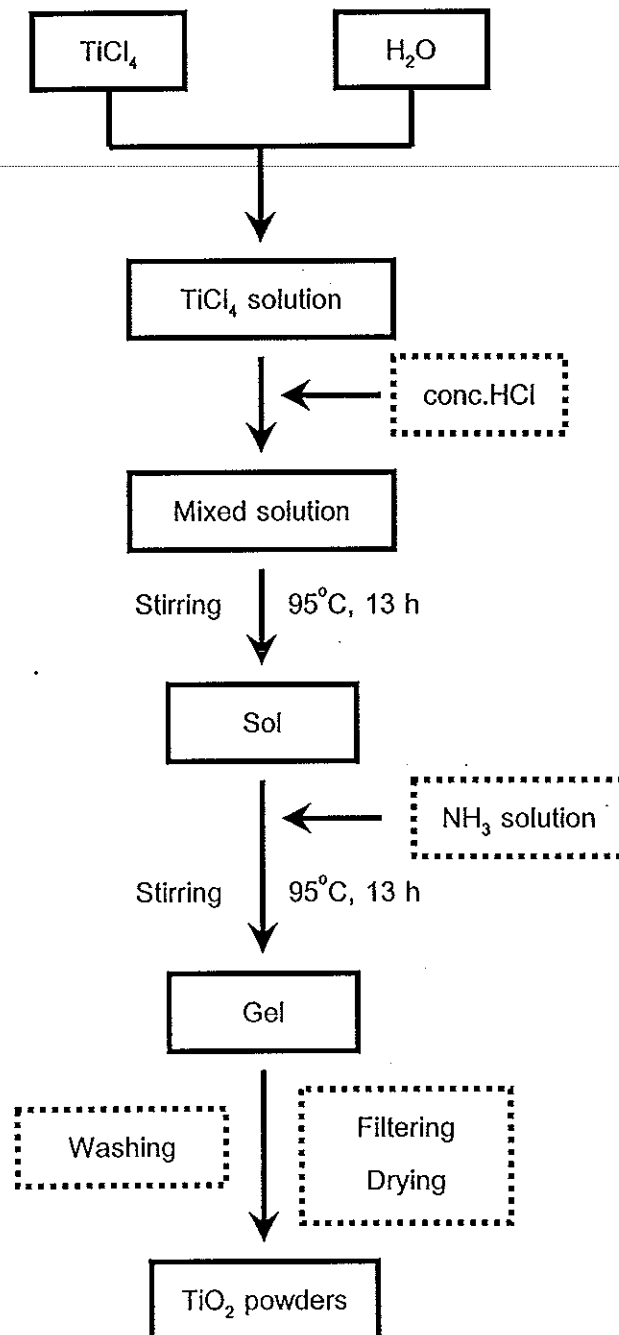


Figure 5 Flow chart of the preparation of TiO_2 powders by sol-gel method

2.3.2.7 Transmission electron microscope (TEM)

The morphology of materials on an atomic scale with resolution larger than 2 Å was achieved by TEM (TEM: JEOL JEM 2010,) using high voltage condition about 200 kV and electron micrograph technique. All data were acquired by the Scientific Equipment Center, Prince of Songkla University, Hat Yai , Songkla.

2.3.2.8 Ultraviolet-visible spectrophotometry (UV-VIS)

UV diffused reflectance studies were performed on a UV absorption spectrophotometer at the scan range 240-800 nm (UV-2401,) with a 2.0 nm slit width and BaSO₄ as reference to establish the absorption edge, band gap energy, and the type of band-to-band transition of titanium dioxide.

3. Results

3.1 Synthesis and characterization of titanium dioxide

3.1.1 Synthesis of titanium dioxide

In this study, two sets of titanium dioxide powders were prepared by sol-gel method with varying amount of water for preparing TiCl_4 aqueous solution. One set was prepared by using 100 mL distilled water (denoted as RU) while the other using 200 mL distilled water (denoted as AR). In sol-gel synthesis of titanium dioxide, the reaction consisted of hydrolysis and condensation reactions of titanium tetrachloride aqueous solution. Titanium tetrachloride was first diluted in cold-distilled water to reduce the high heat of exothermic reaction. The hydrolysis and condensation reaction started immediately upon heating the titanium tetrachloride solution at 95°C as indicated by the rapid increase in turbidity and the formation of flocs which precipitated at the bottom of the reaction vessel. The product is shown in

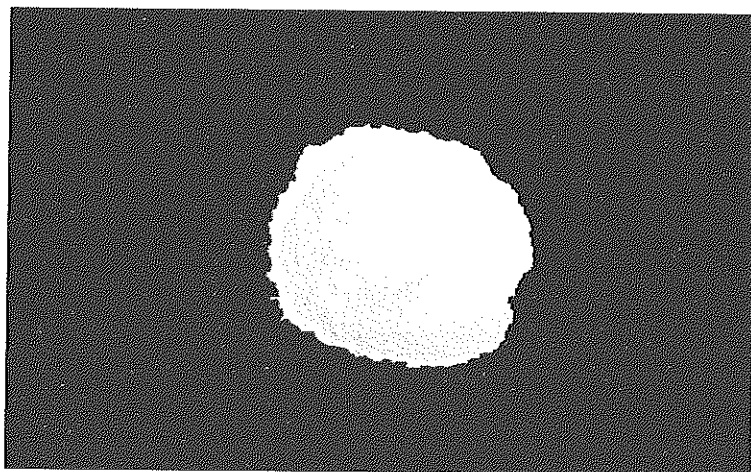


Figure 6 Synthesized TiO_2 .

Figure 6. In this work, hydrochloric acid was used as hydrolysis catalyst which added to the solution in order to monitor the hydrolysis reaction of titanium tetrachloride in water.

3.1.2 Characterization of titanium dioxide

3.1.2.1 X-ray powder diffraction patterns (XRD)

The x-ray powder diffraction method is usually used for the crystal identification and estimation of the crystallite sizes of each phase present. The identification of a species from its powder diffraction pattern is based upon the position of the lines (in terms of 2θ) and their relative intensities (Skoog and Leary, 1992). The XRD pattern at $2\theta = 25.50$ (101) and 48.0° in the spectrum of titanium dioxide are easily identified as the crystal of anatase form whereas the peaks at $2\theta = 27.50$ (110) and 54.5° arise from the crystal of rutile form (Yoshio, et al., 1998). The XRD intensities of both anatase (101) and rutile (110) peaks were analyzed.

The content of anatase or rutile phase in the samples could be determined using the standard addition method by mixing the commercial anatase (Carlo Erba) or rutile (TOA) titanium dioxide with the original titanium dioxide samples in different percent weight; 0, 10, 20, 40 and 60 % and then measured the total peak area. A calibration curve was made by plotting the total XRD-peak-area against the concentration of the added standard. The original concentration of analyte was obtained by the interception point on the concentration axis (Ingle, et al., 1988 : 178-180).

The average particle size can also be determined from the broadening of corresponding x-ray spectra peaks by the Scherrer formula:

$$D_{hkl} = \frac{k\lambda}{\beta_{hkl} \cos \theta} \quad (1)$$

where D_{hkl} is the average particle size, λ the wavelength of the x-ray radiation ($\text{CuK}\alpha = 0.154056 \text{ nm}$), k is usually taken as 0.9, β_{hkl} the line width at the half-maximum height, and θ the diffraction angles (Reddy, et al., 2001).

The x-ray pattern of titanium dioxide denoted as RU in Figure 7a shows diffraction peaks at (2θ) 27.5, 36.1, 41.3, 43.9, 54.3, 56.6, 62.9, and 70.0 which correspond to 110, 101, 111, 210, 211, 220, 002 and 310 reflections of rutile (Park, et al., 1999). In Figure 7b shows XRD pattern of titanium dioxide denoted as AR which has diffraction peaks at (2θ) 25.5, 27.5, 36.2, 37.9, 41.3, 54.3, 56.4 and 62.9 corresponding to 110, 110, 101, 004, 111, 105, 211 and 002 reflections of anatase and rutile (Park, et al., 1999). Figure 7c shows XRD pattern of Degussa P25 at (2θ) 25.4, 38, 48, 53, and 55 that correspond to 101, 004, 200, 105, and 211 reflections of anatase and (2θ) at 27.5, 36, 41, and 56 that correspond to 110, 101, 111, and 220 reflections of rutile (Park, et al., 1999). Figure 7d shows XRD pattern of TiO_2 (anatase), the commercial product from Carlo Erba, at (2θ) 25.4, 38, 48, 53, and 55 that correspond to 101, 004, 200, 105, and 211 reflections of anatase (Park, et al., 1999). XRD pattern of TiO_2 (rutile : TOA Co, Thailand) in Figure 7e shows peaks at (2θ) 27.5, 36, 41, and 56 that correspond to 110, 101, 111, and 220 reflections of rutile (Park, et al., 1999).

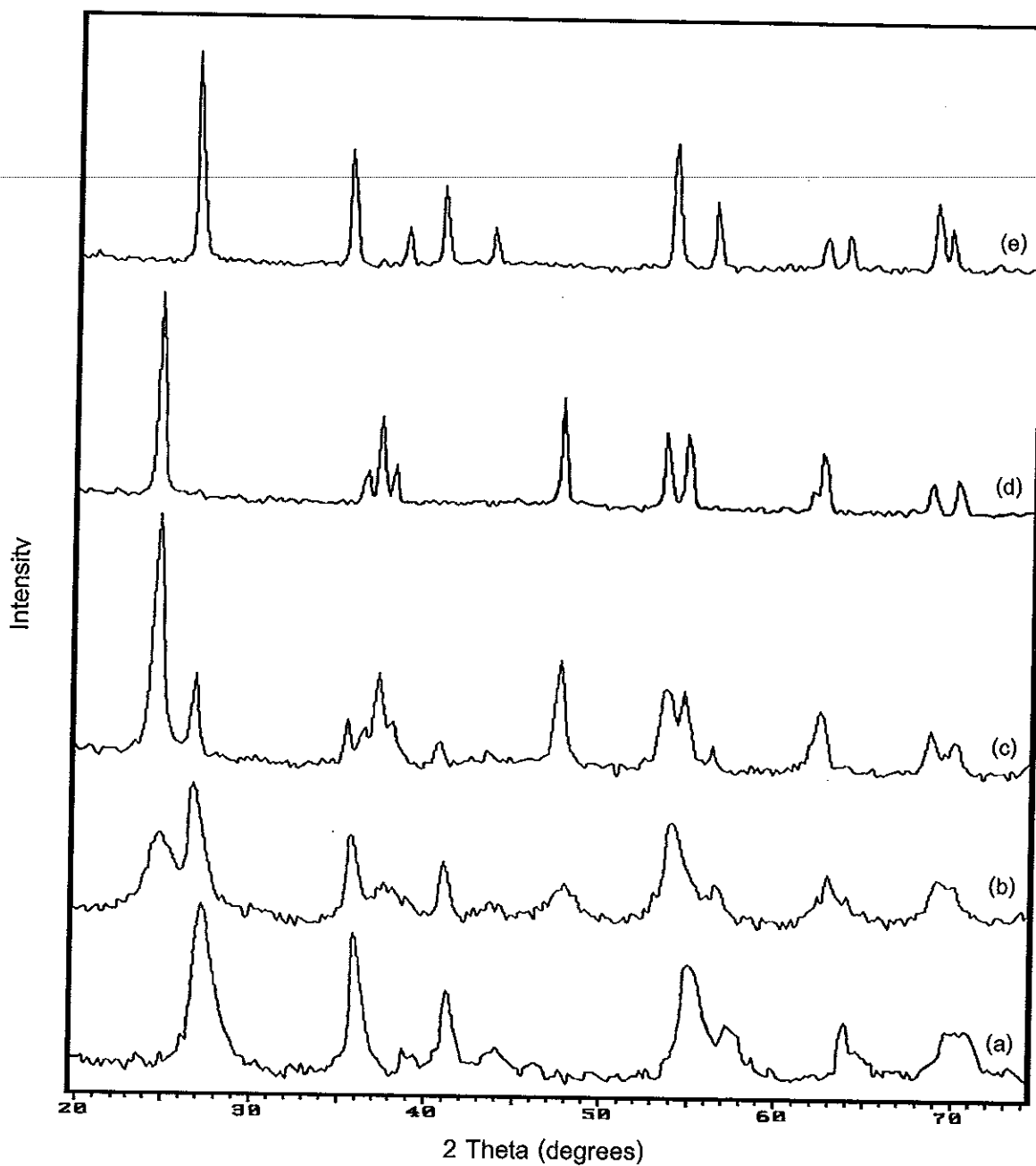


Figure 7 XRD patterns of the TiO₂. (a) RU TiO₂ (b) AR TiO₂ (c) P25:Degussa (d) anatase : Carlo Erba and (e) rutile : TOA Co, Thailand.

The content of rutile crystalline in the synthetic titanium dioxide samples calculated from the standard addition method which is shown in Table 4 and Figure 7 indicates that, in the case of RU sample, only rutile with

30 % by weight is obtained. For AR sample, it is a mixture consisting of rutile 30 % by weight and 15 % anatase by weight .

Table 4 Percent weight and peak area of rutile at $2\theta = 27.5$ of RU and AR TiO_2 .

Percent weight of rutile	Sample weight (g)		Peak area at $2\theta = 27.5$	
	Rutile (TOA)	TiO_2 sample	RU	AR
0	0	1.301	590.50	500.55
10	0.130	1.170	800.25	670.68
20	0.260	1.040	980.45	860.01
40	0.520	0.780	1360.35	1220.64
60	0.780	0.520	1700.45	1550.23

Table 5 Percent weight and peak area of anatase at $2\theta = 25.5$ of AR TiO_2 .

Percent weight of anatase	Sample weight (g)		Peak area at $2\theta = 25.5$
	Anatase (Carlo Erba)	TiO_2 sample	AR
0	0	1.301	203.28
10	0.146	1.167	581.20
20	0.263	1.049	639.17
40	0.538	0.786	919.95
60	0.797	0.541	1307.88

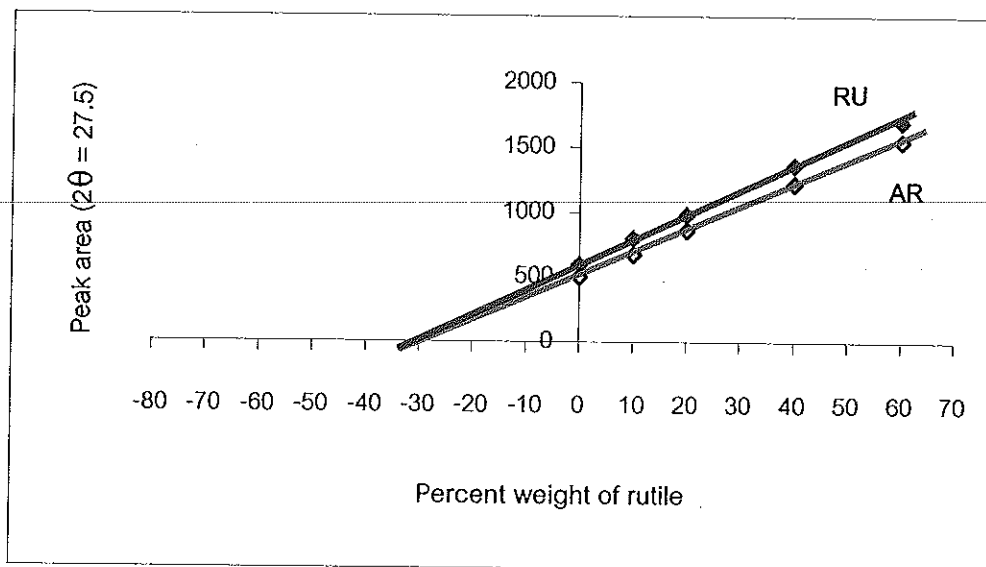


Figure 8 Standard addition calibration curve of synthetic rutile.

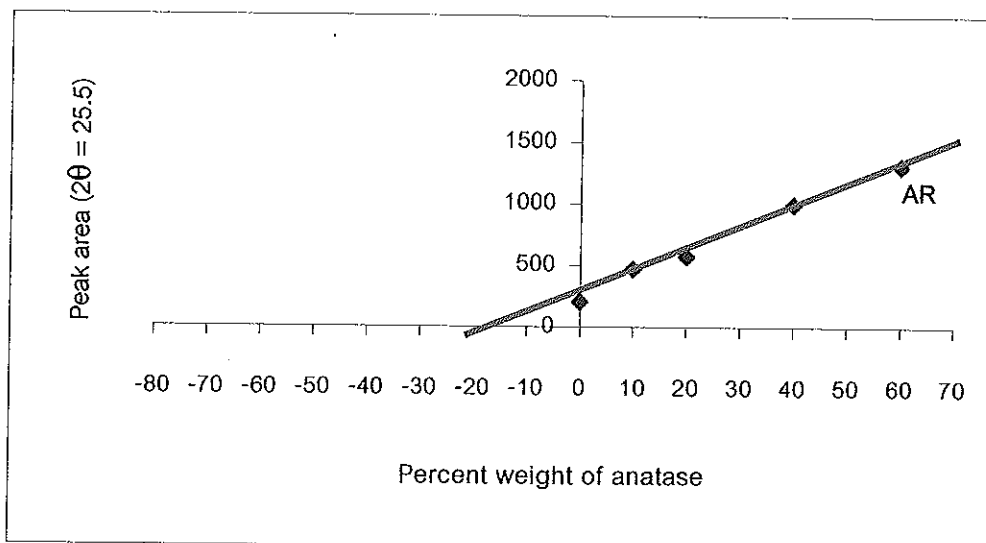


Figure 9 Standard addition calibration curve of synthetic anatase.

The particle size of the sample was estimated by the Scherer formula and is shown in Table 6. This method is generally the accepted methods to estimate the mean crystallite size. The crystalline size is found to be in nanometer region for the sample RU and AR. The data were compared between synthetic titanium dioxide and commercial products.

Table 6 Particle size of TiO₂

Titanium dioxide samples	Particle size (nm)	
	anatase	rutile
TiO ₂ (RU)	-	9.0 ^a
TiO ₂ (AR)	5.2 ^a	7.8 ^a
Anatase (Carlo Erba)	30.0 ^a	-
Rutile (TOA)	-	32.0 ^a
P25 (Degussa)	24.5 ^a	11.8 ^a

^a Data were determined by the Scherer formula.

3.1.2.2 Surface area and pore size.

The surface area is an average measurement of the external surface of a large number of particles and expressed in term of the area per unit mass (m²/g). There are two main analysis techniques for measuring surface area; gas adsorption and gas permeability. In this work gas adsorption surface area analysis was used.

The gas adsorption approach starts with a clean surface achieved through vacuum or inert gas bake-out. The clean powder surface is

exposed to varying partial pressures of known adsorbing vapors. A measurement is made of the amount of gas adsorbed on the powder surface versus the partial pressure. The measurement is often referred to as the BET specific surface area after Brunauer, Emmett and Teller who developed the concept in 1938.

Under equilibrium, the rate of adsorption equals the rate of evaporation. Letting P equals the partial pressure of adsorbate, P_0 equals the saturation pressure of adsorbate (which depends on the gas and temperature), X equals the amount of gas adsorbed at a pressure P , X_m equals the monolayer capacity of the powder (the amount of gas necessary to form a uniform surface coating one atomic layer thick), and C equal a constant relating to the adsorption enthalpy, gives

$$\frac{P}{X(P_0 - P)} = \frac{1}{X_m C} + \frac{C-1}{X_m C} \frac{P}{P_0} \quad (2)$$

Note that the term on the left of equal sign is linear to the partial pressure ratio P/P_0 . This is the BET equation, and is generally valid for powders in the range P/P_0 from 0.05 to 0.30. Equation (2) can be rewritten in a general form as,

$$\frac{P}{X(P_0 - P)} = B + A \frac{P}{P_0} \quad (3)$$

$$X_m = \frac{1}{A + B} \quad (4)$$

where

giving A as the slope and B as the intercept of the linear equation. Finally, the surface area is calculated as

$$S = \frac{X_m N_0 A_0}{WM} \quad (5)$$

using M as the molecular weight of adsorbate, A_0 as the average occupational areas of an adsorbate molecule, N_0 as Avogadro's number, and w as the sample weight (German, 1984).

Surface area and porosity of titanium dioxide are shown in Table 7 and Table 8, respectively. The data were compared between synthesized titanium dioxide and commercial product. Moreover, the porosity study of synthesized samples are shown in Figures 10-15.

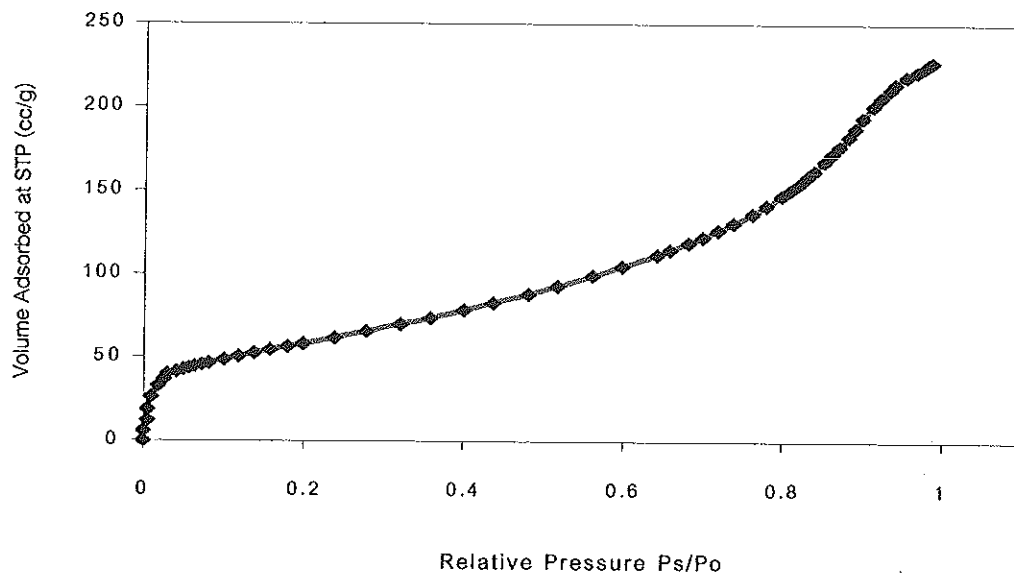
Table 7 Surface area of titanium dioxide.

Titanium dioxide samples	Surface area ^a (m ² /g)
TiO ₂ (RU)	101.36
TiO ₂ (AR)	218.38
Anatase (Carlo Erba)	9.65
Rutile (TOA)	13.08
P25 (Degussa)	51.41

^a Data were determined by using SA3100, Coulter.

Table 8 Porosity of titanium dioxide.

sample	Pore volume (%) for pore diameter :								Porosity (ml/g)
	<6	6-8	8-10	10-12	12-16	16-20	20-80	>80(nm)	
TiO ₂ (RU)	5	10	5	6	7	7	32	28	0.029
TiO ₂ (AR)	23	12	7	9	12	13	21	3	0.291
Anatase (Carlo Erba)	2	1	1	1	1	1	15	78	0.019
Rutile (TOA)	7	5	4	4	6	6	34	34	0.049
P25 (Degussa)	5	3	2	2	3	4	38	43	0.235

Figure 10 Nitrogen adsorption isotherm of RU TiO₂.

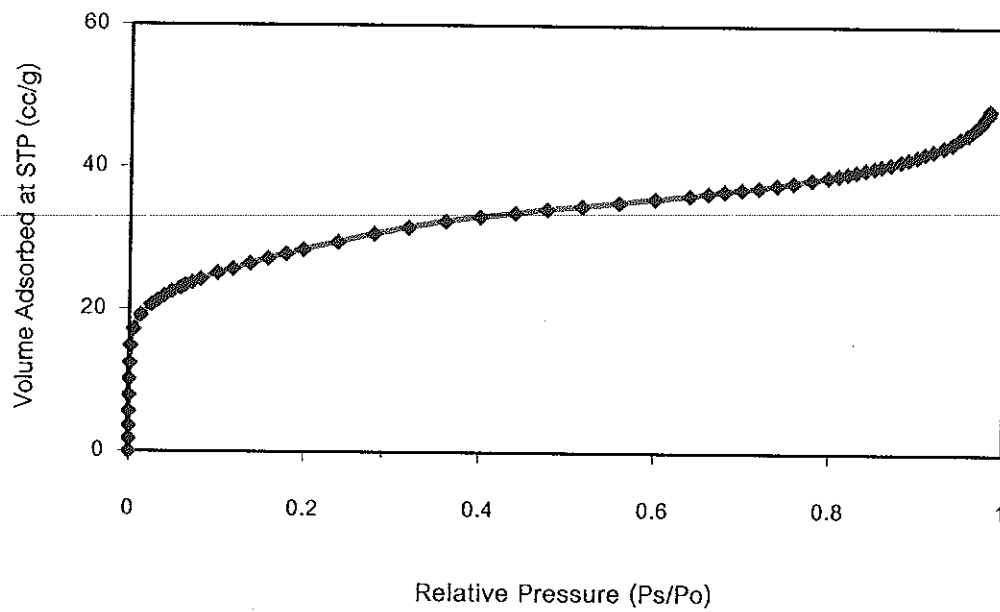


Figure 11 Nitrogen adsorption isotherm of AR TiO₂.

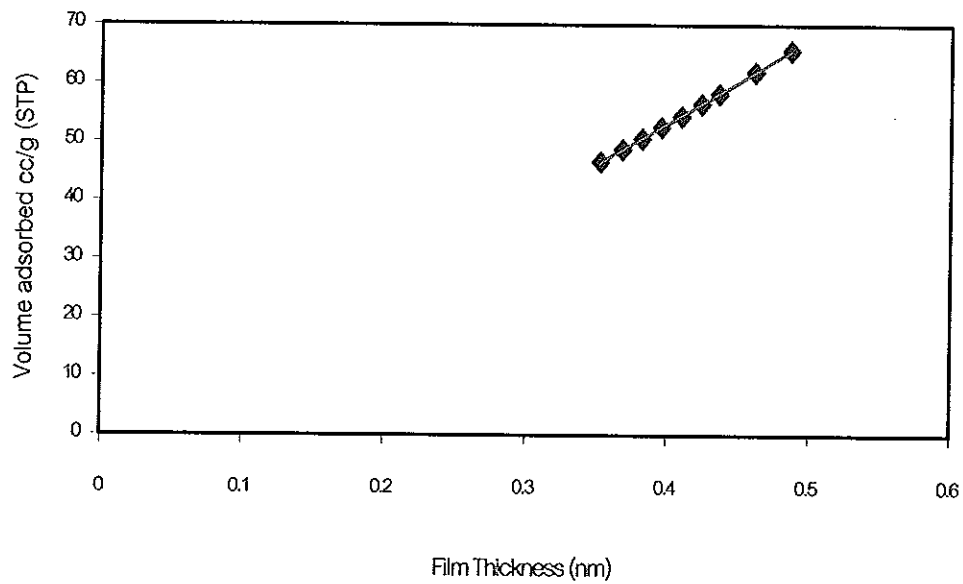


Figure 12 *t*-plot of Nitrogen adsorption isotherm of RU TiO₂.

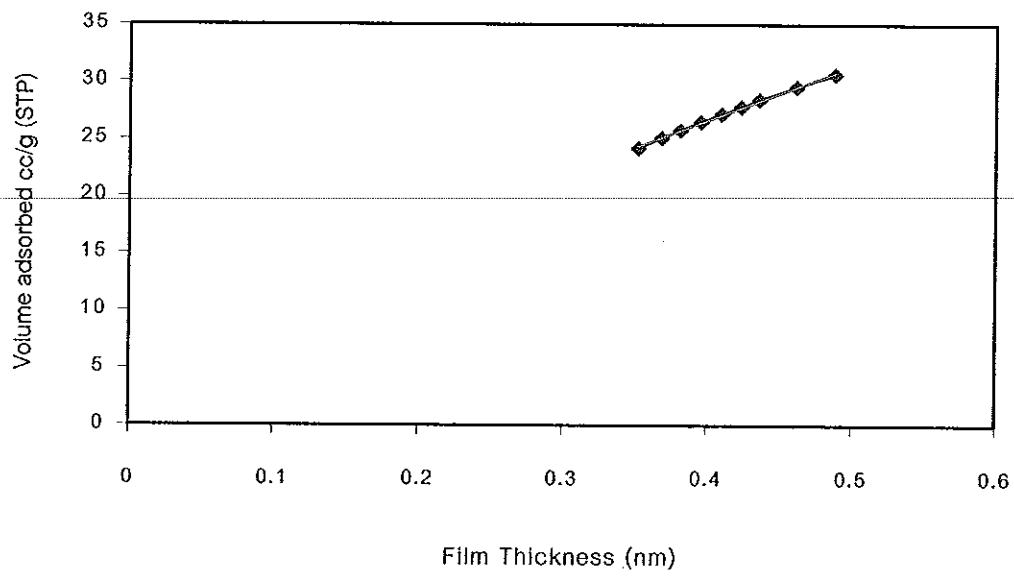


Figure 13 Nitrogen adsorption isotherm of AR TiO₂.

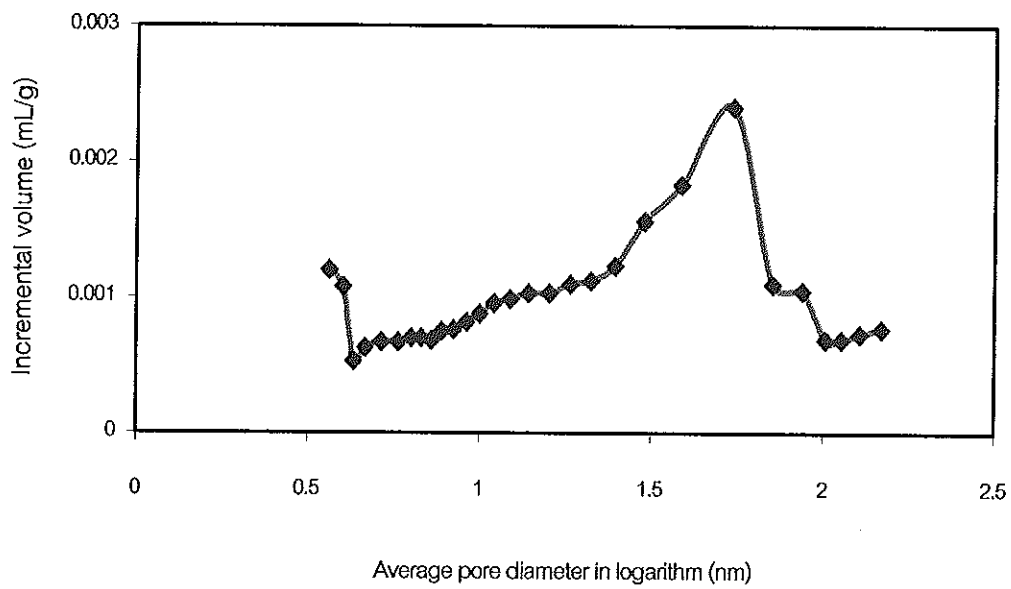


Figure 14 Pore size distribution curve of RU TiO₂

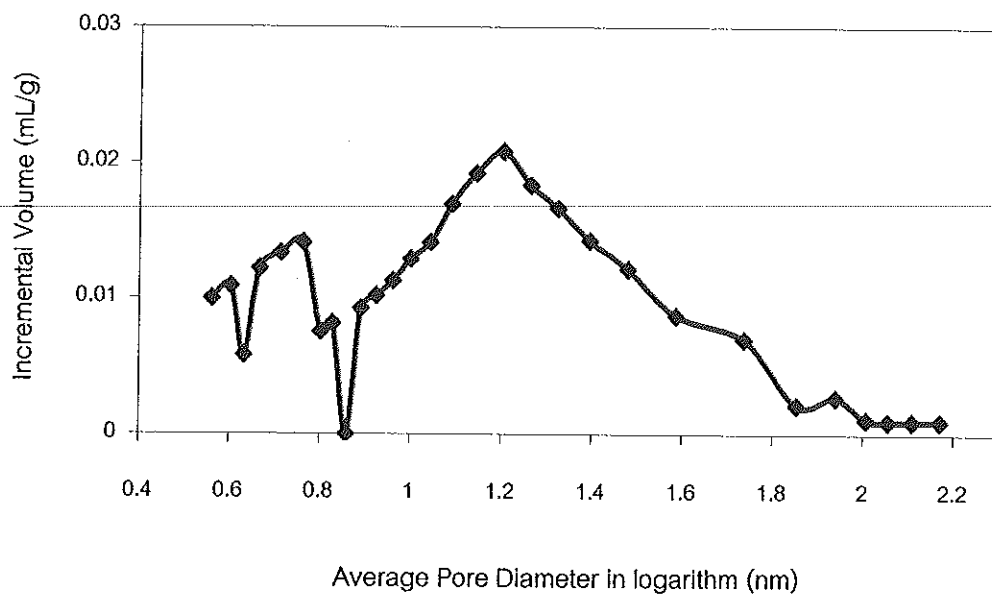


Figure 15 Pore size distribution curve of AR TiO₂.

3.1.2.3 Fourier-transformed infrared spectroscopy (FT-IR)

Infrared spectroscopy is a technique for determining the functional groups within the compounds. The spectrum range of greatest use is in the mid-infrared region, which covers the frequency from 400 to 4000 cm⁻¹. In Figure 16 and 17 show the FT-IR spectrum of titanium dioxide (RU and AR) and Table 9 lists the assigned modes of the functional groups that are responsible for the vibration bands in Figure 16 and 17.

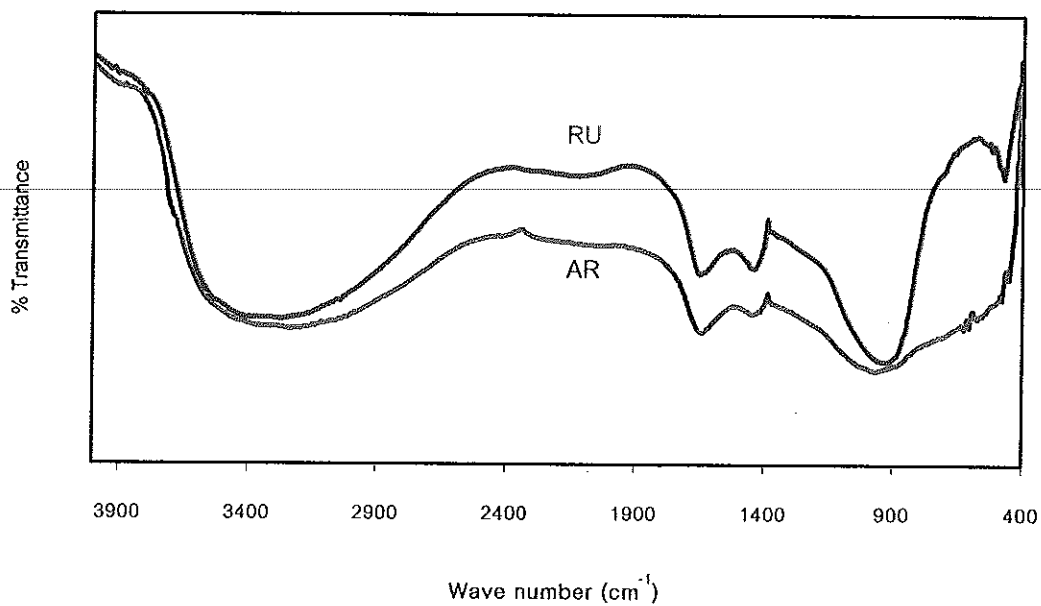


Figure 16 FT-IR spectrum (reflectance mode) of TiO₂ in the range 4000-400 cm⁻¹.

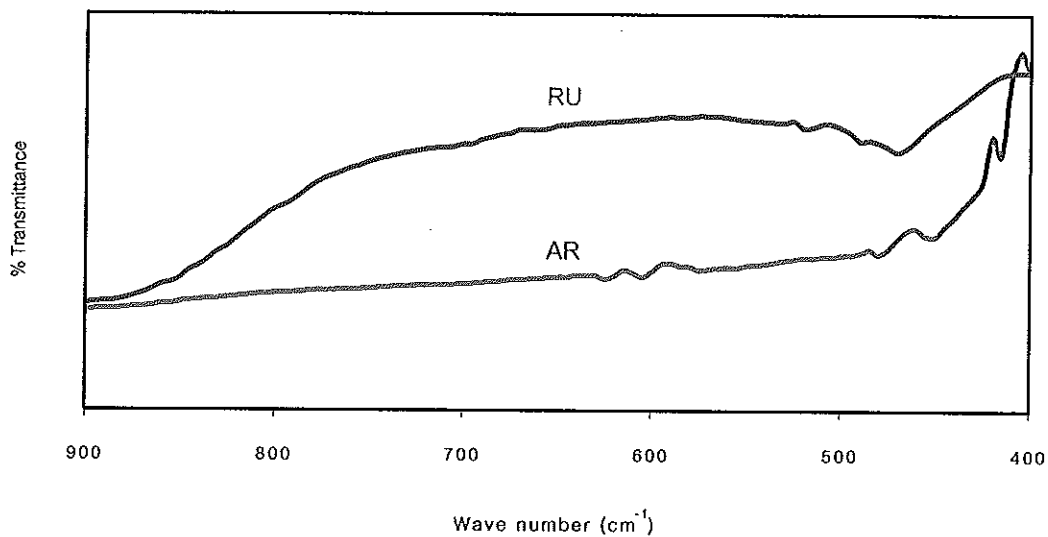


Figure 17 FT-IR spectrum (reflectance mode) of TiO₂ in the range 900-400 cm⁻¹.

Table 9 Assignment of the FT-IR bands of RU TiO₂ (from Figures 16 and 17).

Wave number (cm ⁻¹)	Assignment	Functional groups / molecule	References
3,500-3,000	-OH and -NH stretching	H ₂ O and NH ₄ ⁺	Wang et al., 2000
1,642	O-H bending	OH groups	Velasco et al., 1999
1,431	N-H bending	NH ₄ ⁺ (composite)	Sanobez et al., 1999
930	OH out of plane	H ₂ O or OH groups	Sanobez et al., 1999
470	Ti-O stretching	TiO ₂ (rutile)	Zhang et al., 2001

Table 10 Assignment of the FT-IR bands of AR TiO₂ (from Figures 16 and 17).

Wave number (cm ⁻¹)	Assignment	Functional groups / molecule	References
3,500-3,000	-OH and -NH stretching	H ₂ O and NH ₄ ⁺	Wang et al., 2000
1,642	O-H bending	OH groups	Velasco et al., 1999
1,431	N-H bending	NH ₄ ⁺ (composite)	Sanobez et al., 1999
930	OH out of plane	H ₂ O or OH groups	Sanobez et al., 1999
624	Ti-O stretching	TiO ₂ (anatase)	Zhang et al., 2001
468	Ti-O stretching	TiO ₂ (rutile)	Zhang et al., 2001
414	Ti-O stretching	TiO ₂ (anatase and rutile)	Zhang et al., 2001

3.1.2.4 Thermogravimetric analysis (TGA)

Thermogravimetric analysis provides the analyst with a quantitative measurement of any weight change associated with a transition. It can directly record the loss in weight with time or temperature due to dehydration or decomposition (Willard, et al., 1974). The TG curve of synthesized titanium dioxide is shown in Figure 18 where the different pattern of decomposition with a total weight loss of 5 and 12 % for RU and AR sample, respectively, can be seen. The RU sample shows two stages during the weight loss process. One was that the weight loss is about 5% in the temperature range from the room temperature to 700°C; the next stage shows no significant weight loss after 700°C. The three stages of weight loss could be found in AR sample. The first stage of weight loss is about 8 % in the range from room temperature to 745°C; the second stage was about 1 % in the range 745-1,045°C and the last stage from 1,045-1,348°C shows the weight loss about 3 %.

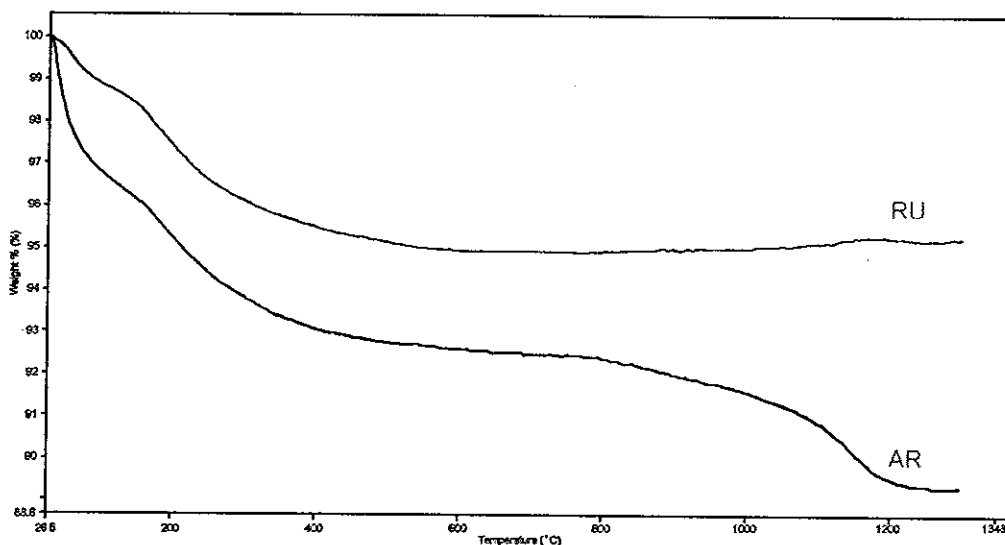


Figure 18 TGA curve of synthesized TiO_2 .

3.1.2.5 Differential thermal analysis (DTA)

Differential thermal analysis is a thermal technique in order to determine the temperatures of possible decomposition and phase changes. (Reddy, et al., 2000). Figure 19 shows the DTA curves of as-prepared titanium dioxide powders. The DTA curve of RU shows the endothermic peaks around 100 and 266°C and the exothermic peaks at 576 and 800°C. For AR curve there are endothermic peaks around 100 and 250°C and exothermic peaks around 452 and 800°C after which no significant peaks can be detected even up to 1,250°C.

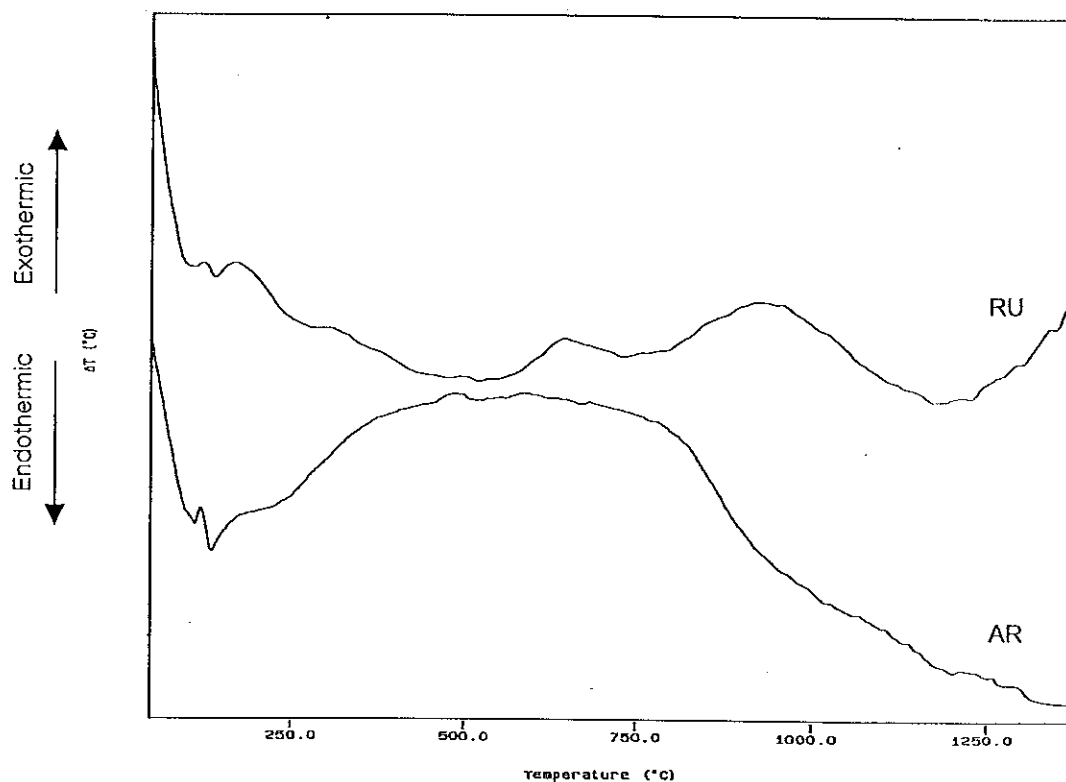


Figure 19 DTA curve of synthesized TiO_2 .

3.1.2.6 Scanning electron microscope (SEM)

Scanning electron microscope is a technique for investigation the network structure and the texture of sample as shown in Figure 20. It can be seen that the photomicrograph of the RU sample appears highly regular aggregated and uniform structure produced by the agglomeration of particles of nearly spherical shape. But for the AR sample, it shows a dense and non-uniform structure with fewer aggregates than RU sample.

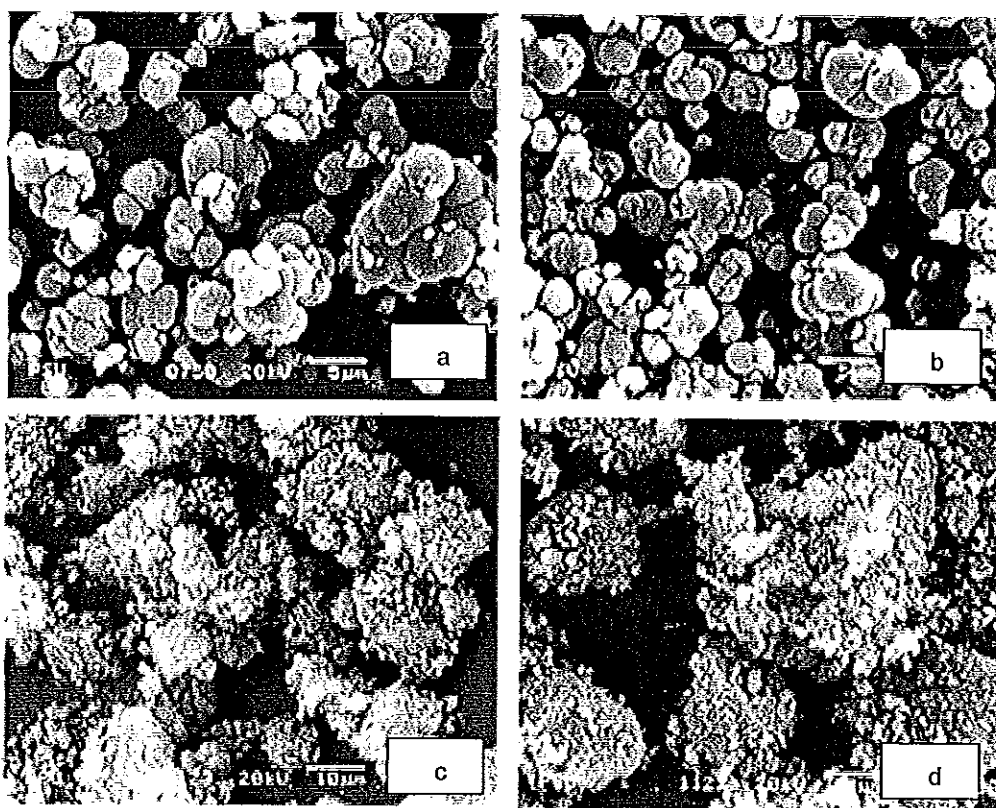


Figure 20 SEM images of synthesized TiO_2 (RU : a and b, AR : c and d).

3.1.2.7 Transmission electron microscope. (TEM)

Transmission electron microscope technique is employed for estimating the particle size and shape of particles. The TEM micrograph of synthesized titanium dioxide samples are shown in Figure 21. It appears that sample RU consisted of tenuous fibers (Figure 21a). The dark areas in Figure 21a were the result of aggregation of fibers as shown at higher magnification (Figure 21b). In Figure 21c and 21d, a TEM picture of the AR sample is shown. The structure consists of point-like primary particles (small black spots) which are partially aggregated of particles. The AR samples have also consisted of tenuous fibers particles. In this study, the TEM image could not determine the particle size of the product because it was not shape enough.

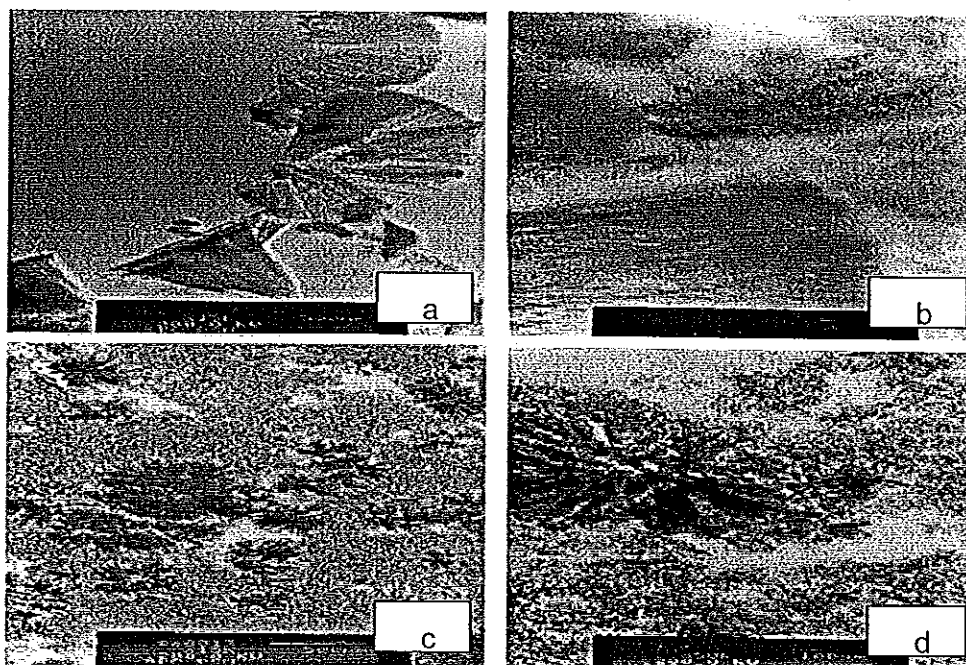


Figure 21 TEM images of synthesized TiO_2 (RU : a and b, AR : c and d).

3.1.2.8 Ultraviolet -Visible spectrophotometry (UV-Vis)

Ultraviolet-Visible diffuse reflectance spectroscopy is used to probe the molecular energy levels in materials since UV-Vis light excitation creates photo-generated electrons and holes (Tanaka, et al., 2002). Figure 22 shows the UV absorption edge which determined by the linear extrapolation of the steep part of the UV adsorption toward the baseline. The corresponding band gap energy of each titanium dioxide can be calculated from the following Plank's equation:

$$E_g = \frac{hc}{\lambda} = \frac{1240}{\lambda} \quad (6)$$

where E_g is the band gap energy (eV), h is the Plank's constant (6.67×10^{-34} J.s), c is the velocity of light (3×10^8 m.s⁻¹) and λ is the onset of absorption. The diffuse UV-vis absorption spectra and the onset of absorption as well as the band gap energy of the samples are shown in Figure 22 and Table 11.

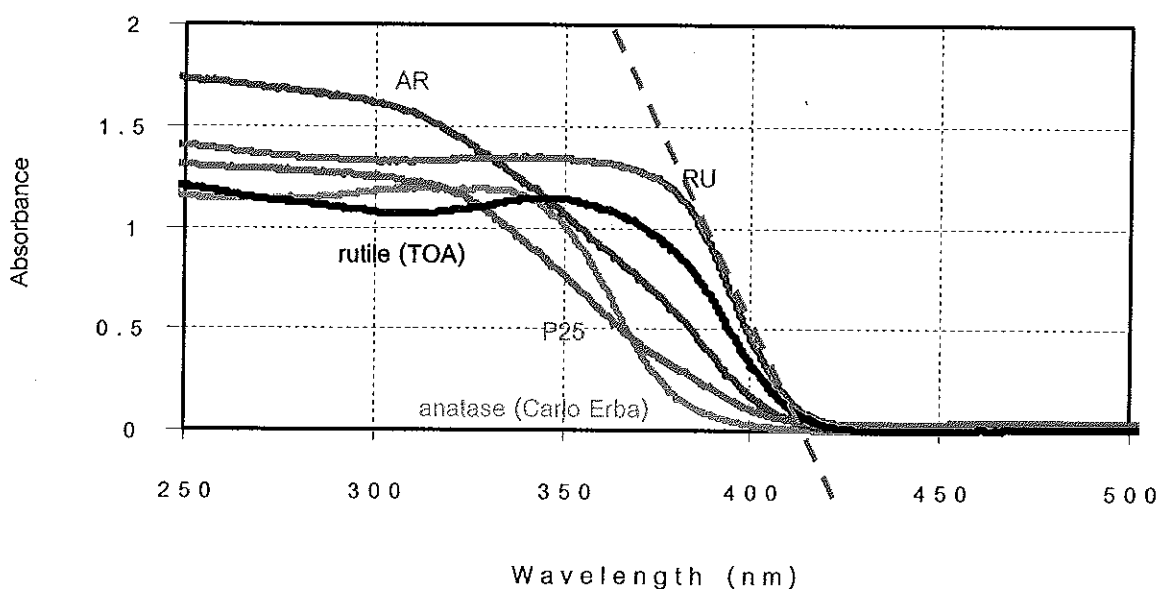


Figure 22 Diffuse UV-vis absorption spectra of TiO₂.

Table 11 The onset of absorption and band gap energy of TiO₂.

Titanium dioxide samples	Onset of absorption (λ_{os})	Band gap energy (eV)
TiO ₂ (RU)	415	2.98
TiO ₂ (AR)	410	3.03
Rutile (TOA)	413	3.00
Anatase(Carlo Elba)	385	3.22
TiO ₂ (P25)	387	3.20

In order to establish the type of band-to-band transition in these synthesized particles, the absorption data were fitted to equation for both indirect and direct band gap transitions. The equation of both transitions is given by the following equation (Kumar, et al., 2000):

$$(\alpha \cdot h\nu) = B_{i,d}(h\nu - E_g)^n \quad (7)$$

where α is the absorption coefficient (cm⁻¹), $B_{i,d}$ is the absorption constant for an indirect transition (subscript i) and direct transition (subscript d), n is 2 for indirect transition and $1/2$ for direct transition, $h\nu$ is the energy of excitation, E_g is the band gap energy. The value of E_{phot} extrapolated to $\alpha = 0$ gives an absorption energy, which corresponds to band gap energy (E_g).

The absorption coefficient (α) for reflectivity measurements could be calculated by the following equation (Zhao, et al., 1991):

$$\alpha = \frac{A}{d_s} \quad (8)$$

where A is the measured absorbance and d_s is the thickness of sample in UV-Vis cell (0.4 cm).

Thus, the plot of $(\alpha E_{\text{phot}})^{1/2}$ versus E_{phot} and $(\alpha E_{\text{phot}})^2$ versus E_{phot} should determine the nature of the transition in the sample and are shown in Figures 23 and 24, respectively. The band gap values calculated from Figures 23 and 24 are shown in Table 12.

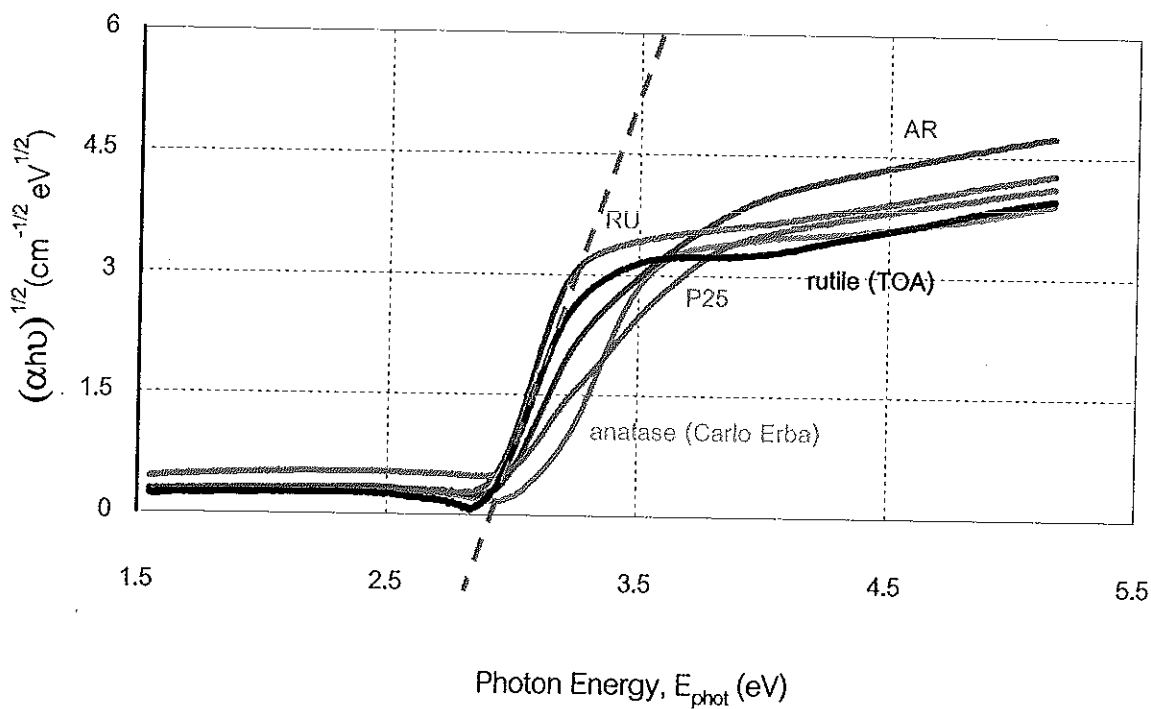


Figure 23 Plot of $(\alpha h\nu)^{1/2}$ versus E_{phot} for indirect transition of TiO_2 . The band gap (E_g) are obtained by extrapolation to $\alpha = 0$.

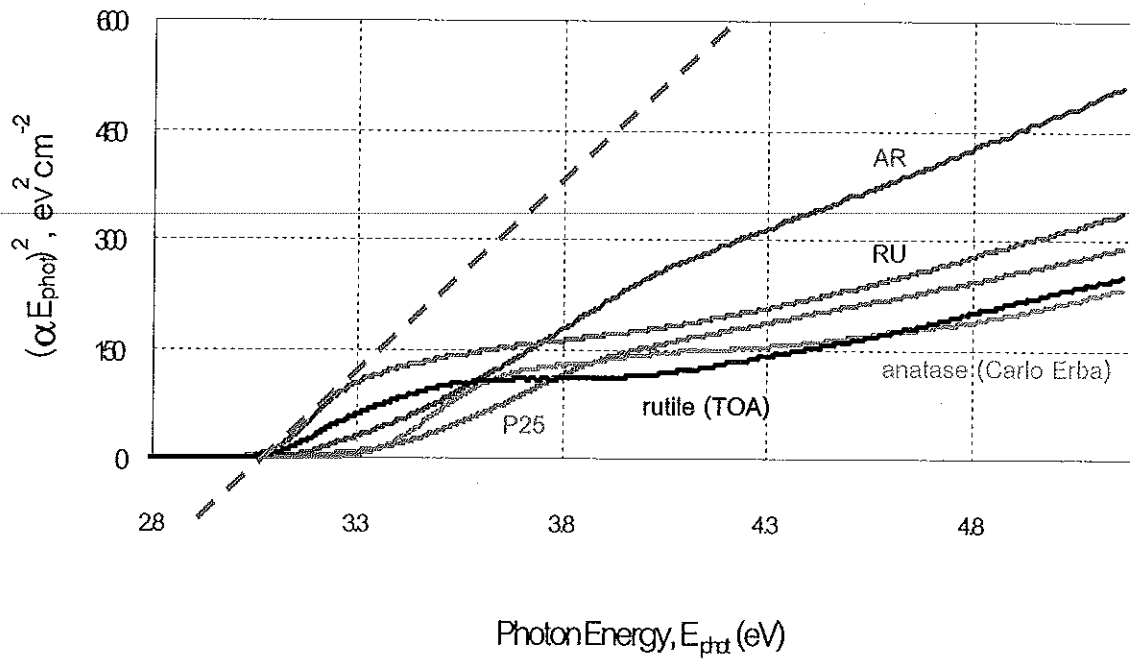


Figure 24 Plot of $(\alpha h\nu)^2$ versus E_{phot} for direct transition of TiO_2 . The band gap (E_g) are obtained by extrapolation to $\alpha = 0$.

Table 12 Band gap energy from direct and indirect method.

Titanium dioxide sample	Band gap energy (eV)		
	Equation 6	Indirect method	Direct method
$\text{TiO}_2(\text{RU})$	2.98	2.97	3.16
$\text{TiO}_2(\text{AR})$	3.02	2.98	3.38
Rutile (TOA)	3.00	2.98	3.10
Anatase (Carlo Erba)	3.22	3.18	3.34
$\text{TiO}_2(\text{P25})$	3.20	2.97	3.36

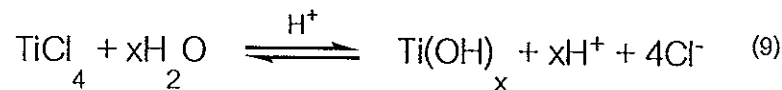
4. Discussion

4.1 Synthesis and characterization of titanium dioxide

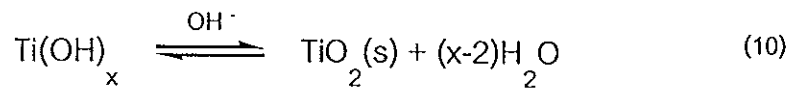
4.1.1 Synthesis of titanium dioxide

The sol-gel method consists of the hydrolysis and condensation reactions which are catalysed in the presence of acid. The hydrolysis reaction leads to the formation of original nuclei of titanium dioxide while the condensation reaction leads to the growth of network system of original nuclei (Kumar et al., 1999). The general reactions are as follows.

The hydrolysis reaction



The condensation reaction



Zhang et al., (2000) suggested the equilibrium between the hydrolysis reaction (nucleation stage) and the condensation reaction (growth stage) made the formation of titanium dioxide particles in the rutile phase possible. After the neutralization of ammonia solution, the equilibrium between the hydrolysis and condensation was broken and the condensation reaction or the growth rate was possible to accelerate for the formation of anatase phase (Zhang et al., 2000). According to Tang et al., (2002), the formation of anatase and rutile titanium dioxide is determined by the hydrolysis and condensation reactions. If the condensation starts before completion of hydrolysis, either amorphous or anatase titanium dioxide will form. And also, in neutral and basic conditions, condensation starts before complete hydrolysis, while acid

condition promotes the hydrolysis and decreases the condensation (Tang et al., 2002).

In the present study, it could be seen that only rutile phase (RU sample) and mixture of anatase and rutile (AR sample) were obtained. It could be suggested that both products might have formed by the different in reaction mechanism as described below.

For both samples, the reaction that carried out with the heating of titanium tetrachloride aqueous solution at 95°C could be considered as a two-step processes, hydrolysis and condensation reactions. As seen in the reaction steps that the reaction was carried out at pH 7 because it was close to the point of zero-charge (PZC) of titanium dioxide at pH about 6.8. At this point, titanium dioxide has a neutral surface ($\text{O}^- \text{OH}_2^+$) with minimal electronic repulsion among particles; thus the rates of coagulation of titanium dioxide particles are the fastest and an equilibrium is also reached easily to give titanium dioxide crystalline (O'Sheam, et al., 1999). Moreover, the reaction appeared in the prolonged time (26 h.) because titanium dioxide crystalline could grow larger and more stable than shorter time (Yanqing et al., 2001). Because both samples have the same reaction time (13 h. before adding ammonia solution and 13 h. after adding ammonia solution), volume of HCl, and pH value but different water volume in preparation step, so there is the difference in hydrolysis and condensation rate between them. The different in crystalline phase may be due to the content of water in the preparation step. As seen in this study that only rutile phase appears in RU sample, this could be attributed to only the equilibrium between hydrolysis and condensation is appeared in the RU sample which result from the low volume of water in the reaction stabilized the equilibrium between hydrolysis and condensation

reactions. For AR sample, it consists not only rutile phase but also anatase phase. This could be explained that the equilibrium between hydrolysis and condensation reaction is broken from the larger amount of water which result in faster condensation and slower hydrolysis. As a result, the possibility to form structure unit of anatase phase is obtained. Therefore, the high volume of water in the reaction catalyzed the rearrangement of TiO_6 octahedral in amorphous titanium dioxide, promoting the formation of anatase structure.

4.2 Characterization of titanium dioxide

4.2.1 X-ray diffraction (XRD)

The crystalline structure of the phases in the sample is obtained by x-ray powder diffraction which is shown in Figure 7. From the XRD patterns, it could be seen that titanium dioxide in rutile or mixture of anatase and rutile phase was obtained as the reaction product at low temperature about $95^{\circ}C$. In the case of RU sample (Figure 7a), only pure rutile phase was obtained. For AR sample (Figure 7b), it was a mixture consisting of anatase and rutile phases. The percentage of anatase and rutile in the sample was determined by XRD using the standard addition method to be 30 % of rutile for both samples and 15 % anatase for AR sample. From the XRD measurement, the information on the size of anatase and rutile crystallites was also obtained by using the Scherrer formula which is generally the accepted method to estimate the average crystallite size (Ohtani et al., 1997). It is clear from Figure 7 that the crystallite size is found to be in nanometer region; 5.2 and 7.8 nm for anatase and rutile, respectively, in AR sample, and 9.0 nm for rutile in RU sample. It should be noticed that the XRD spectra of AR and RU sample are broader and weaker than those of commercial titanium dioxide indicating the

predominantly amorphous phase being present in the sample. The broader and weaker peaks in XRD spectrum of AR and RU samples compared to commercial products indicated that both samples were nanoparticles ((Liqiang et al., 2003).

The differences in the crystallographic phase of AR and RU sample can be attributed to different in ratio of volume of water and titanium tetrachloride ($H_2O/TiCl_4$) under the same conditions. It can be seen that only rutile phase was obtained at $[H_2O/TiCl_4] = 5$ (Figure 7a), whereas a mixture of anatase and rutile was obtained when the volume ratio was 10 (Figure 7b). These results indicated that the amount of water determined the structure of the samples. This result corresponded to those observed by Ding et al., (1997) who studied the hydrolysis reaction of $Ti(O-Bu)_4$ with water. They found that the amount of water determined the chemical and structure changes of the gel-derived titanium dioxide powders (Ding et al., 1997). But their results were different from this study in term of structure stability that the sample prepared by smaller amount of water has more stable phase of anatase than those with larger amount of water. They only discussed that the difference in amount of water determined the degree of hydrolysis which directly responsible for the structure of TiO_2 . Their result was opposite to this study where it was found that rutile is more stable than anatase phase at lower amount of water as evidenced from XRD study which showed only diffraction peaks of rutile phase in Ru sample. The different of phase stability may be the result of starting material and also from the volume of water for the preparation of titanium dioxide which may affect the crystal structure of sample.

Yanagisawa and Overtone et al., (1999) also studied the effect of water for the crystallization of anatase by using dry vapor and hydrothermal conditions. Their results showed that in all cases where water was present, anatase was produced, with no rutile present. They discussed that the presence of water in the reaction catalyzed the crystallization step of anatase structure (Yanagisawa and Overtone., 1999). However, they did not demonstrate the effect of water content on the crystallization of titanium dioxide. Their results did not agree with this work which found the present of rutile phase in both samples (AR and RU) as evidenced by XRD study. The change in the crystalline structure of titanium dioxide could be due to the different in preparation method. Thus, the change in the amount of water could affect the crystallinity of titanium dioxide and sometime it may be also responsible for the porous properties (Samantaray et al., 2003).

4.2.2 Surface area and pore size

The specific surface areas of RU and AR sample were shown in Table 7. In order to compare this value, other samples of titanium dioxide were also subjected to the same measurement under the same conditions, such as the commercially available anatase from Carlo Erba, rutile from a paint factory (TOA, Co., Thailand), and the Degussa P25. It can be seen in Table 7 that both synthesized titanium dioxide have higher surface area than commercial titanium dioxide due to lower crystallinity of the synthesized samples. The AR sample shows the highest surface area with value of $218.38 \text{ m}^2/\text{g}$, much higher than RU and commercial sample. This result is in agreement with TGA study which shows greater weight loss of AR sample than RU sample. The larger surface area of AR sample could be attributed to highly network system from

condensation reaction which is caused by the high volume of water in AR sample (Zhang et al., 2001).

The porous nature of synthesized titanium dioxide was studied by nitrogen adsorption isotherm. In order to utilize the information within the adsorption isotherms, it is necessary to inspect the shape of physisorption isotherm and the identification of the principle mechanism of adsorption. The majority of physisorption isotherms could be grouped into six types, as shown in Figure 25.

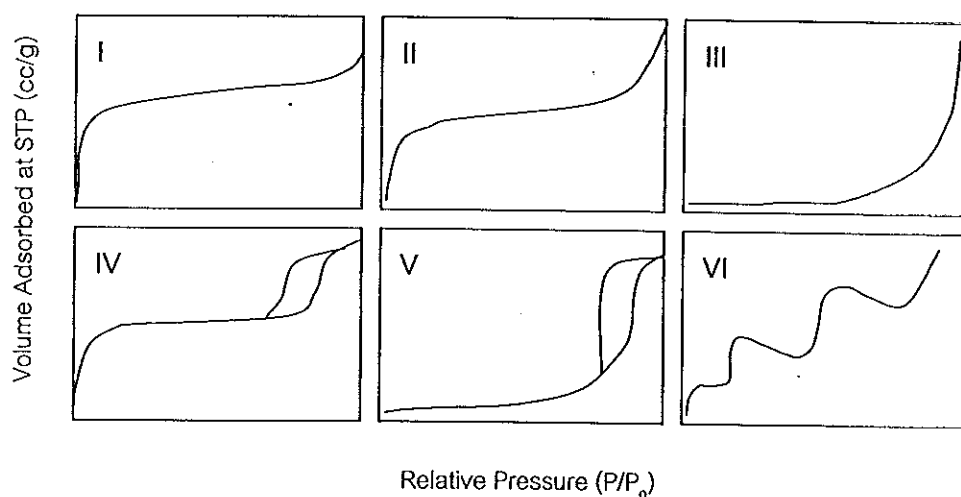


Figure 25 IUPAC classification of adsorption isotherms (Ryu et al., 1999).

Table 13 IUPAC classification of the pore (Khalil et al., 2001).

Porosity type	Size(d)
Ultramicropores	< typical molecule diameter of the adsorptive about 0.6 nm
Micropores	$d < 2 \text{ nm}$
Mesopores	$2 \text{ nm} < d < 50 \text{ nm}$
Macropores	$d > 50 \text{ nm}$

The Type I isotherm is given by microporous solids. The very steep region at low P/P_0 is due to the filling of very narrow pores and limiting uptake is dependent on the accessible micropore volume rather than on the internal surface area. The Type II isotherm is normally given by a non-porous solids which unrestricted monolayer-multilayer adsorption can occur. The Type III isotherm is generally associated with weak adsorbent-adsorbate and relatively strong adsorbate-adsorbate interactions. In this case cooperative effects lead to the development of patches of multilayer before a uniform monolayer has been formed. Type IV isotherm with hysteresis loop is the characteristic features of the adsorbate-adsorbate interactions which is associated with capillary condensation. Some microporous or mesoporous solids are amongst the few adsorbents to give Type V isotherm. The Type VI isotherm is relatively rare, it presents stepwise multilayer adsorption on a uniform non-porous surface. (Ryu et al., 1999).

The nitrogen adsorption isotherms for RU and AR samples are shown in Figures 10 and 11, respectively. The isotherms corresponding to the RU sample is of Type IV (BDDT classification) (Ryu et al., 1999), indicating that the pore size is in the mesoporous region. For AR sample, the isotherm is a combination of Type I and IV (BDDT classification) with two distinct regions; at low relative pressure, the isotherm exhibits high adsorption, indicating that the sample contains micropore (Type I). However, at high relative pressure, the curve exhibits the presence of mesopores (Type IV). In this study, the hysteresis loop in the isotherm could not be determined due to the limited capability of the equipment (SA3100 coulter) which was not able to determine the desorption study. The present of micropore could be checked by plotting the adsorbed layer called "*t*-plot" as seen in Figures 12 and 13 for RU and AR,

respectively. It seems that for RU sample, there is an early linear section passing the origin. This behavior indicated that the specimen lacks of micropore but contains only mesopores (Khalil et al., 2001). However, t -plot of AR sample shows that linear section is not pass the origin, suggesting that it contains not only mesopore but also micropore (Khalil et al., 2001).

The pore size distribution of synthesized titanium dioxide are shown in Figures 14 and 15 for RU and AR sample, respectively. The AR sample shows bimodal pore size distribution consisting of intra-particle pores (4-8 nm) and larger inter-particle pores (8-100 nm). Usually, there are two types of pores present in the bimodal pore size distribution. One is made from the intra-aggregated pores at lower P/P_0 range (the pores within the hard aggregates) and the other is larger inter-aggregated pores in the higher P/P_0 range arising from hard aggregated (the void between hard aggregates) (Yu et al., 2003). For RU sample, it exhibits monomodal pore size distribution due to the collapse of the intra-particle pores. The main cause of the disappearance of intra-particle pores could be attributed to the non-growth of anatase, leading to the disappearance of the void among anatase crystallite which results in the collapse of intra-particle pores. As seen in the study of Yu et al., (2003) who investigated the microstructures of titanium dioxide powders doped F^- at various temperatures by scanning electron microscope. They found that after calcined at 700°C , the intra-particle pores of pure and doped titanium dioxide completely disappeared. This could be attributed to grain growth from the phase transformation of anatase to rutile, leading to the disappearance of the intra-particle pores (Yu et al., 2003). It is also interesting to note that the pore volumes in RU sample is less than those in AR sample. This indicated that AR sample consisted of more hard aggregated than RU

sample, since the inter-particle pores arise from the voids between aggregates as seen in SEM image. The difference in the inter-particle pore volumes between samples can be explained by influence of the content of HCl which obtained from the sol-gel reaction. For RU sample prepared by lower volume of water, the hydrolysis and condensation reaction rates are extremely high. It generated the large amount of HCl which was then adsorbed as H^+ and Cl^- on the surface of the particles. On the other hand, AR sample prepared by higher volume of water, slower hydrolysis and condensation reaction rates occurred, so, the lower quantity of H^+ and Cl^- from HCl are partially adsorbed on the surface of the particle. The lower in pore volume of RU sample is in agreement with the decreasing of surface area observed for this sample, ascribed to the higher aggregate of particle and subsequent creation of smaller pores.

4.2.3 Fourier-transformed infrared spectrophotometer (FT-IR)

The infrared spectra of titanium dioxide, both AR and RU, in the range 4,000-400 and 900-400 cm^{-1} are shown in Figures 16 and 17, respectively. The band at around 3,180 cm^{-1} in both spectra is the stretching vibration of Ti-OH bonding which could not be removed easily until at relatively higher temperature (Wang et al., 2000). Near this band at 3,050 cm^{-1} , a shoulder was generated by an asymmetric vibration mode of the residual ammonium ions (Sanobez et al., 1996). The intensity of the 3,180 cm^{-1} band was high, suggesting that the Ti-OH bonding dominated the sol-gel reaction (Sanobez et al., 1996). This result supports the fact that the current reaction favors hydrolysis and slow condensation since titanium dioxide crystallines were very small, the local environment of the Ti-OH bonding was not

homogeneous, widening the $3,180\text{ cm}^{-1}$ band. The bending vibration of the Ti-OH bonding appeared at around $1,642\text{ cm}^{-1}$ for both samples (Velasco et al., 1999). In the low energy region ($900\text{-}400\text{ cm}^{-1}$) shows in Figure 17, the band due to stretching mode of Ti-O could be assigned. The presence of band in this spectral region could be assigned the crystalline structure (anatase or rutile phase) of titanium dioxide (Valesco et al., 1999). For RU sample appears the band at 470 cm^{-1} corresponding to Ti-O stretching mode of rutile structure (Zhang et al., 2001). The AR sample shows a different in the profile of the spectrum from that of RU sample, although the profile is somewhat similar to those of RU sample. The character of bands at 414 cm^{-1} indicated that sample consists of the mixture phases of anatase and rutile (Zhang et al., 2001). In addition, AR sample also had bands at 624 and 468 cm^{-1} due to the crystalline phases of anatase and rutile, respectively. But for the bands at 624 and 414 cm^{-1} , they disappeared when the amount of water is lower to 100 mL (RU sample). The product had rutile as the only crystalline phase and its FT-IR spectrum showed only band at 470 cm^{-1} which also supported by XRD technique. Thus, the IR studies indicated that only rutile or mixture of anatase and rutile phases resulted under sol-gel conditions. From an assignment of the FT-IR bands, it suggested that RU sample should exist in the mixed form of TiO_2 (rutile) and $[\text{Ti}(\text{H}_2\text{O})_x(\text{OH})_2]^{2+}$ (amorphous), and AR sample in TiO_2 (anatase and rutile) and $[\text{Ti}(\text{H}_2\text{O})_x(\text{OH})_2]^{2+}$ (amorphous). (Shao et al., 2001). This summary helps explain that both samples have low crystallinity and yet high content of amorphous.

4.2.4 Thermogravimetric analysis (TGA)

The results of TGA analysis of synthesized sample also indicated that the difference in the volume of water influences the decomposition behavior. The greater weight loss found in AR sample implies that there was larger amount of hydroxyls as free water and impurity in sample (Ding et al., 1997). This indicated that the residual components in the AR sample were more difficult to eliminate at the washing step than RU sample. The RU sample shows the decomposition of adsorbed water at the temperature below 700°C. The loss of weight was not very obvious at the temperature after 700 °C which possibly resulted from the desorption of the hydroxyl group (Ti-OH) on the particle (Liqiang et al., 2003). It is known that there are two types of surface hydroxyl groups, i.e. terminal Ti-OH and bridge Ti(OH)Ti. Dissociation temperature of these surface hydroxyl groups differs from each other and each temperature also could be affected by the chemical surrounding. Thus, the decrease in the weight appears at the wide range of temperature (Yoshio et al., 1998). The AR sample shows the decomposition stage different from RU sample. The first stage of weight lost is about 8 % which is higher than the other stage. It is corresponding to the decomposition of free water. The small weight loss in second stage implies the decomposition of some residual contamination such as N as NH_4^+ . The present of N was confirmed by CHN-O analyses which showed only small amount less than 1 %. The last stage of TGA could be assigned to the desorption of the hydroxyl groups (Ti-OH) on the particles (Liquiang et al., 2003).

4.2.5 Differential thermal analysis (DTA)

According to differential thermal analysis curves of the as-prepared samples, it could be found that the endothermic peak around 120°C assigned to the expulsion of free water from sample which is more prominent in AR sample (Liqang et al., 2003). This is in confirmation with the TGA analysis which shows a greater weight loss in AR sample as compared to that in RU sample. An endothermic peak at around 250°C associated with the removal of water from the network (Kumar et al., 1999). The exothermic peak indicated the onset of anatase phase formation near 462 and 576°C for AR and RU sample, respectively (Reddy et al., 2001). The phase transformation from anatase to rutile appears around 800°C for both samples. It is worth mentioning that the transformation temperature from amorphous to anatase of AR sample is shifted to lower temperature around 462°C which due to the inductive effect of anatase nuclei which is produced by sol-gel conditions (Yanagisawa et al., 1999). The area of peak could also suggest the content of amorphous in both samples. It could be seen that the exothermic peak of RU sample shows the area of peak larger than that of AR sample. This means that RU sample containing more amorphous than AR sample (Xie et al., 2002). Moreover, RU sample shows broader exothermic peak of amorphous to anatase than that of AR sample which indicates that amorphous to anatase phase transformation of RU sample is slower than that of AR sample (Xie et al., 2002).

4.2.6 Scanning electron microscope (SEM)

The SEM study gives only the information about the aggregation of particle. The morphology of commercial titanium dioxide; anatase, rutile and Degussa P25 are shown in Figure 26. It could be seen that the habit of the commercial specimens are rather similar with almost spherical shape. Thus, the result of SEM could not give the difference in the particle structure of anatase and rutile phase of titanium dioxide.

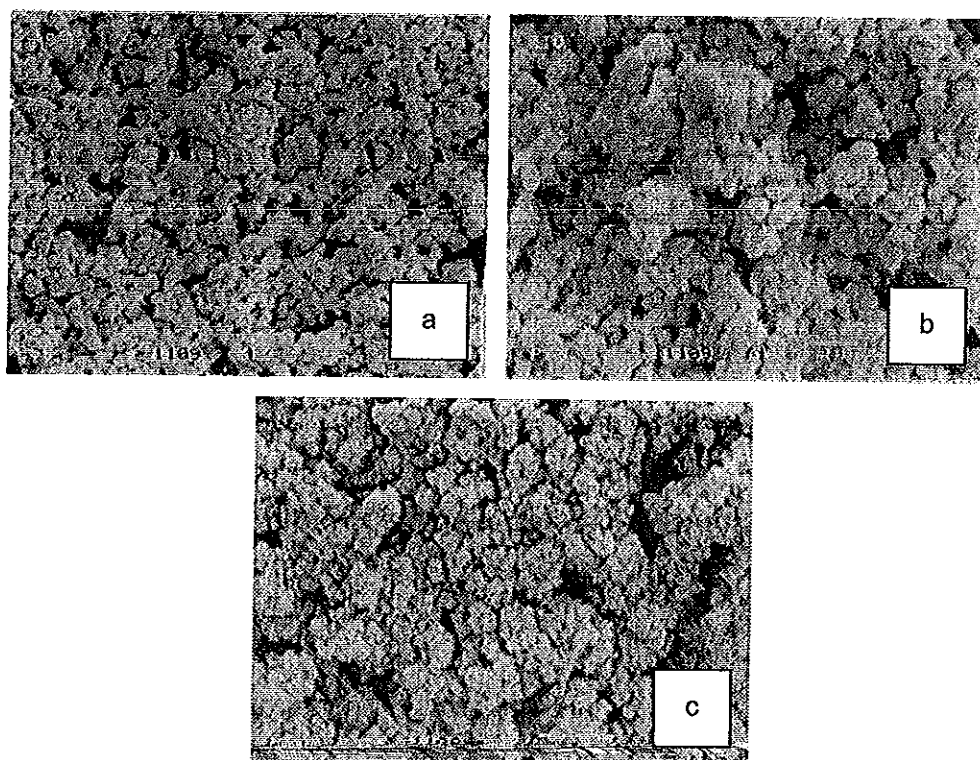


Figure 26 SEM images of commercial TiO_2 ; (a) anatase : Carlo Erba
(b) rutile : TOA Co, Thailand. and (c) P25:Degussa.

From SEM images of this study, it could be seen that there is the important difference in the morphology of AR and RU sample. For RU sample, it appears higher aggregation of spherical shape particle than AR sample and

also uniform structure. But for AR sample, it appears a dense and non-uniform structure with fewer aggregates than RU sample. The difference in the morphology could be ascribed to different preparation conditions, especially, the volume of water which may affect the aggregation of each sample. The morphology of AR sample is similar to the results of Yu et al., (2003) who investigated the effect of acidic and basic hydrolysis catalysts on the photocatalytic activity and microstructure of titanium dioxide prepared by sol-gel process. Their results showed that the morphology of titanium dioxide prepared by the hydrolysis of titanium tetraisopropoxide at pH 6.8 and without using HNO_3 as catalyst appears a dense structure and fewer in aggregation (Yu et al., 2003). The morphology of RU sample corresponds to that of commercial titanium dioxide which appear to constitute of regular aggregates produced by the agglomeration of particles with spherical shape.

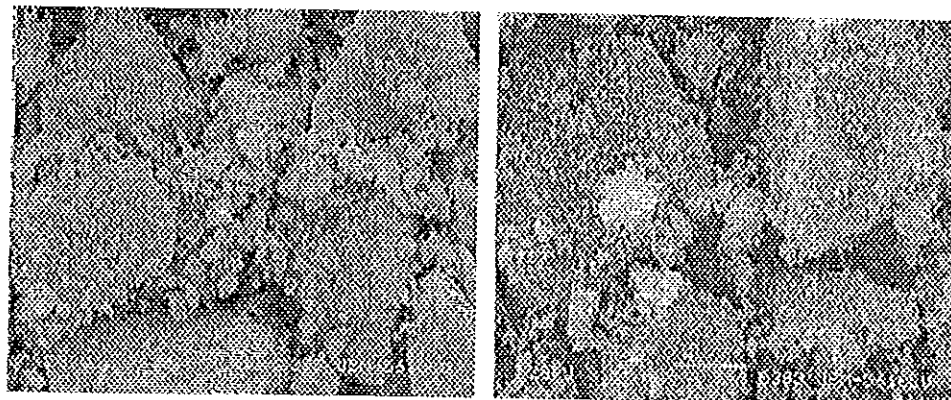


Figure 27 SEM images of TiO_2 from the study of Yu et al., (2003)

4.2.7 Transmission electron microscope (TEM)

The exact microstructure of synthesized titanium dioxide could be investigated by TEM. The typical microstructure of three kinds of titanium dioxide are shown in Figure 28. It could be seen that anatase, rutile, and Degussa P25 show point-like (Jalava et al., 1998), rod-like structure (Zhang et al., 2001), and ball-like (Liqiang et al., 2003). The TEM images showed that RU sample only consisted of tenuous fibers of rutile which agreed with the study of Wang et al., (2001) who synthesized nanocrystalline rutile titanium dioxide in

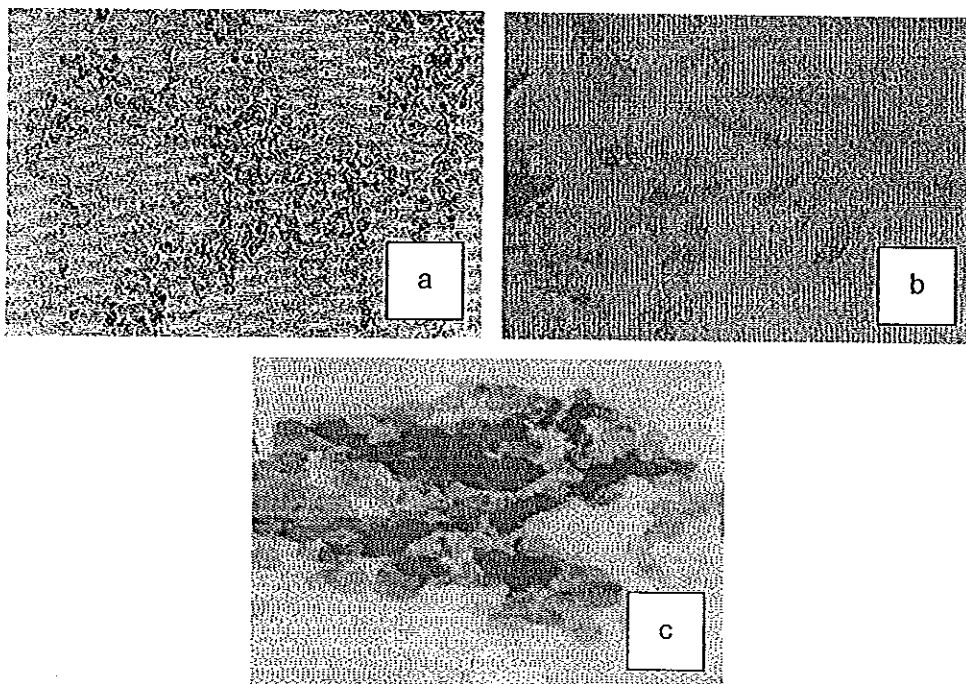


Figure 28 TEM images of TiO_2 ; (a) anatase : Zhang et al., (2000)
(b) rutile : Yang et al., (2002) and (c) P25:Degussa :
Liquang et al., (2003).

mixed organic solvents (alcohol and acetic acid) by hydrothermal method. They found that the product consisted of tenuous fibers of rutile as shown in Figure 29. Other researchers suggested that rutile consisted of rod-like shape (Yang et al., 2002). The difference in microstructure of rutile could be due to the difference of preparation methods (Yang et al., 2002). On the other hand, the particle of AR sample has two shapes owing to the formation of anatase and rutile phases. It could be found that AR sample consisted of point-like of anatase (Jalava et al., 1998) and also tenuous fibers of rutile (Xie et al., 2002). This result corresponds to the study of Seo et al., (2001) who prepared titanium dioxide in anatase and rutile phases from the reaction of TiOCl_2 and NH_4OH and then aging in 0.5 M HCl for 24 h. Their study showed that the product consisted of anatase and rutile phases with spherical and tenuous fibers shaped of anatase and rutile, respectively. Moreover, it can be seen from TEM images of synthesized titanium dioxide (Figure. 21) that their shapes are different from Figure 28 because of low crystallinity of the synthesized samples.

4.2.8 Ultraviolet-visible spectroscopy (UV-VIS)

UV-Vis spectroscopy has been used to characterize the bulk structure of crystalline titanium dioxide. Titanium dioxide is a semiconducting oxide with easily measured optical band gap. UV-Vis diffuse reflectance spectroscopy is used to probe the band structure or molecular energy levels in the materials since UV-Vis light excitation creates photo-generated electron and holes (Reddy et al., 2001). Figure 22 shows the UV-Vis diffuse reflectance spectra of two kinds of the sample, RU and AR, together with the commercial

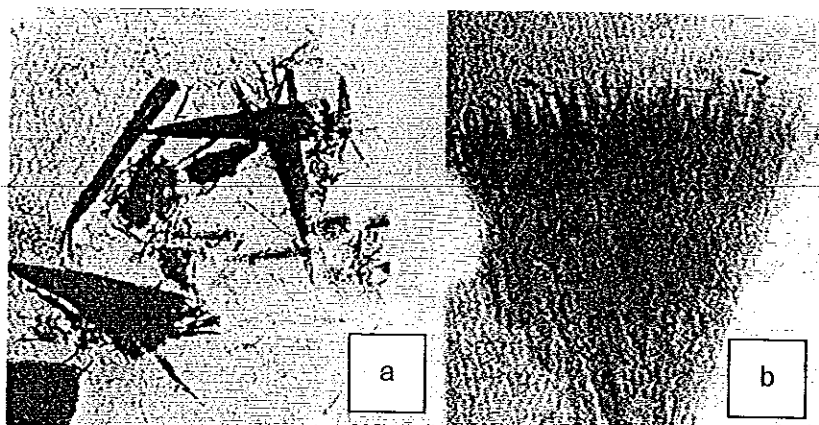


Figure 29 TEM images of rutile TiO_2 ; Wang et al., 2001 (a) tenuous fiber of rutile phase (b) : higher magnification of the dark area in (a)

materials, rutile (TOA Co., Thailand), anatase (Carlo Erba) and Degussa P25. Degussa P25 is known as a mixture of anatase and rutile and exhibits the spectrum showing the mixed profile of anatase and rutile. The absorption edge of rutile (TOA Co., Thailand) is found to be at the longer wavelength than that of anatase (Carlo Erba). It can be seen that the position of the absorption edge of RU is red-shifted by about 2 nm in comparison to rutile (TOA Co., Thailand) due to the difference in particle size of sample. The UV-Vis spectrum of the AR sample is steep line in comparison to other samples. Its absorption edge shows the mixed value of anatase and rutile structure which more similar to those of bulk rutile than anatase phase. This could be attributed to the higher content of rutile in sample. The band gap energy from the absorption edge shows in Table 11. It could be seen that the onsets of RU and AR samples were about 415 and 410 nm corresponding to the electron transition from the valence band which composed of 2p atomic orbitals of oxygen (π

band orbitals) to the conduction band which originated from the 3d atomic orbitals of titanium (Sanchez et al., 1995), giving the band gap energy of RU and AR at 2.98 and 3.03 eV, respectively. The experimental result for band gap energy of bulk anatase, rutile and Degussa P25 is in reasonable agreement to the accepted literature values of 3.2, 3.0 and 3.20 eV (Miao et al., 2003). It should be noticed that there was the difference in band gap energy between RU sample and rutile (TOA Co., Thailand). This phenomenal might be result of the smaller particle size, poor crystallinity and also defects on crystal planes of RU sample (Zhang et al., 2000). Because of the difference in the particle size of synthesized titanium dioxide and commercial product, it is clear that the band gap energy of synthesized titanium dioxide should be larger than those commercial products and not less as observed in the present case. It had been known and demonstrated by many that the properties of nanosized particles depend very sensitively on the particle size. This is the so-called "quantum size effect". As the diameter of crystallite approaches the exciton Bohr diameter, a splitting of the energy bands into discrete quantised energy level occur, it leads to a blue-shift in the absorption spectrum due to increased band gap nonlinear optical properties (Reddy et al., 2001). Thus, it means that as the particle size decrease the band gap energies increase. In order to determine the nature of the band gap and the type of band-to-band transition in synthesized titanium dioxide, either indirect or direct transition has to consider the expression for the variation of the absorption coefficient with energy. Figures 23 and 24 show the plot of $(\alpha E_{phot})^{1/2}$ versus E_{phot} for an indirect transition and $(\alpha E_{phot})^2$ versus E_{phot} for a direct transition, respectively. The value of E_{phot} extrapolated to $\alpha = 0$ gives an absorption energy which corresponds to a band gap energy (E_g). As seen in Figure 23 for indirect

transition, the commercial sample: rutile (TOA Co., Thailand), anatase (Carlo Erba) and Degussa P25 show a perfect fit and the extrapolation yields an E_g value of 2.98, 3.18 and 2.97 eV, respectively. But for the RU and AR sample, the indirect fit plot yield band gap of 2.97 and 2.98 eV, respectively, which does not seem realistic. This is so because for the sample with particle size 5-10 nm which is much less than that of the commercial product, there must be an increase in the band gap energy (Reddy et al., 2002). Hence, their band gap energy should be larger than that of commercial product and should not be equal or less than as obtained by Plank's equation (equation 6). Therefore, the data is then fit to the direct transition for two samples. Figure 24 shows the $(\alpha E_{phot})^2$ versus E_{phot} for these two samples. These data is a better fit than the corresponding indirect band gap fit, result in value of E_g estimated from the $\alpha = 0$ extrapolation as 3.16 eV for sample RU and 3.38 eV for sample AR. This could be explained due to the reduced ionicity of the synthesized titanium dioxide which comes from the mixing of the O 2p -Ti 3d orbitals. This result is in agreement with those of Reddy et al., (2002), who studied the band gap energy of anatase titanium dioxide nanocrystalline compared to the commercial one. Their result indicated that the anatase commercial sample shows an indirect transition, whereas anatase titanium dioxide nanocrystalline shows a direct transition (Reddy et al., 2002). There was also report where the nanoparticles have been reported to follow the direct transition. Sepone et al., (1995) had established the mechanism believed being operatively in nanophase titanium dioxide. These author had attributed the spectral blue shifts due to quantum size effects in titanium dioxide colloids as a result of direct transitions (Serpane et al., 1995). The electronic band structure of titanium dioxide had been reported by Daude and co-workers. Titanium

dioxide possesses a highly ionic lattice with the valence band composed principally of oxygen 2p orbitals, with the corresponding wave functions considerably localized on the O^{2-} lattice size. The conduction band consisted mostly of excited states of Ti^{4+} . The width of the O^{2-} 2p valence bands is about 16 eV, the breadth of the 3d conduction bands is about 27 eV. The energy level diagram is shown in Figure 30, where X denoted as the edge and Γ as the center of the Brillouin zone (BZ) (Serpone et al., 1995). The electronic transition and their energy summarized in Table 14.

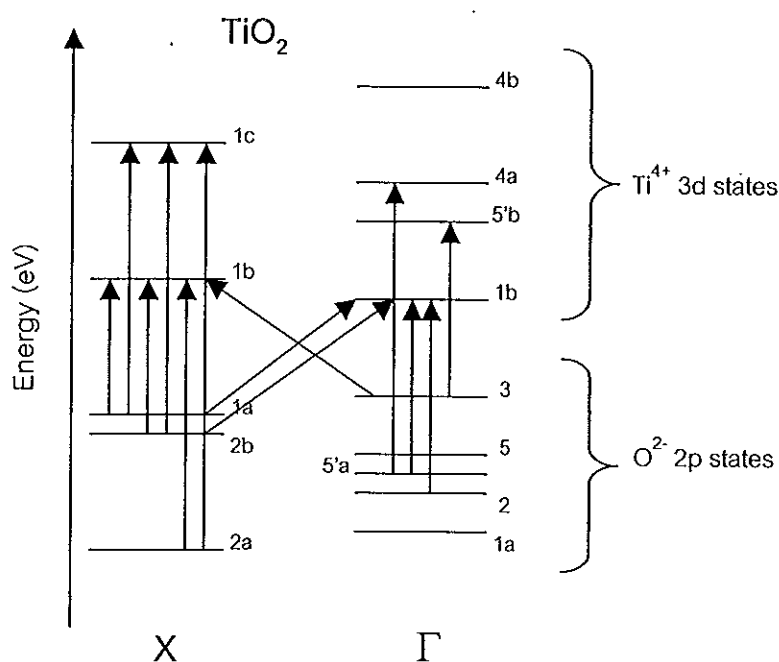


Figure 30 Short energy level diagram illustrating the relative energy level in TiO_2 (Serpone et al., 1995).

By using Table 14, it could be assigned the electronic transition of synthesized titanium dioxide and commercial products, so, it could be seen

that the band gap energy of anatase (Carlo Elba) and Degussa P25 correspond to the band gap energy of value 3.22 and 3.20 eV are ascribed to the indirect transition, $\Gamma_3 \rightarrow X_{1b}$. Different from rutile (TOA CO., Thailand) with

Table 14 Energies of Direct and Indirect Transitions in a TiO_2 Semiconductor (Serpone et al., 1995)

transition	nature	Energy (eV)
		Bulk crystals
$X_{1a} \rightarrow \Gamma_{1b}$	Indirect	2.91-3.02
$X_{1b} \rightarrow \Gamma_{1b}$	indirect	3.02-3.05
$\Gamma_3 \rightarrow X_{1b}$	indirect	3.11-3.21
$X_{1a} \rightarrow X_{1b}$	direct	3.22-3.45
$X_{2b} \rightarrow X_{1b}$	direct	3.48-3.68
$\Gamma_{5a} \rightarrow \Gamma_{1b}$	direct	4.00-4.07
$\Gamma_\gamma \rightarrow \Gamma_{1b}$	direct	4.11-4.15

band gap value of 3.00 eV has the indirect transition namely, $X_{1a} \rightarrow \Gamma_{1b}$. For the band gap energy of synthesized sample both AR and RU calculated by direct method, it shows the band gap energy of AR sample corresponds to the electronic transition namely, $X_{1a} \rightarrow X_{1b}$. The lowest energy of direct transition is not found for RU sample although it was nanocrystalline powders. This result had been reported by Ghosh et al., (1969), who found nanophase rutile titanium dioxide (band gap 3.2 eV) had the onset of absorption of the lowest-energy indirect transition. For these study, it suggests that nanocrystalline titanium dioxide in rutile phase shows the band gap energy at 3.16 eV corresponding to the indirect transition namely, $\Gamma_3 \rightarrow X_{1b}$. This could be

attributed to the defect energy levels in synthesized rutile titanium dioxide from crystal face. Because the reflectance spectra of rutile does not reveal all structure at the band edge, the band gap of rutile is dependent on the crystal face which shows the band gap value of 3.0 eV for (110) and (001) crystal face and 3.2 eV for (100) crystal face. Thus, It was proposed that the band gap in RU is due to (100) crystal face (Ghosh et al., 1969).

4.3 The possible mechanism for the formation of anatase and rutile in sol-gel method

4.3.1 Yanqing mechanism

A mechanism for the crystallization of anatase and rutile has been postulated by Yanqing et al., (2001). The key to the differences in anatase and rutile formation stems from the structure of two polymorphs. Anatase consists of TiO_6 octahedra which shared faces while rutile TiO_6 octahedra share edges and the phase transformation is accomplished by the rearrangement of these octahedra. The mechanism for anatase and rutile titanium dioxide formation may be explained by using the concepts of microscopic model which had been proposed to explain the polymorphs partition behavior of TiO_2 studied by Yanqing et al., (2001). They prepared TiO_2 by the hydrothermal method using an aqueous solution of TiCl_4 as precursor and then investigated the influence of TiCl_4 concentration, reaction time, and reaction temperature. Their results showed that the crystalline phase of TiO_2 prepared by the hydrothermal route was found to be influenced by those conditions. They also proposed that the phase formation mechanism of TiO_2 was similar to those of ZrO_2 because both substances have similar solubility-temperature behavior. According to this model, the first hydrolysis of Ti^{4+} at reaction temperature leads to the formation

of hydroxo complex monomer: $[\text{Ti}(\text{OH})(\text{OH}_2)_5]^{3+}$ species which are stable under strong acid conditions (Aruna et al., 2000). This species cannot condense because of its high positive charge. When pH is not sufficiently low to stabilize these precursors as a result of changing TiCl_4 concentration, deprotonation takes place, forming $[\text{Ti}(\text{OH})_2(\text{OH}_2)_4]^{2+}$ monomers. These species will form original nuclei in the form of corner-sharing octahedral dimers in the solution and can grow further continuously either by sharing apical edges for anatase, and also equatorial edges for rutile as shown in Figure 31 (Yanqing et al., 2001).

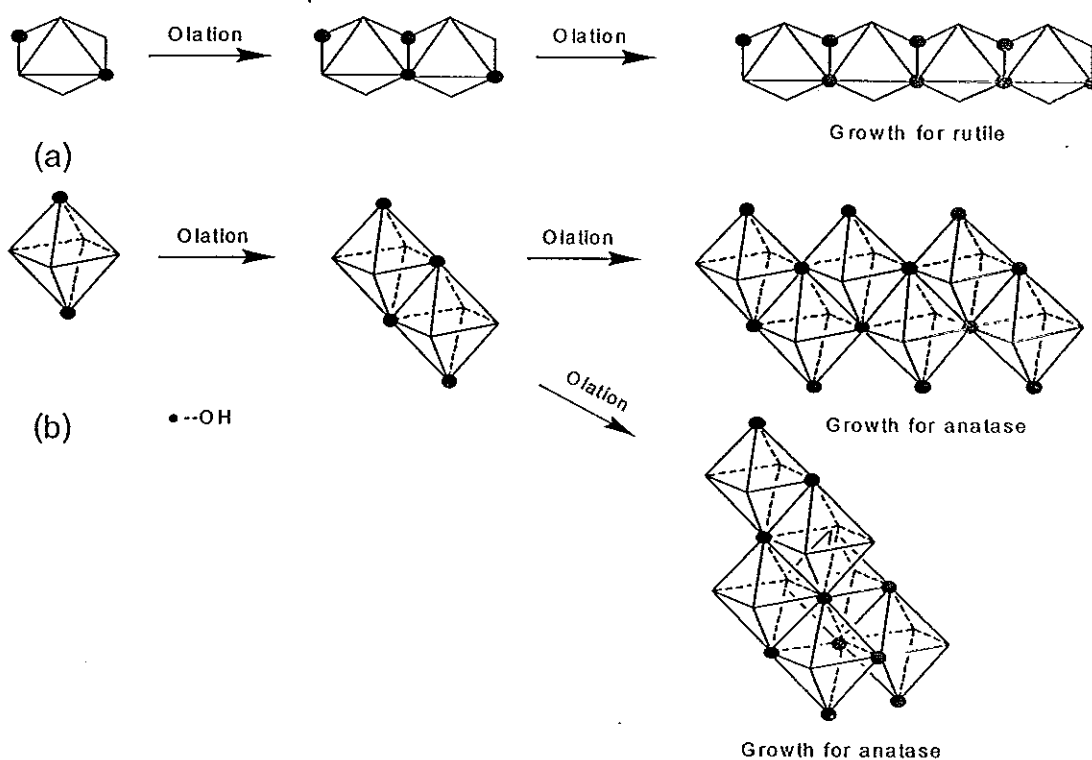
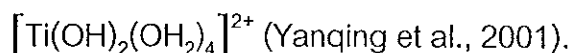


Figure 31 Proposed pathway for the TiO_2 nuclei of rutile (a) and anatase (b) starting from octahedral cations



4.3.2 Extension to Yanqing' s mechnism

According to the mechanism proposed by Yanqing et al., (2001), we can see that linear chains can only form rutile crystallites while skewed chains can only form anatase crystallites. We would like to further the Yanqing' s proposal slightly by invoking the concepts of stereochemistry of $[\text{Ti}(\text{OH})_2(\text{OH}_2)_4]^{2+}$. Our reasoning arises from the fact that the $[\text{Ti}(\text{OH})_2(\text{OH}_2)_4]^{2+}$ monomers in the solution may exist in two forms: *cis*- and *trans*-forms depending on the experimental conditions as shown in Figure 32.

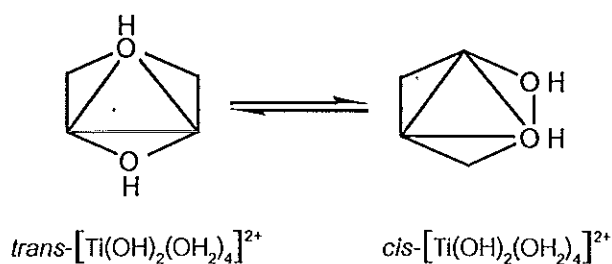


Figure 32 The *cis*- and *trans*-isomers of $[\text{Ti}(\text{OH})_2(\text{OH}_2)_4]^{2+}$ monomers.

The formation of *cis*- and *trans*-forms of the above monomers may be described as a result of different amount of water used to prepare TiCl_4 aqueous solution. When small amount of water is used, only *trans*-isomers are formed and when amount of water is increased, the *trans*-form isomerizes to *cis*-form. The solution of $[\text{Ti}(\text{OH})_2(\text{OH}_2)_4]^{2+}$ monomers will then exist as mixture of both forms.

In solution, the *trans*-isomer can condense with another *trans*-isomer (Figure 33a) or the *cis*-isomer can do the same with another *cis*-isomer at the opposite edge parallel to the two OH' s, or equatorial positions, (Figure 33b) to form the starting nuclei for the rutile phase. The *cis* and *cis* can also condense

using other edges, apical positions, leading to the anatase nuclei as in Figure 33c or the condensation of *trans* and *cis* isomers also leads to the anatase nuclei as in Figure 33d. [Note: Products nuclei c1 is the same as that obtained in Figure 33b].

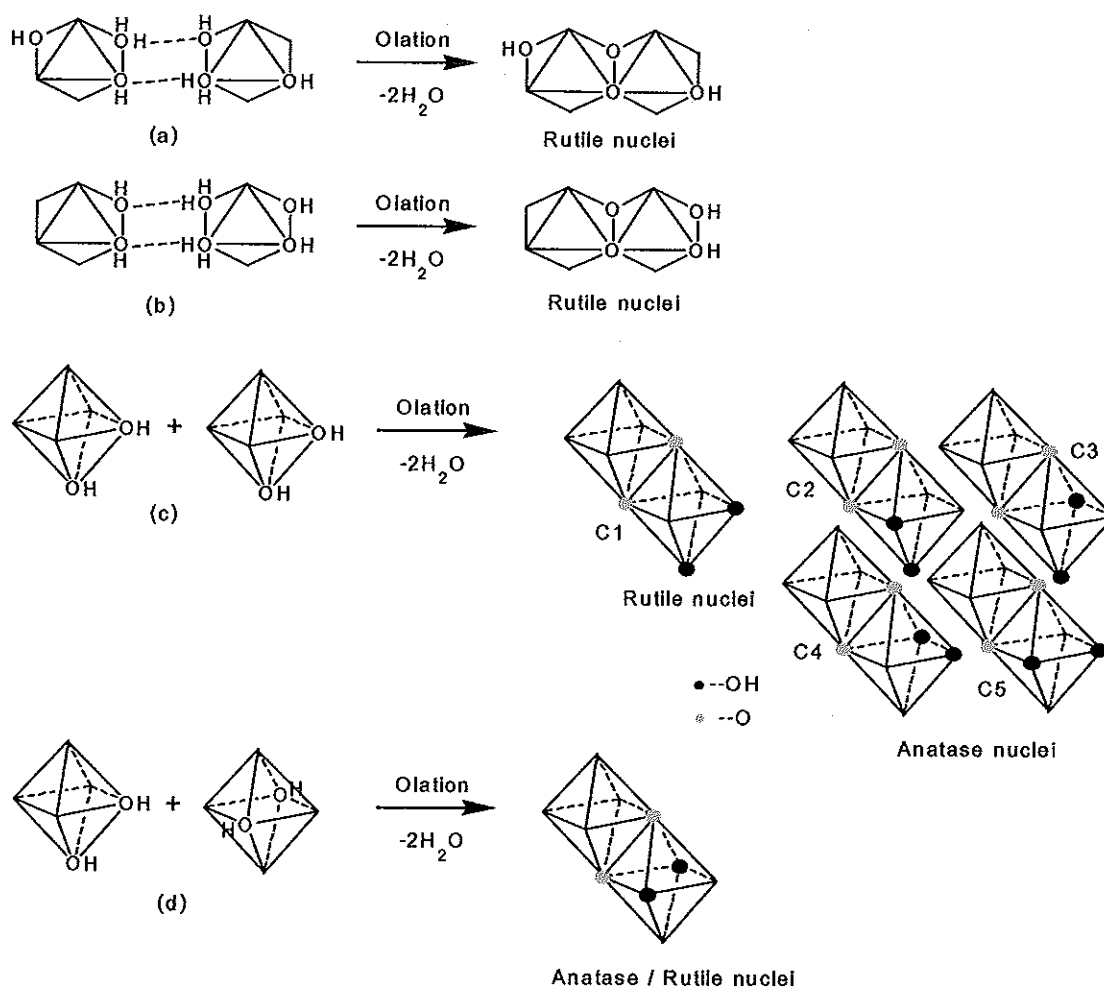


Figure 33 Possible pathways for the formation of anatase and rutile type

nuclei starting from octahedral cations (a) $\text{trans-}[\text{Ti}(\text{OH})_2(\text{OH}_2)_4]^{2+}$,

(b) $\text{cis-}[\text{Ti}(\text{OH})_2(\text{OH}_2)_4]^{2+}$ in equatorial positions,

(c) $\text{cis-}[\text{Ti}(\text{OH})_2(\text{OH}_2)_4]^{2+}$ in apical positions, and

(d) $\text{trans- and cis-}[\text{Ti}(\text{OH})_2(\text{OH}_2)_4]^{2+}$.

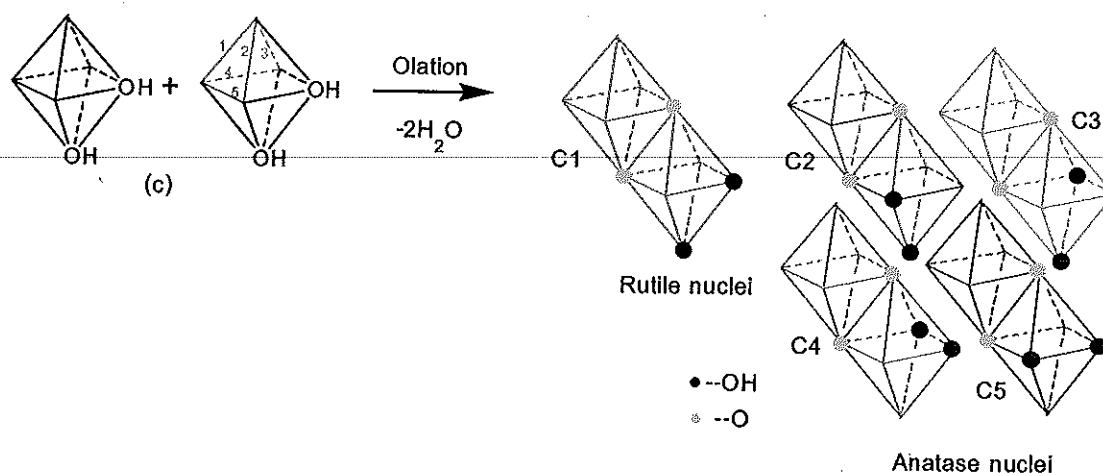


Figure 34 Details of Figure 33 (c) showing the formation of each nuclei.

In Figure 35, the product nuclei obtained from (a), (b), and c1 can only grow linearly leading to rutile crystallites whereas c2, c3, c4, and c5 can grow to anatase crystallite, and the product from d can grow one end to rutile and at the other end to anatase.

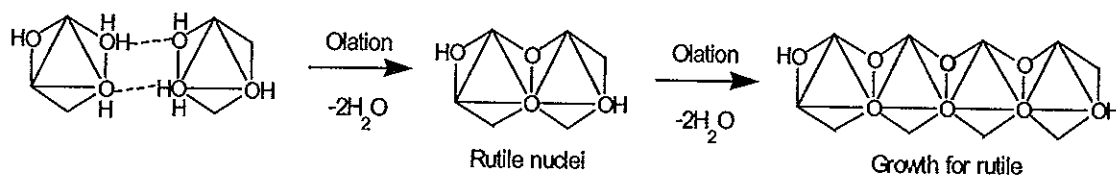


Figure 35 Possible pathway for the TiO_2 of RU sample starting from octahedral cations $\text{trans-}[\text{Ti}(\text{OH})_2(\text{OH}_2)_4]^{2+}$.

Based on above idea, the experimental results can be explained that only pure rutile phase formation in RU sample resulted from the growth of $trans\text{-}[\text{Ti}(\text{OH})_2(\text{OH}_2)_4]^{2+}$ monomers by sharing equatorial edge. The formation of these monomers took place at high concentration of titanium tetrachloride in solution (low volume of water). For AR sample, The formation of anatase and rutile phase could be due to the isomerization of $[\text{Ti}(\text{OH})_2(\text{OH}_2)_4]^{2+}$ monomers which took place at low concentration of titanium tetrachloride in solution (high volume of water). The formation of rutile structure in AR sample could result from the growth of $trans\text{-}[\text{Ti}(\text{OH})_2(\text{OH}_2)_4]^{2+}$ and $cis\text{-}[\text{Ti}(\text{OH})_2(\text{OH}_2)_4]^{2+}$ monomers by sharing equatorial edges (Figure 36a, 36b) and also partially from the growth of nuclei in 36c, 36d, while the formation of anatase phase in AR sample could be due to the growth of $cis\text{-}[\text{Ti}(\text{OH})_2(\text{OH}_2)_4]^{2+}$ monomers by sharing apical edges as in Figure 36c (c2 to c5) and partially from 36d. The fact that RU sample contains only rutile and AR sample contains mixture of rutile and anatase with the former as major product. This can be explained that at high concentration of titanium tetrachloride only $trans\text{-}[\text{Ti}(\text{OH})_2(\text{OH}_2)_4]^{2+}$ monomer exist in solution whereas at lower concentration of titanium tetrachloride mixture of $trans\text{-}[\text{Ti}(\text{OH})_2(\text{OH}_2)_4]^{2+}$ and $cis\text{-}[\text{Ti}(\text{OH})_2(\text{OH}_2)_4]^{2+}$ exist in solution but the $trans\text{-}[\text{Ti}(\text{OH})_2(\text{OH}_2)_4]^{2+}$ is present in much larger amount. Therefore, the AR sample has rutile as the major product.

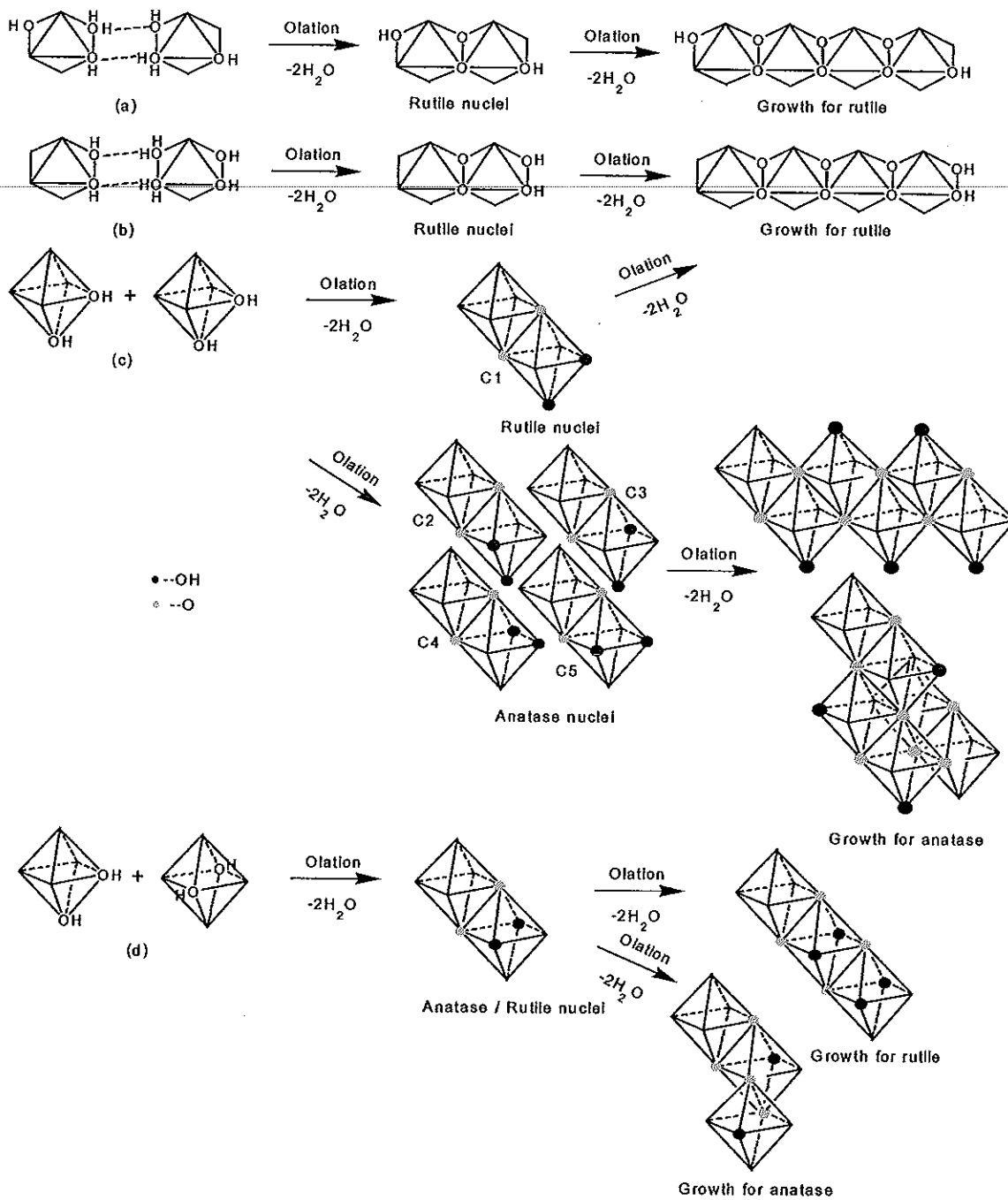


Figure 36 Possible pathways for the TiO_2 of AR sample starting from octahedral cations (a) $\text{trans-}[\text{Ti}(\text{OH})_2(\text{OH}_2)_4]^{2+}$, (b) $\text{cis-}[\text{Ti}(\text{OH})_2(\text{OH}_2)_4]^{2+}$ in equatorial positions and (c) $\text{cis-}[\text{Ti}(\text{OH})_2(\text{OH}_2)_4]^{2+}$ in apical positions and (d) both cis- and $\text{trans-}[\text{Ti}(\text{OH})_2(\text{OH}_2)_4]^{2+}$.

5. Summary

Titanium dioxide (TiO_2) in rutile phase or mixture of anatase and rutile phases was prepared by the sol-gel technique at relatively low temperature (95°C) from the hydrolysis and condensation reaction of titanium tetrachloride (TiCl_4) and then neutralized by ammonia solution until the pH value was 7. The XRD spectrum of synthesized TiO_2 indicated that in the case of RU sample only rutile phase was obtained. For AR sample, it was a mixture consisting of anatase and rutile phases. The percentage of anatase and rutile in the sample was determined by XRD technique using the standard addition method to be 30 % by weight of rutile for both samples and 15 % by weight of anatase for AR sample. From the XRD measurement the information on the size of anatase and rutile crystallites was also obtained by using the Scherrer formula which indicated that the crystallite size was found to be in nanometer region; 5.2 and 7.8 nm for anatase and rutile, respectively, in AR sample, and 9.0 nm for rutile in RU sample. The broader and weaker peaks in XRD spectrum of AR and RU samples compared to those of commercial titanium dioxide commercial products indicated that both samples were predominantly amorphous phase being present in the sample as nanoparticles. The surface area of RU and AR samples were 101.36 and 218.38 m^2/g , respectively, which were higher than that of commercial TiO_2 . This could be due to lower crystallinity of the synthesized samples. The porous nature of synthesized titanium dioxide was studied by nitrogen adsorption isotherm indicated that the pore size is in the mesoporous region for RU sample and both mesoporous and microporous for AR sample. The FT-IR spectrum showed the presence of H_2O and NH_4^+

presumably on their surfaces and also Ti-O band which corresponding to anatase and rutile structure. The general formula of both synthesized TiO_2 thus can be written in the mixed form as TiO_2 for anatase or rutile crystalline and also $[\text{Ti}(\text{H}_2\text{O})_x(\text{OH})_2]^{2+}$ for amorphous phase. This summary help explain that both samples have low crystallinity and yet high content of amorphous. The results of TGA analysis of synthesized sample indicated that AR sample showed the greater weight loss than RU sample implies that there was larger amount of hydroxyls as free water and impurity in sample. Data from DTA analysis of the as-prepared samples, it could be found that the endothermic peak around 120°C assigned to the expulsion of free water from sample is more prominent in AR sample. This was in confirmation with the TGA analysis which showed a greater weight loss in AR sample as compared to that in RU sample. An endothermic peak at around 250°C associated with the removal of water from the network. The exothermic peak indicated the onset of anatase phase formation near 462 and 576°C for AR and RU sample, respectively. The phase transformation from anatase to rutile appears around 800°C for both samples. The transformation temperature from amorphous to anatase of AR sample shifted to lower temperature than that of RU sample due to the inductive effect of anatase nuclei which was produced by sol-gel conditions. The area of exothermic peaks in DTA spectrum also suggested that RU sample containing more amorphous than AR sample. The SEM image indicated the higher aggregation of spherical shape particle and also uniform structure for RU sample. But for AR sample, it appears a dense and non-uniform structure with fewer aggregates than RU sample. The TEM images showed RU sample only consisted of tenuous fibers of rutile. While AR sample consisted of point-like of anatase and also tenuous fibers of rutile. The UV-Vis

diffuse reflectance study indicated the adsorption edge of RU and AR samples were about 415 and 410 nm, respectively. The band gap energy of synthesized samples determined by quantum size effect was 3.16 eV for sample RU and 3.38 eV for sample AR. This band gap values were corresponding to the indirect transition namely, $\Gamma_3 \rightarrow X_{1b}$, and the direct transition namely, $X_{1a} \rightarrow X_{1b}$, respectively. The formation of anatase and rutile phase in this study proposed from the difference in the stereochemistry of original nuclei. Rutile phase in RU sample resulted from the growth of *trans*- $[\text{Ti}(\text{OH})_2(\text{OH}_2)_4]^{2+}$ monomers by sharing equatorial edge. Anatase and rutile phase in AR sample were due to the isomerization of $[\text{Ti}(\text{OH})_2(\text{OH}_2)_4]^{2+}$ monomers. The formation of rutile structure in AR sample was mainly from the growth of *trans*- $[\text{Ti}(\text{OH})_2(\text{OH}_2)_4]^{2+}$ and *cis*- $[\text{Ti}(\text{OH})_2(\text{OH}_2)_4]^{2+}$ monomers by sharing equatorial edges while the formation of anatase phase in AR sample was mainly due to the growth of *cis*- $[\text{Ti}(\text{OH})_2(\text{OH}_2)_4]^{2+}$ monomers by sharing apical edges. The difference in crystallite phase and the other properties of synthesized samples may result from the different of water content in the preparation condition.

References

- Arroyo, R.; Cordoba, G.; Padilla, J. and Lara, V. H. 2002. "Influence of manganese ions on the anatase-rutile phase transition of TiO₂ prepared by the sol-gel process", Materials Letters. 54(2002), 397-402.
- Aruna, S. T.; Tirosh, S. and Zaban, A. 2000. "Nanosize rutile titania particle synthesis *via* a hydrothermal method without mineralizers", Journal of Materials Chemistry. 10(2000), 2388-2391.
- Balong, Z.; Baishun, C.; Keyu, S.; Shangjin, H.; Xiaodong, L.; Zongjie, D. and Kelian, Y. 2003. "Preparation and characterization of nanocrystal grain TiO₂ porous microspheres", Applied Catalysis B: Environmental. 40 (2003), 253-258.
- Bankmann, M.; Brand, R.; Engler, B. H. and Ohmer, J. 1992. "Forming of high surface area TiO₂ to catalyst supports", Catalysis Today. 14(1992), 225-242.
- Brunauer, S.; Deming, L. S.; Deming, W. E. and Teller, E. 1940. "On a Theory of the Van Der Waals adsorption of gases", Journal of American Chemical Society. 62(1940), 1723-1732.
- Buchner, W.; Schliebs, S.; Winter, G. and Buchel, K. H. 1989. Industrial Inorganic Chemistry. New York : VCH.

Chemat.1998. Sol-Gel Technology. <http://www.chemat.com/html/solgel.html>.

Chemat Technology, Inc.

Clark, R. J. H. 1968. The Chemistry of Titanium and Vanadium. Amsterdam : Elsevier.

Cristallo, G.; Roncari, E.; Rinaldo, A. and Trifiro, F. 2001. "Study of anatase-rutile transition phase in monolithic catalyst V_2O_5/TiO_2 and WO_3/TiO_2 ", Applied Catalysis A: General. 209(2001), 249-256.

Cun, W.; Jincai, Z.; Xinming, W.; Bixian, M.; Guoying, S.; Ping' an, P. and Jiamo, F. 2002. "Preparation, characterization and photocatalytic activity of nano-sized ZnO/SnO_2 coupled photocatalysts", Applied Catalysis B: Environmental. 39(2002), 269-279.

Ding, Z.; Lu, G. Q. and Greenfield, P. F. 2000. "Role of the crystallite phase of TiO_2 in heterogeneous photocatalysis for phenol oxidation in water", Journal of Physical Chemistry. 104(2000), 4815-4820.

Ding, X. and Liu, X. 1997. "Synthesis and microstructure control of nanocrystalline titania powders via a sol-gel process", Materials Science and Engineering A. 224(1997), 210-215.

Escobar, J.; Reyes, J. D. and Viveros, T. 2000. "Influence of the synthesis additive on the texture and structural characteristic of Sol-Gel Al_2O_3 -

TiO₂", Industrial and Engineering Chemistry Research. 39(2000), 666-672.

Ghosh, A. K.; Wakim, F. G. and Addiss Jr. R. R. 1969. "Photoelectronic processes in rutile", Physical Review. 184(1969), 979-988.

Harizanov, O.; Ivanova, T. and Harixanova, A. 2001. "Study of sol-gel TiO₂ and TiO₂-MnO obtained from a peptized solution", Materials Letters. 49 (2001), 165-171.

Hirasawa, M.; Seto, T.; Orii, T.; Aya, N. and Shimura, H. 2002. "Synthesis of size-selected TiO_x nanoparticles", Applied Surface Science. 197-198 (2002), 661-665.

Hu, Z. and Srinivasan, M. P. 1999. "Preparation of high-surface-area activated carbons from coconut shell", Microporous and Mesoporous Materials. 27 (1999), 11-18.

Ingle, Jr. J. D. and Crouch, S. R. 1988. Spectrochemical Analysis. U.S.A.: Prentice-Hall International, Inc.

Jalava, J. P.; Heikkila, L.; Hovi, O; Laiho, R.; Hiltunen, E.; Hakanen, A. and Harma, H. 1998. "Structural investigate of hydrous TiO₂ precipitates and their aging product by X-ray diffraction, atomic force microscopy, and transmission electron microscopy", Industrial and Engineering Chemistry Research. 37(1998), 1317-1323.

Joselevich, E. and Willner, I. 1994. "Photosensitization of quantum Size TiO_2 particles in water-in-oil microemulsion", Journal of Physical Chemistry. 98 (1994), 7628-7635.

Khalil, T.; Abou El-Nour, F.; El-Gammal, B and Boccaccini. 2001. "Determination of surface area and porosity of sol-gel derived ceramic powders in the system $\text{TiO}_2\text{-SiO}_2\text{-Al}_2\text{O}_3$ ", Powder Technology. 114(2001), 106-111.

Kim, j.; Song, K. C.; Foncillas, S. and Pratsinis, S. E. 2001. "Dopants for synthesis of stable bimodally porous titania", Journal of European Ceramic Society. 21(2001), 2863-2872.

Kormann, C.; Bahnemann, D. W. and Hoffman, M. R. 1988. "Preparation and characterization of quantum-Size titanium dioxide", Journal of Physical Chemistry. 92(1988), 5196-5201.

Kumar, P. M.; Barinarayanan, S. and Sastry, M. 2000. "Nanocrystalline TiO_2 studied by optical, FT-IR and X-ray photoelectron spectroscopy: correlation to presence of surface states", Thin Solid Films. 358(2000), 122-130.

Kumar, S. R.; Suresh, C.; Vasudevan, A. K.; Suja, N. R. and Mukundan, P. 1999. "Phase transformation in sol-gel titania containing silica", Materials Letters. 38(1999), 161-166.

Lee, S. K.; Robertson, P. K. J.; Mills, A.; McStay, M.; Elliott, N. and McPhail, D. 2003. "The alternation of the structure properties and photocatalytic activity of TiO₂ following exposure to non-linear irradiation sources", Applied Catalysis B: Environment. xxx(2003), xxx-xxx. (Article in press)

Li, W. J.; Shi, E. W. and Yin, Z. W. 2002. "Growth habit of rutile and α -Al₂O₃ crystals", Journal of Crystal Growth. 208(2000), 546-554.

Liqiang, J.; Xiaojun, S.; Weimin, C.; Zili, X.; Yaoguo, D. and Honggang, F. 2003. "The preparation and characterization of nanoparticle of TiO₂/Ti films and their photocatalytic activity", Journal of Physics and Chemistry of Solids. 64(2003), 615-623.

Lopez, T.; Gomez, R.; Pecci, G.; Reyes, P.; Bokhimi, X. and Novaro, O. 1999. "Effects of pH on the incorporation of platinum into the lattice of sol-gel titania phases", Materials Letters. 40(1999), 59-65.

Martin, C. and Rives, V. 1986. "Texture Properties of Titanium Dioxide", Powder Technology. 46(1986), 1-11.

Miao, L.; Jin, P.; Kaneko, K.; Terai, A.; Gabain, N. N. and Tanemura, S. 2003. "Preparation and characterization of polycrystalline anatase and rutile thin films by rf magnetron sputtering", Applied Surface Science. 9775 (2003), 1-9.

Ohno, T.; Sarukawa, K.; Tokieda, K. and Matsumura, M. 2001. "Morphology of a TiO₂ photocatalyst (Degussa P25) consisting of anatase and rutile crystalline phases", Journal of Catalysis. 203(2001), 82-86.

O'Shea K. E.; Pernas, E. and Sakers, J. 1999. "The Influence of mineralization products on the coagulation of TiO₂ photocatalyst", Langmuir. 15(1999), 2071-2076.

Ohtani, B.; Ogawa, Y.; Nishimoto, S. -I. 1997. "Photocatalytic activity of amorphous-anatase mixture of titanium(IV) oxide particles suspended in aqueous solutions", J. Phys. Chem. B. 101(30 January 1997), 3746-3752.

Park, N. -G.; Schlichthörl, G.; van de Lagemaat, J.; Cheong, H. M.; Mascarenhas, A. and Frank, A. I. 1999. "Dye-sensitized TiO₂ solar cells: structural and photoelectrochemical characterization of nanocrystalline electrodes formed from the hydrolysis of TiCl₄", J. Phys. Chem. B. 103 (1999), 3308-3314.

Reddy, K. M.; Manorama, S. V. and Reddy, A. R. 2002. "Band gap studies on anatase titanium dioxide nanoparticles", Materials Chemistry Physics. 78 (2002), 239-245.

Reddy, K. M.; Reddy, R. C. V. and Manorama, S. V. 2001. "Preparation, characterization, and spectra studies on nanocrystalline anatase TiO₂", Journal of Solid State Chemistry. 158(2001), 180-186.

- Ryu, Z.; Zheng, J.; Wang, M. and Zhang, B. 1999. "Characterization of pore size distributions on carbonaceous adsorbents by DFT", Carbon. 37 (1999), 1257-1264.
- Samantary, S. M.; Mohapatra, P. and Parida, K. 2003. "Physico-chemical characterization and photocatalytic activity of nanosized $\text{SO}_4^{2-}/\text{TiO}_2$ towards degradation of 4-nitrophenol", Journal of Molecular Catalysis A: Chemical. 198(2003), 277-287.
- Sanchez, E. and Lopez, T. 1995. "Effects of preparation method on the band gap of titania and platinum-titania sol-gel materials", Materials Letters. 25 (1995), 271-275.
- Sanchez, E.; Lopez, T.; Gomez, R.; Morales, A. and Novaro, O. 1996. "Synthesis and characterization of sol-gel Pt/TiO₂ catalyst", Journal of Solid State Chemistry. 122(1996), 309-314.
- Sathyamoorthy, S.; Hounslow, M. J. and Moggride, G. D. 2001. "Influence of stirrer speed on the precipitation of anatase particle from titanyl sulphate solution", Journal of Crystal Growth. 223(2001), 225-234.
- Sclafani, A.; Palmisano, L. and Schiavello, M. 1990. "Influence of the preparation methods of TiO₂ on the photocatalytic degradation of phenol in aqueous dispersion", J. Phys. Chem. 94(1990), 829-832.

- Seo, D. K.; Lee, J. K. and Kim, H. 2001. "Synthesis of TiO₂ nanocrystalline powder by aging at low temperature", Journal of Crystal Growth, 233 (2001), 298-302.
- Seo, D. K.; Lee, J. K.; Lee, E. G. and Kim, H. 2001. "Effect of aging on the formation of TiO₂ nanocrystalline powder", Materials Letters, 51(2001), 115-119.
- Serpone, N.; Lawless, D. and Khairutdinov, R. 1995. "Size effects on the photophysical properties of colloidal anatase TiO₂ particles: size quantization or direct transition in this Indirect semiconductor", Journal of Physical Chemistry, 99(1995), 16646-16654.
- Shao, L.; Zhang, L.; Chen, M.; Lu, H. and Zhou, M. 2001. "Reactions of titanium oxides with water molecules. A matrix isolation FT-IR and density functional study", Chemical Physics Letters, 343(27 July 2001), 178-184.
- Strelko, V. and Malik, D. J. 2002. "Characterization and metal sorptive properties of oxidized active carbon", Journal of Colloid and Interface Science, 250(2002), 213-220.
- Suresh, C.; Biju, V.; Mukundan, P. and Warriar, K. G.K. 1998. "Anatase to rutile transformation in sol-gel titania by modification of precursor", Polyhedron, 17(1998), 3131-3135.

- Tanaka, T.; Teramura, K.; Yamamoto, T.; Takenaka, S.; Yoshida, S. and Funabiki, T. 2002. "TiO₂/SiO₂ photocatalysts at low levels of loading: preparation, structural and photocatalysis", Journal of Photochemistry and Photobiology. 148(2002), 277-281.
- Tang, Z.; Zhang, J.; Cheng, Z. and Zhang, Z. 2002. "Synthesis of nanosized rutile TiO₂ powder at low temperature", Materials Chemistry and Physics. 9319(2002), 1-4.
- Tonejc, A. M.; Turkovic, A.; Gotic, M.; Music, S.; Vokovic, M.; Trojko, R. and Tonejc, A. 1997. "HREM, TEM and XRD observation of nanocrystalline phases in TiO₂ obtained by the sol-gel method", Materials Letters. 31 (1997), 127-131.
- Vasudevan, A. K.; Prabhakar R. P.; Ghogh, G.; Anilkumar, G. M. and Damodaran, A. D. 1997. "Effect of addition of silver on anatase-rutile transformation as studied by impedance spectroscopy", Journal of Materials Science Letters. 16(1997), 8-11.
- Valasco, M. J.; Rubio, F.; Rubio, J. and Oteo, J. L. 1999. "DSC and FT-IR analysis of the drying process of titanium alkoxide derived precipitates", Thermochimica Acta. 326(1999), 91-97.

- Wang, Z. C.; Chen, J. F. and Hu, X. F. 2000. "Preparation of nanocrystalline TiO₂ powders at near room temperature from peroxo-polytitanic acid gel", Materials Letters. 43(2000), 87-90.
- Wang, C; Deng, Z. X. and Li, Y. 2001. "The synthesis of nanocrystalline anatase and rutile titania in mixed organic media", Inorganic Chemistry. 40(2001), 5210-5214.
- West, A. R. 1987. Solid State Chemistry and its Applications. U.S.A : John Willey and Sons.
- Wu, X.; Wang, D. and Yang, S. 2000. "Preparation and characterization of sterate-capped titanium dioxide nanoparticles", Journal of Colloid and Interface Science. 222(2000), 37-40.
- Xie, H.; Zhang, Q.; Xi, T.; Wang, J. and Liu, Y. 2002. "Thermal analysis on nanosized TiO₂ prepared by hydrolysis", Thermochimica Acta. 381 (2002), 45-48.
- Xu, N.; Shi, Z.; Fan, Y.; Dong, J.; Shi, J. and H U, M. Z. C. 1999. "Effects of particle size of TiO₂ on photocatalytic degradation of methylene blue in aqueous suspension", Industry and Engineering Chemistry Research. 38 (1999), 373-379.
- Yanagisawa, K. and Ovenstone, J. 1999. "Crystallization of anatase from amorphous titania using the hydrothermal technique: Effects of starting

- material and temperature", Journal of Physicals Chemistry B. 103(1999), 7781-7787.
- Yang, J. and Ferreira, J. M. F. 1998. "Inhibitory effect of the Al_2O_3 - SiO_2 mixed additives on the anatase-rutile phase transformation", Materials Letters. 36(1998), 320-324.
- Yang, S.; Liu, Y.; Guo, Y.; Zhao, J.; Xu, H. and Wang, Z. 2002. "Preparation of rutile titania nanocrystals by liquid method at room temperature", Materials Chemistry and Physics. 9430(2002), 1-6.
- Yanqing, Z.; Erwel, S.; Zhinzhan, C.; Wenjun, L. and Xingfang, H. 2001. "Influence of solution concentration on the hydrothermal preparation of titania crystallines", Journal of Material Chemistry. 11(2001), 1547-1551.
- Youn, H. -J.; Ha, P. S.; Jung, H. S.; Hong, K. S.; Park, Y. H. and Ko, K. H. 1999. "Alcohol rinsing and crystallization behavior of precipitated titanium dioxide", Journal of Colloid and Interface Science. 211(1998), 321-325.
- Yu, J.; Yu, J. C.; Leung, M. K. P.; Ho, W.; Cheng, B.; Zhao, X. and Xhao, J. 2003. "Effects of acidic and basic hydrolysis catalysts on the photocatalytic activity and microstructures of bimodal mesoporous titania", Journal of Catalysis. 217(2003), 69-78.

- Yu, J. G. Y.; Yu, J. C.; Cheng, B.; Hark, S. K. and Lu, K. 2003. "The effect of F-doping and temperature on the structural and textural evolution of mesoporous TiO₂ powders", Journal of Solid State Chemistry. 174(2003), 372-380.
- Zaban, A.; Aruna, S. T.; Tirosh, S.; Gregg, B. A. and Mastai, Y. 2000. "The effect of the preparation condition of TiO₂ ", Journal of Physical Chemistry B. 104(2000), 4130-4133.
- Zhang, Q. -H.; Gao, L. and Guo, J. -K. 1999. "Preparation and characterization of nanosized TiO₂ powders from aqueous TiCl₄ solution", Nanostructured Materials. 11(5 November 1999), 1293-1300.
- Zhang, Q.; Gao, L. and Guo, J. 2000. "Effects of calcination on the photocatalytic properties of nanosized TiO₂ powders prepared by TiCl₄ hydrolysis", Applied Catalysis B: Environment. 26(2000), 207-216.
- Zhang, Q.; Gao, L. and Guo, J. 2000. "Effects of hydrolysis conditions on morphology and crystallization of nanosized TiO₂ powders", Journal of the European Ceramic Society. 20(2000), 2153-2158.
- Zhang, R. and Gao, L. 2001. "Effect of peptization on phase transformation of TiO₂ nanoparticles", Materials Research Bulletin. 36(2001), 1957-1965.

Zhang, Y. H. and Reller, A. 2001. "Nanocrystallite iron-doped mesoporous titania and its phase transition", Journal of Materials Chemistry. 11(2001), 2537-2541.

Zhang, Y.; Weidenkaff, A. and Reller, A. 2002. "Mesoporous structure and phase transition of nanocrystalline TiO_2 ", Materials Letters. 54(June 2002), 375-381.

Zhao, X. K. and Fendler, J. H. 1991. "Size quantization in semiconductor particulate films", Journal of Physical Chemistry. 95(1991), 3716-3723.

Vitae

Name Mister Wissanu Choychangtong

Birth Date 21 December 1977

Educational Attainment

Degree	Name of Institution	Year of Graduate
Bachelor of Science (Chemistry)	Prince of Songkla University	2000

Scholarship Awards during Enrolment

The Development and Promotion of Science and Technology Talents Project (DPST).

Postgraduate Education and Research Program in Chemistry (PERCH).